AD-A172 945 THE APPLICATION OF LASER SATURATION TO THE EFFICIENT GENERATION OF SHORT (U) TORONTO UNIV DOWNSVIEW (ONTARIO) INST FOR AEROSPACE STUDIES R M MEASURES

1/2

UNCLASSIFIED MAY 86 AFOSR-TR-86-0986 AFOSR-85-0020 F/G 20/5 NL

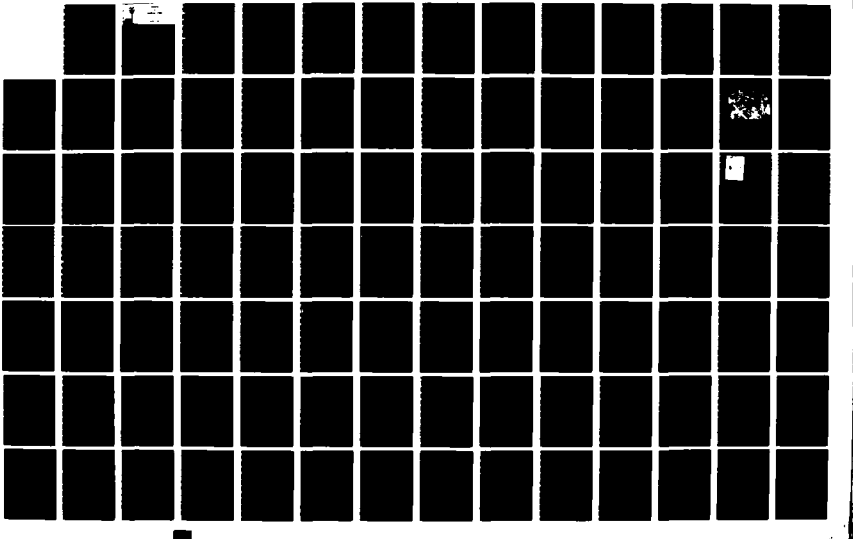

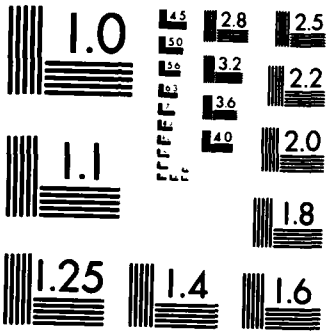

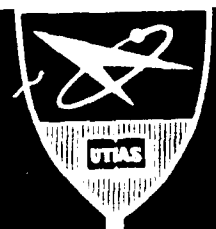


# INSTITUTE
# FOR
# AEROSPACE STUDIES

UNIVERSITY OF TORONTO

UNCLASSIFIED
SECURITY CLASSIFICATION OF THIS PAGE

AD-A172 945

# REPORT DOCUMENTATION PAGE

| | |
|---|---|
| 1a. REPORT SECURITY CLASSIFICATION: Unclassified | 1b. RESTRICTIVE MARKINGS |
| 2a. SECURITY CLASSIFICATION AUTHORITY | 3. DISTRIBUTION/AVAILABILITY OF REPORT: Approved for public release; distribution unlimited |
| 2b. DECLASSIFICATION/DOWNGRADING SCHEDULE | |
| 4. PERFORMING ORGANIZATION REPORT NUMBER(S) | 5. MONITORING ORGANIZATION REPORT NUMBER(S): AFOSR-TR- 86-0906 |
| 6a. NAME OF PERFORMING ORGANIZATION: University of Toronto Inst. for Aerospace Studies; 6b. OFFICE SYMBOL (If applicable) | 7a. NAME OF MONITORING ORGANIZATION: AFOSR |
| 6c. ADDRESS (City, State and ZIP Code): 4925 Dufferin Street, Downsview, Ontario, Canada M3H 5T6 | 7b. ADDRESS (City, State and ZIP Code): AFOSR/NP Bolling AFB DC 20 |
| 8a. NAME OF FUNDING/SPONSORING ORGANIZATION: Air Force Office of Scientific Research/NA; 8b. OFFICE SYMBOL (If applicable): NP | 9. PROCUREMENT INSTRUMENT IDENTIFICATION NUMBER: AF-AFOSR 85-0020 |
| 8c. ADDRESS (City, State and ZIP Code): Bldg. 410, Bolling Air Force Base, DC 20332, U.S.A. | 10. SOURCE OF FUNDING NOS. |

| PROGRAM ELEMENT NO. | PROJECT NO. | TASK NO. | WORK UNIT NO. |
|---|---|---|---|
| 61102F | 2301 | A8 | N/A |

11. TITLE (Include Security Classification): The Application of Laser Saturation to the Efficient Generation of Short Wavelength Radiation from Plasmas

12. PERSONAL AUTHOR(S): Dr. R. M. Measures

| 13a. TYPE OF REPORT | 13b. TIME COVERED | 14. DATE OF REPORT (Yr., Mo., Day) | 15. PAGE COUNT |
|---|---|---|---|
| Annual | FROM Nov. 1/84 TO Oct 31/85 | May 1986 | |

16. SUPPLEMENTARY NOTATION

| 17. COSATI CODES | | |
|---|---|---|
| FIELD | GROUP | SUB. GR. |
| | | |
| | | |

18. SUBJECT TERMS (Continue on reverse if necessary and identify by block number): 1. Strontium plasma, 2. Sodium plasma, 3. Laser resonance saturation, 4. Laser ionization, 5. Electron temperature measurement, 6. Stark broadening. (Continued on reverse)

19. ABSTRACT (Continue on reverse if necessary and identify by block number)

Resonant laser pumping of transitions within atoms or ions represents a powerful mode of coupling laser energy into a gas or plasma. In the case of laser saturation of a resonance transition rapid heating of the free electrons by superelastic collision quenching of the laser pumped state has been shown to play the central role in this process. We have developed a computer code that models this "laser ionization based on resonance saturation" (LIBORS) and permits us to map the three dimensional nature of this complex interaction. We have been able to show by comparison with

(Continued on reverse)

| 20. DISTRIBUTION/AVAILABILITY OF ABSTRACT | 21. ABSTRACT SECURITY CLASSIFICATION |
|---|---|
| UNCLASSIFIED/UNLIMITED ☒ SAME AS RPT. ☐ DTIC USERS ☐ | Unclassified |

| 22a. NAME OF RESPONSIBLE INDIVIDUAL | 22b. TELEPHONE NUMBER (Include Area Code) | 22c. OFFICE SYMBOL |
|---|---|---|
| Dr. ROBERT J BARKER | 202/767-5011 | NP |

DD FORM 1473, 83 APR — EDITION OF 1 JAN 73 IS OBSOLETE.

UNCLASSIFIED
SECURITY CLASSIFICATION OF THIS PAGE

Abstract - Continued:

experiment that this LIBORS computer code can predict the radial and axial electron density and temperature profiles of the plasma formed along the path of the laser pulse. These experimental results in themselves represent the first detailed measurements of a sodium plasma created by laser resonance saturation and reveal the importance of laser attenuation in the formation of the plasma.

We have also shown that both one and two photon resonant laser pumping of a cold, unexcited plasma created by two photon ionization of strontium vapor can lead to rapid excitation of high lying states of the strontium ion. Lastly, we have demonstrated parametric generation within this same strontium plasma when the laser is tuned close to a two photon transition of the ion.

18 Subject Terms - Continued.

7. Electron density measurements, 8. Parametric generation, 9. Atom density measurements, 10. Laser diagnostics, 11. Alkali oven, 12. Superelastic plasma heating, 13. Four wave difference mixing, 14. Metal vapor plasmas.

# THE APPLICATION OF LASER SATURATION TO THE EFFICIENT GENERATION OF SHORT WAVELENGTH RADIATION FROM PLASMAS

Final Technical Report, May 1986

U.S. AFOSR 85-0020

Prepared by

Dr. R. M. Measures

Professor of Applied Science and Engineering

University of Toronto, Institute for Aerospace Studies
4925 Dufferin Street
Downsview, Ontario, Canada
M3H 5T6

CONTENTS


| | Page |
|---|---|
| ABSTRACT | 4 |
| RESEARCH OBJECTIVES | 5 |
| STATUS REPORT | 6 |
| Laser Ionization Based on Resonance Saturation (LIBORS) Program | 6 |
| LIBORS Experimental Facility | 7 |
| Electron Density Radial Profile Measurements | 8 |
| Electron Temperature Measurements | 8 |
| Multishot Average Multiplet Spectrum | 9 |
| LIBORS Computer Code | 10 |
| Computational and Experimental Comparison | 10 |
| Development of New LIBORS Code Including Thermal Conduction and Using an Adaptive Grid | 11 |
| Multiphoton Interactions in Strontium | 12 |
| Strontium Experimental Facility | 12 |
| Superelastic Heating of a Strontium Plasma by Resonant One and Two Photon Laser Pumping | 13 |
| Parametric Generation within a Strontium Plasma Created by Two Photon Ionization | 15 |
| REFERENCES | 15 |
| CUMULATIVE CHRONOLOGICAL LIST OF PUBLICATIONS (1980-present) | 17 |
| PROFESSIONAL PERSONNEL | 19 |
| INTERACTIONS | 19 |
| NEW DISCOVERIES STEMMING FROM RESEARCH | 19 |
| FIGURES | |
| APPENDICES: A - Sodium Atom Distribution Within a Heat Sandwich Oven | |
| B - Electron Density Radial Profiles Derived from Stark Broadening in a Sodium Plasma Produced by Laser Resonance Saturation | |
| C - Effect of Inhomogeneities, Optical Depth and Finite Bandwidth on Electron Temperature Measurements in Cylindrically Symmetric Plasmas | |
| D - Computer Modeling of the Multishot Averaged Spectral Emission from a Laser Created Sodium Plasma | |
| E - Plasma Channel Formation Through Laser Resonance Saturation | |
| F - Superelastic Collisional Excitation of a Strontium Plasma Induced Through One and Two Photon Laser Pumping | |
| G - Parametric Generation Within a Strontium Plasma Created by Two Photon Ionization | |

ABSTRACT

Resonant laser pumping of transitions within atoms or ions represents a powerful mode of coupling laser energy into a gas or plasma. In the case of laser saturation of a resonance transition rapid heating of the free electrons by superelastic collision quenching of the laser pumped state has been shown to play the central role in this process. We have developed a computer code that models this "laser ionization based on resonance saturation" (LIBORS) and permits us to map the three dimensional nature of this complex interaction. We have been able to show by comparison with experiment that this LIBORS computer code can predict the radial and axial electron density and temperature profiles of the plasma formed along the path of the laser pulse. These experimental results in themselves represent the first detailed measurements of a sodium plasma created by laser resonance saturation and reveal the importance of laser attenuation in the formation of the plasma.

We have also shown that both one and two photon resonant laser pumping of a cold, unexcited plasma created by two photon ionization of strontium vapor can lead to rapid excitation of high lying states of the strontium ion. Lastly, we have demonstrated parametric generation within this same strontium plasma when the laser is tuned close to a two photon transition of the ion.

## RESEARCH OBJECTIVES

Over the years research towards the development of short wavelength (VUV to X-ray) lasers has proceeded down many paths. Recently, groups at Livermore and Princeton appear to have had some success using very powerful lasers.[1-3] In each of these cases the wavelength of the pumping laser was non-specific and the density of the plasma was very high. Alternatively, the generation of coherent short wavelength radiation can be achieved through multiphoton induced nonlinear processes such as: two photon four-wave sum mixing and third harmonic generation.

The prospects of achieving high conversion efficiency are greatly facilitated by selecting the exciting and generated fields to be near resonant with allowed optical transitions of the atom. In the past, these interactions have usually involved atomic vapors,[4-7] but the quest for coherent short wavelength radiation will invariably require multiphoton pumping of an ionic species within a plasma. However, the fulfilment of this promise is only likely to be achieved if a cool (relatively unexcited), uniform plasma column of considerable length can be created. At modest densities laser resonance saturation has been shown to be very effective at rapidly producing near total ionization of the laser pumped species.[8-15]

The main objective of our current research program has been to study "laser ionization based on resonance saturation" (LIBORS), both theoretically and experimentally in order to gain a better understanding of this complex laser interaction and to provide some insight into the capability of this mode of ionization to create long, cool dense plasma channels. To accomplish this we have undertaken the development of a computer code that attempts to model LIBORS in both space and time. We have also performed a set of experiments designed to evaluate the properties of the plasma channel created by LIBORS and to test the predictions of our computational model in this regard.

Laser saturation of an ion resonance line within a plasma offers the prospect of very rapid heating of the free electrons through superelastic collision quenching of the laser pumped resonance state population.[16] This mode of coupling laser energy into a plasma could be very competitive with inverse bremsstahlung[17] and could lead to a form of shock heating of the free electrons. If the initial plasma was cold and relatively unexcited, it

might be possible with this technique to create a population inversion that could lead to efficient short wavelength laser action. Consequently, another of our objectives has been to undertake a preliminary investigation of laser pumping of an ion resonance line within a plasma.

Near resonance multiphoton excitation can also lead to certain enhanced nonlinear interactions and we have undertaken a preliminary investigation of one such process.

## STATUS REPORT

### Laser Ionization Based on Resonance Saturation (LIBORS) Program

Laser saturation of a resonance transition within an atom or an ion represents a new class of laser-plasma interactions In the case of a neutral atomic vapor, laser resonance saturation gives rise to many processes that quickly lead to ionization.[18] Once an appreciably degree of ionization has been achieved the primary mechanism for converting laser energy into plasma energy is superelastic electron collision quenching of the laser pumped resonance state population. This is an extremely efficient method of laser energy transfer which, in effect, rapidly cycles the bound electrons between the ground and resonance states, converting the energy of one photon into free electron kinetic energy during each cycle per atom.[9-11]

Laser resonance saturation can be viewed as complementary to inverse bremsstrahlung, for although it can lead to energy deposition that is many orders of magnitude greater than attainable through inverse bremsstrahlung for modest values of laser irradiance — the free electron temperature achieved is limited by the characteristics of the atom or ion being irradiated.[16] Laser saturation of an ion resonance line within a plasma saturation can lead to extremely rapid electron heating, in effect, creating a well defined electron temperature jump[16] and a commensurate sharp burst in the emission of short wavelength radiation from a suitable plasma.

The objective of our research program is to study this new form of laser-plasma interaction and explore some of its potential applications. In any practical application, the laser pulse has to propagate through a finite depth of the medium being irradiated and as a result of the strong nature of the resonance interaction, the laser pulse will undergo an appreciable

degree of attenuation and temporal and spatial distortion. Consequently, any theoretical modeling of this interaction should take account of this fact.

To date, we are the first to develop a computational analysis that attempts to model the three dimensional nature of this interaction by taking account of the attenuation and distortion suffered by the laser pulse as it burns its way through a realistic atomic vapor distribution. In order to assess the reliability of our theoretical work we are comparing our computer simulations with the results attained from experiments involving a new facililty.

LIBORS Experimental Facility

This new facility basically comprises: a Nd-YAG laser pumped dye laser, a specially designed sodium heat sandwich oven which provides 360° optical access and a photodetection system tht includes an RCA C31034 photomultiplier mounted on the exit slit of a SPEX monochromator. A photograph of the facility is displayed as figure 1, and a schematic overview is presented in figure 2. Detailed descriptions of this facility are provided in Appendices A, B and C — which constitute three papers describing our experimental work. *Appendix A is a* paper that has recently been published, while Appendices B and C represent two new papers that will shortly be submitted for publication.

The sodium atom density distribution across this novel oven was evaluated by measuring the absorption of a narrow, well collimated beam of continuum radiation from a xenon lamp. These measurements were undertaken at a number of locations across the heat sandwich oven and are made possible by the design of this oven. The width of the spectral hole created by the sodium resonance line was evaluated for the beam passing through the high density vapor core, while the depth of the 589 nm spectral hole was determined in the low density rim of the vapor disc. The experimental technique is described in detail in Appendix A.

Our principal plasma measurements have involved evaluating the radial profiles of the free electron density and temperature along the path of the laser pulse. We have also looked with some depth into the accuracy of such measurements and the care needed in their interpretation. This work is presented briefly in the body of this report as the full details are

included in Appendices B and C in the form of papers that will shortly be submitted for publication.

## Electron Density Radial Profile Measurements

We have undertaken the first spatially resolved measurement of the free electron density in a sodium plasma produced by laser resonance saturation. This evaluation involved fitting the radially inverted experimental $4^2D$-$3^2P$ multiplet spectrum with convoluted Stark (electron impact) and instrument broadened profiles. A pair of representative radial profiles of the free electron density, evaluated at two equidensity locations along the path of the laser pulse ($z = -2$ and 2 cm) are displayed as figure 3. These results clearly reveal that the plasma narrows and the peak degree of ionization diminishes with axial location. We attribute this to absorption of the laser pulse as it propagates through the sodium vapor. A detailed description of this work is presented as Appendix B and Cappelli.[19]

## Electron Temperature Measurements

The free electron temperature, $T_e$, of a sodium plasma created by laser resonance saturation has been evaluated by two independent methods. The first involves the measurement of the spectrally integrated emission of several sodium multiplets and the deduction of the $T_e$ from the slope of the least square linear fit to this data when plotted logarithmically (this is termed a Boltzmann plot). A representative example of such a measurement for our plasma is presented as figure 4. Although this technique has been used by a number of researchers,[20,21] we have shown (see Appendix C) that this kind of measurement can be subject to appreciable errors if the plasma is not uniform and optically thin.

In particular, we have undertaken a numerical simulation of the emission observed from a cylindrical plasma and have shown that if the core is highly ionized, then the bulk of the emission originates from a cooler outer angular zone where the upper state population density is a maximum and, under these circumstances, the measured temperature fails to reflect the value in the plasma core. This could explain some of the low temperatures observed.[20,21] In addition self absorption has been found to lead to a large scatter of the multiplet emission data on a Boltzmann plot,

and even more deviation from linearity can arise in high density plasmas (where Stark broadening can be significant) if the photodetection bandwidth is inadequate.

The second technique is indirect, nevertheless it provides us with the radial variation of $T_e$. In this approach the free electron density radial profile, discussed above and in Appendix B, is used in conjunction with the sodium atom density and the Saha-equation, assuming the establishment of Local Thermodynamic Equilibrium (LTE), to calculate the free electron temperature radial profile $T_e$. Two such $T_e$-radial profiles corresponding to the two $N_e$-radial profiles displayed in figure 3, are presented in figure 5 and reveal that the temperature tends to decrease monitonically with increasing radius and also decreases along the path of the 37 mJ laser pulse (from z = -2 to 2 cm). The peak sodium density in this run was also $1.5\times10^{16}$ $cm^{-3}$ and the value at the axial locations of interest was about $10^{16}$ $cm^{-3}$. Furthermore, since these measurements were undertaken about 65 ns after the start of the laser pulse (duration 40 ns) the plasma is expected to be in LTE.

The observed decline of the free electron temperature along the path of the laser pulse represents an important observation for it also reflects the progressive attenuation of the laser pulse with increasing penetration of the sodium vapor. Moreover, the low value of the electron temperature corresponding to propagation distances of several centimeters at a mean sodium atom density of around $10^{16}$ $cm^{-3}$ is similar to that observed by others under similar experimental conditions.[20,21]

Multishot Average Multiplet Spectrum

In our experimental measurements, as with many others, the spectral distribution of the emission is determined from a series of measurements at different wavelengths. If the shot-to-shot reproducibility is poor, or the signal is weak, the emission recorded in each spectral interval is an average of several shots. When the results of such experiments are to be compared with those predicted by a computational model the question of whether the laser pulse can be represented by a Gaussian radial profile arises. This is particularly true if the interaction is highly nonlinear,

as in the case of LIBORS, and if the experimental laser pulse has a noisy radial profile.

We have undertaken a computational simulation of this problem and have shown, in Appendix D, that computer modeling of LIBORS based on a Gaussian approximation for the laser pulse radial profile is acceptable provided the experimental results are averaged over at least 16 shots.

## LIBORS Computer Code

We have developed the first computer code for modeling the formation of a cylindrical sodium plasma, through laser resonance saturation, that takes account of the nonuniform sodium atom distribution along the path of the laser pulse and the temporal and spatial distortion of the laser pulse arising from absorption as it propagates through the sodium vapor.

This LIBORS computer code represents a major development of our research group and is described in detail in Appendix E and Wong[22] and Kissack.[23] The predictions of this code have provided us with the first insight into the three dimensional nature of LIBORS and have been tested by comparison with the results of experiments using the facility described above and in Appendices A, B, C and E. One of the most significant results of this work has been the recognition that considerable attenuation of the laser pulse can arise within a few centimeters of vapor at a density of about $10^{16}$ $cm^{-3}$ and that this can lead to the formation of a low temperature low density plasma at these locations.

An idea of the predictive capability of this code is provided in figures 6 and 7 which reveal two views of the plasma channel expected to be formed in one of our experiments. In figure 6, the axial variation of the electron density for several radial positions is displayed, while in figure 7 the radial variation of the electron density is presented for several axial locations. Also shown in figure 6 is the experimentally based sodium atom density distribution along the path of the laser pulse used in the computer code.

## Computational and Experimental Comparison

In order to test the modeling capability of our LIBORS computer code we have compared its predictions regarding the radial and axial distributions

of the free electron density and temperature with the results obtained from an experiment. In general the agreement is very good when the uncertainty in the experimental measurements is taken into account and it is borne in mind that many of the cross-sections used in the code are not accurately known. The 20% uncertainty in the sodium atom density measurements are particularly troublesome because this distribution is used in the computer code and as a consequence leads to two kinds of theoretical uncertainty: a direct uncertainty in the local value of the free electron density and an uncertainty that results from the cumulative uncertainty in the laser energy fluence that penetrates to that location.

With this in mind we present in figure 8 a comparison of the experimentally measured (see Appendix B) and computer predicted electron density radial profile at Z = -2 cm and t = 65 ns for the sodium atom distribution displayed in figure 6. The two computed profiles are seen to flank the experimental values and arise from using two values for the cross-section of the dominant seed ionization (laser assisted associative ionization). The computer code based on the cross section derived by Roussel et al, 1980, $\sigma_A = \sigma_A(F)$ [$5 \times 10^{-15}$ $cm^2$ for most of our conditions] fits closest to the experimental data on axis, while for large radial positions this code overestimates the electron density. Reference to figure 9 shows good agreement between the predictions of this code and the experimentally determined axial profiles of the free electron density and temperature. We believe that the divergence observed for large Z could result from error in the sodium atom density measurements while the radial difference could be attributed to an overestimate in the radius of the laser beam. The experimental electron temperature data were derived from the electron density data assuming LTE. A more detailed discussion of this work is provided in Appendix E, which will serve as the basis of a paper to be submitted for publication.

## Development of New LIBORS Computer Code Including Thermal Conduction and Using an Adaptive Grid

The previous section clearly indicates that our current LIBORS computer code is capable of predicting with reasonable accuracy the long term state of a plasma created by laser resonance saturation. However, for certain

kinds of applications the state of the plasma during the formation stage could be of interest. Indeed, some applications may even rely on the kind of temperature shocks predicted to occur during the formation phase of the plasma. For example we present in figure 10(a) and (b) the radial variation of the free electron density and temperature at t = 58 ns and Z = 0 where $N_o = 1.7 \times 10^{16}$ $cm^{-3}$. The incident laser pulse was assumed to have an energy of 37 mJ and its radial distribution of energy fluence is also depicted in figure 10(a). In figure 10(b) we display the corresponding radial variation of the thermal conduction and net time rate of change of the free electron thermal energy density. This figure clearly indicates that thermal conduction can become very large and even dominate in the energy equation where steep gradients in $T_e$ exist.

We surmize that the omission of thermal conduction and electron diffusion may not be justified during the formation phase and we are in the process of including these effects into the energy and ionization equations. These major advances in our theoretical treatment have forced us to reformulate our LIBORS computer code so that integration in time is now undertaken at a set of so called "nodal positions" in space. To accomplish this with a minimum use of computer time, we are employing an "adaptive grid" to constantly move a limited number of nodal positions into the regions of strong gradients. In this way the code should be able to accommodate the formation and propagation of the ionization front and the associated steep gradient in the electron temperature, Kissack.[23]

## MULTIPHOTON INTERACTIONS IN STRONTIUM

### Strontium Experimental Facility

Our experimental facility for studying the formation of a strontium plasma and the subsequent one and two photon excitation of the SrII ions is schematically presented as figure 11. The strontium vapor is contained in a specially designed crossed heat pipe heated to around 800°C. Our Nd-YAG laser (JK HY750) is used with a DCDA doubler and KD*P mixer crystal to generate third harmonic radiation at 355 nm for pumping Stillbene 420 within our dye laser (Quanta-Ray PDL-1).

The performance of this dye declines fairly rapidly, the laser output dropping by about 50% within 20 minutes. The subsequent decline is then

much slower. For most of our initial work we have used an output pulse energy of about 2-5 mJ. A lens was used just ahead of the crossed heat pipe to focus the laser pulse and produce maximum two photon ionization in the centre of the oven in order that the side light fluorescence could be observed.

A SPEX 1700 II monochromator was employed to spectrally select the radiation detected by our RCA-4526 photomultiplier. Radiation emitted colinear and parallel with the laser pulse was sampled by a beam splitter and two mirrors. The mirror positioned in front of the monochromator is rotatable through 90 degrees so that it can also be used in conjunction with another beam splitter and mirror to sample any radiation emitted in the opposite direction to the laser pulse. This mirror can also be removed and a lens introduced to focus some of the strontium plasma side light emission (i.e., that emitted perpendicular to the laser beam) onto the entrance slit of the monochromator. Two photodiodes were also used in the experiments: one to monitor the output of the dye laser, the other was used to provide a trigger pulse to the signal averager (EG&G 4420) used for data acquisition of the photomultiplier signal.

Superelastic Heating of a Strontium Plasma by Resonant One and Two Photon Laser Pumping

A number of years ago we had theoretically predicted that laser saturation of an ion resonance line, within a dense plasma, could lead to extremely rapid rates of electron heating through superelastic collision quenching of the laser pumped state.[16] We had also shown that, under certain circumstances, this superelastic laser energy conversion process could couple laser energy into the plasma several orders of magnitude faster than through inverse bremsstrahlung.[17] Furthermore, we suggested that multiphoton laser pumping might be used to expand the capabilities of this interaction.[17]

We have recently undertaken the first test of superelastic electron heating of a strontium plasma created by two photon ionization of strontium vapor. The details of this work are provided in Appendix F, which constitutes a paper that will shortly be submitted for publication and Menard.[24]

In essence strontium vapor confined within our crossed heat pipe oven is two photon ionized with a pulse of laser radiation of wavelength ($\lambda_L$) less than 431 nm. When the wavelength of the laser was tuned to the $5^2P_{1/2}$-$5^2S_{1/2}$ SrII resonance transition at 421.67 nm, strong emission was observed from the high lying transition, $5^2F_{5/2,7/2}$-$5^2D_{5/2}$, at 565.20 nm. We believe that this excitation represents clear evidence of free electron heating resulting from superelastic electron collision quenching of the laser pumped $5^2P_{1/2}$-$5^2S_{1/2}$ transition. The $5^2S_{1/2}$ ion ground state population being created by two photon ionization with the same laser pulse. We were able to eliminate the possibility that this 565.2 nm emission arose through three photon excitation on the grounds that the intensity of the emission failed to peak as the laser was tuned through the wavelength for exact three photon resonance at 422.14 nm, while it did peak when the laser was tuned through the 421.67 nm wavelength corresponding to the ion resonance wavelength, see figure 12(a). Although the emission increases sharply as the laser wavelength approaches 421.67 nm from the blue, the emission falls much more slowly on the red side of 421.67 nm. We attribute this asymmetry to some form of self-focussing effect. Both the intensity of this emission and its spectral asymmetry are seen to decline with decreasing strontium density, figure 12. The most convincing evidence that the excitation mechanism is collisional in origin rather than laser induced stems from the long lived nature of the emission.

The emission at 565.2 nm is also found to peak sharply when the laser is tuned through the two photon $5^2S_{1/2}$-$6^2S_{1/2}$ transition at 418.97 nm, which leads us to suspect that again superelastic collision quenching of the laser pumped $6^2S_{1/2}$ level population could be heating the free electrons and enabling them to excite the high lying $5^2F$ levels. In this instance the 565.2 nm emission arises only when the laser wavelength exactly matches the value needed to excite the two photon transition because only then is the $6^2S_{1/2}$ state actually populated. Verification of the collisional origin of the interaction is again provided by the long lived nature of the 565.2 emission.

We conclude that this work constitutes the first proof of principle that one or two photon laser pumping of an ion can lead to superelastic

heating of the free electrons and concomitant rapid excitation of high lying ion states.

Parametric Generation Within a Strontium Plasma Created by Two-Photon Ionization

The study of nonlinear optical effects in plasmas has in the past primarily been associated with the nonlinear polarization of the free electrons. However, when the exciting laser is tuned to be in close resonance with a two photon transition within the ions of the plasma the nonlinear susceptibility of the ions can dominate. As part of our study of resonant multiphoton interactions in strontium we have found that an intense beam of radiation almost colinear with the pump laser beam can be generated parametrically within a strontium plasma that is created by two photon ionization. What is particularly interesting is that this four-wave difference mixing is achieved with the same laser that is responsible for the ionization of the strontium.

This complex sequence of interactions can be understood by reference to figure 13 which shows how laser radiation at 418.97 nm can two photon ionize SrI and excite the four-wave difference mixing process leading to beams of radiation at 430.67, 416.30, 407.89 and 421.67 nm that are close to colinear with the laser pump beam. The details of this experiment and a formulation of its theoretical basis is provided as Appendix G, which constitutes another paper that will shortly be submitted for publication, and in the M.A.Sc. thesis of K. Menard.[24]

## REFERENCES


1 M. D. Rosen, et al., Phys. Rev. Lett., 54, 106-109, 1985.

2 D. L. Mathews, et al., Phys. Rev. Lett., 54, 110-113, 1985.

3 S. Suckewer, et al., in "Laser Techniques in the Extreme Ultraviolet", Eds. S. E. Harris and T. B. Lucatorto, AIP Conf. Proc. No. 119, Subseries 5, p. 55, 1984.

4 W. Hartig, Appl. Phys., 15, 427-432, 1978.

5 A. V. Smith and J. F. Ward, J. of Quant. Elect. QE-17, 525-529, 1981.

6 F. S. Tomkins and R. Mahon, Optics Lett., 7, 304-306, 1982.

7 C. Y. R. Wu and J. K. Chen, Optics Commun. 50, 317-319, 1984.

8 (a) T. B. Lucatorto and T. J. McIlrath, Phys. Rev. Letters, 37, 428-431, 1976.

(b) T. J. McIlrath and T. B. Lucatorto, Phys. Rev. Letters, 38, 1390-1393, 1977.

9 C. H. Skinner, J. Phys. B: Atom. Molec. Phys., 13, 55-68, 1980.

10 C. Bréchignac and Ph. Cahuzac, Optics Commun., 43, 270-273, 1982.

11 (a) F. Roussel, P. Breger, G. Spiess, C. Manus and S. Geltman, J. Phys. B: Atom. Molec. Phys. 13, L631-L636, 1980.

(b) B. Carré, F. Roussel, P. Breger and G. Spiess, J. Phys. B: Atom. Molec. Phys. 14, 4289-4300, 1981.

12 L. Jahreiss and M. C. E. Huber, Phys. Rev. A, 28, 3382-3401, 1983.

13 R. M. Measures and P. G. Cardinal, Physical Review A, 23, 804-815, 1981.

14 R. M. Measures, P. G. Cardinal and G. W. Schinn, J. Appl. Phys. 52, 1269-1277, 1981, and 52, 7459, 1981.

15 R. M. Measures, "Laser Resonance Saturation: An Efficient and Rapid Means of Ionization and Electron Heating". Invited paper at the Society for Optical and Quantum Electronics LASER'S 82 Meeting, New Orleans, Dec. 12-17, 1982.

16 R. M. Measures, P. L. Wizinowich and P. G. Cardinal, J. Appl. Phys., 51, 3622-3628, 1980.

17 R. M. Measures, N Drewell and P. G. Cardinal, Appl. Optics, 18, 1824-1827, 1979.

18 P. G. Cardinal, UTIAS Report No. 299, 1985.

19. M. A. Cappelli, UTIAS Report No. 306, 1986.

20 O. L. Landen, R. J. Windfield, D. D. Burgess, J. D. Kilkenny, and R. W. Lee, Phys. Rev. A 32, 2963, 1985.

21 D. J. Krebs and L. D. Schearer, J. Chem. Phys. 76, 2925, 1982.

22 S. K. Wong, UTIAS Report No. 292, 1985.

23 R. Kissack, UTIAS Report No. 305, 1986.

24. K. A. Menard, University of Toronto, Institute for Aerospace Studies M.A.Sc. Thesis, 1986.

## CUMULATIVE CHRONOLOGICAL LIST OF PUBLICATIONS (1980-PRESENT)

1. M. A. Cappelli and R. M. Measures, "Electron Density Radial Profiles Derived from Stark Broadening in a Sodium Plasma Produced by Laser Resonance Saturation" (to be submitted for publication).
2. M. A. Cappelli and R. M. Measures, "Effects of Inhomogeneities Optical Depth and Finite Bandwidth on Electron Temperature Measurements in Cylindrically Symmetric Plamas" (to be submitted for publication).
3. R. S. Kissack, M. A. Cappelli and R. M. Measures, "Computer Modeling of the Multishot Averaged Spectral Emission from a Laser Created Sodium Plasma" (to be submitted for publiction).
4. R. S. Kissack, M. A. Cappelli and R. M. Measures, "Plasma Channel Formation Through Laser Resonance Saturation" (to be submitted for publication).
5. K. A. Menard and R. M. Measures, "Superelastic Collisional Excitation of a Strontium Plasma Induced Through One and Two Photon Lasre Pumping" (to be submitted for publication).
6. K. A. Menard and R. M. Measures, "Parametric Generation within a Strontium Plasma Created by Two Photon Ionization" (to be submitted for publication).
7. M. A. Cappelli, P. G. Cardinal, H. Herchen and R. M. Measures, "Sodium Atom Distribution Within a Heat Sandwich Oven", Rev. Sci. Instrum., 56, 2030-2037, 1985.
8. M. A. Cappelli and R. M. Measures, "Two Channel Technique for Stark Measurements of Electron Density Within a Laser Produced Sodium Plasma", Appl. Optics 23, 2107-2114, 1984.
9. G. W. Schinn and R. M. Measures, "STROPE - A New Species Density Gradient Measurement Technique", Appl. Optics 23, 1258-1266, 1984.
10. R. M. Measures, "Laser Resonance Saturation: An Efficient and Rapid Means of Ionization and Electron Heating", Invited Paper in the Proc. of Soc. for Optical and Quantum Electronics LASERS 82 Meeting, New Orleans, Dec. 12-17, 1982.
11. R. M. Measures and H. Herchen, "Laser Absorption Under Saturation Conditions with Allowance for Spectral Hole Burning", J. Quant. Spectrosc. Radiat. Transfer 29, 9-18, 1983.

12. R. M. Measures, S. K. Wong and P. G. Cardinal, "The Influence of Molecular Nitrogen Upon Plasma Channel Formation by Laser Resonance Saturation", J. Appl. Physics 53, 5541-5551, 1982.
13. M. R. Arnfield and R. M. Measures, "Ion to Neutral Atom Measurements within an Ablation Plasma Through Laser Selective Excittion Spectroscopy", Physical Review A, 24 535-539, 1981.
14. R. M. Measures, P. G. Cardinal and G. W. Schinn, "Theoretical Model of Laser Ionization of Alkali Vapours Based on Resonance Saturation", J. Appl. Phys. 52, 1269-1277, 1981.
15. P. G. Cardinal, P. L. Wizinowich and R. M. Measures, "Anomalous Laser Energy Absorption Associated with Resonance Saturation", J. Quant. Spectrosc. Radiat. transfer 25, 537-545, 1981.
16. R. M. Measures and P. G. Cardinal, "Laser Ionization Based on Resonance Saturation - A Simple Model Description", Physical Review A, 23, 804-815, 1981.
17. R. M. Measures, P. L. Wizinowich and P. G. Cardinal, "Fast and Efficient Plasma Heating Through Superelastic Laser Energy Conversion", J. Appl. Phys., 51, 3622-3628, 1980.
18. H. S. Kwong and R. M. Measures, "Lifetime Measurements on Atoms in Compounds Embedded in Matrices Using Laser Selective Excitation and Ablation Dynamics", Appl. Optics, 19, 1025-1027, 1980.

Books

1. R. M. Measures, "Laser Remote Sensing", J. Wiley & Sons, 1984.

PROFESSIONAL PERSONNEL

Principal Investigator:

Dr. R. M. Measures (Professor of Applied Science and Engineering)

Research Assistants:

P. G. Cardinal, Ph.D., Nov. 1985, Thesis: "A Study of Laser Induced Ionization of Alkali Metal Vapors Based on Saturation of the First Resonance Transition"

S. K. Wong, Ph.D., Sept. 1985, Thesis: "A Computational Study of the Influence of Molecular Nitrogen and Laser Absorption on Plasma Channel Formation Created by Laser Resonance Saturation of Sodium Vapor"

R. S. Kissack (Ph.D. Student)

M. A. Cappelli (Ph.D. Student)

K. Menard (M.A.Sc. Student)

S. D. Hanratty (M.A.Sc. Student)

P. Gomes (M.A.Sc. Student)

Interactions

Professor R. M. Measures served on the Program Committee of the newly formed: "International Laser Science Conference". He organized and chaired a session on Laser Resonance Saturation and Its Application and delivered an invited paper on Laser Resonance Saturation at the First Meeting, November 18-22, Dallas, Texas. Professor Measures also organized a session on Remote Sensing with Lasers and Fiber Optics at the LASERS 85 Meeting, December 2-6, Las Vegas, 1985, and also presented an invited paper on Laser Diagnostics in Plasmas in a session on Laser Diagnostics in Fluids and Plasmas at the same meeting.

NEW DISCOVERIES STEMMING FROM RESEARCH

Saturation of an atomic transition by the intense radiation field of a suitably tuned laser represents an important kind of interaction with a wide range of potential applications. The consequences of laser resonance saturation and the applications stemming from this interaction depend to a very large extent upon the period of saturation. If the resonance to ground level populations are only momentarily locked in the ratio of respective degeneracies (saturation) the principal effect is a burst of intensified spontaneous emission that can be used to diagnose the excited medium.[1,2] On the other hand an extended period of saturation (lasting for much longer than the resonance state lifetime) can lead to extensive perturbation of the

medium.[3,4] Indeed, if the free electron superelastic collision time is short compared to the duration of the laser pulse near total ionization of the laser pumped species is rapidly achieved.[4-19] In the case of an ionic species extremely rapid changes of electron temperature can be produced by this means.[20]

The author was the first to recognize the importance of laser saturation and many of its possible areas of application.[1-4] Subsequent work in the author's laboratory and elsewhere have proven that laser resonance saturation does represent a significant form of interaction between laser radiation and atomic vapors or plasmas.

Momentary laser saturation represents a powerful diagnostic technique that is finding application in many areas ranging from fusion reactor studies[21] to combustion measurements.[22,23] The combination of laser ablation and laser saturation spectroscopy represents a new approach at evaluating fundamental atomic quantities such as: radiative lifetimes, branching ratios, transition probabilities and selected collision cross-sections. A preliminar paper on this subject was published by us in Physical Review.[24] This technique, as well as being convenient and accurate, is particularly well suited for measurements on short lived, highly ionized species created by laser ablation. Furthermore, it is versatile and can use multiphoton or stepwise excitation as the means of generating the bursts of intensified emission.

As a spin-off of this work we have also shown that this concept can also form the basis of a new form of trace element laser microprobe called a TABLASER.[25]

More recently, we have demonstrated in a proof of principle experiment that laser saturation spectroscopy can be used to directly measure, with both spatial and temporal resolution, the ion to neutral atom density ratio in a rapidly expanding ablation plasma.[26]

The ionization capabilities of extended laser resonance saturation have now been indisputably demonstrated with a variety of experiments.[5-17] We have developed a model of this "laser ionization based on resonance saturation" (LIBORS) process and have shown that the interaction can be thought to proceed in four stages.[18,19] Confirmation of certain aspects of our theory has been provided by several research groups.[5-17] Recently,

there has been some success in using laser resonance saturation for the purpose of creating infrared laser action.[27]

Recently we have developed a new form of the LIBORS computer code that enables us to gain some insight into the three dimensional nature of this interaction. The predictions of this code have been found to be in reasonable agreement with experimental measurements of the radial and axial electron density and temperature of the cylindrical plasma created by laser resonance saturation. LIBORS is currently viewed as one of the least risky methods of producing the cold lithium plasma used for ion beam generation in the Sandia National Laboratory's PBFA II.[28]

Recently, we have demonstrated that one and two photon resonant laser pumping of cold, unexcited ions formed by two photon ionization can lead to rapid excitation of high lying states of these ions (Appendix F). We believe that this approach could be used to produce intense sources of short wavelength radiation and possibly an efficient short wavelength laser. We have also shown that two photon resonant pumping of the $6^2S_{1/2}$-$5^2S_{1/2}$ forbidden transition of SrII in a cold strontium plasma can lead to parametric generation of intense radiation that is almost colinear with the pump laser beam.

REFERENCES


1. R. M. Measures, J. Appl. Phys. 39, 5232-5245 (1968).
2. R. M. Measures, Phys. of Fluids, 13, 1889-1890 (1970).
3. R. M. Measures, J. Quant. Spectrosc. Radiat. Transfer, 10, 107-125 (1970).
4. R. M. Measures, J. Appl. Phys., 48, 2673-2675 (1977).
5. T. B. Lucatorto and T. J. McIlrath, Phys. Rev. Letters, 37, 428-431 (1976).
6. T. J. McIlrath and T. B. Lucatorto, Phys. Rev. Letters, 38, 1390-1393 (1977).
7. C. H. Skinner, J. Phys. B: Atom. Molec. Phys., 13, 55-68 (1980).
8. F. Roussel, P. Breger, G. Spiess, C. Manus and S. Geltman, J. Phys. B: Atom Molec. Phys., 13, L631-L636 (1980).
9. T. Stacewicz, Optics Commun. 35, 239-241 (1980).
10. C. H. Skinner, J. Phys. B: Atom. Molec. Phys., 13, L637-L640 (1980).

11. J. Krasinski, T. Stacewicz and C. R. Stroud Jr., Optics Commun. 33, 158-162 (1980).
12. D. J. Krebs and L. D. Shearer, J. Chem. Phys., 75, 3340-3344 (1981).
13. T. Stacewicz and J. Krasinski, Optics Commun., 39, 35-40 (1981).
14. B. Carré, F. Roussel, P. Breger and G. Spiess, J. Phys. B: Atom. Molec. Phys., 14, 4289-4300 (1981).
15. B. Carré, F. Roussel, P. Breger and G. Spiess, J. Phys. B: Atom. Molec. Phys., 14, 4271-4288 (1981).
16. J. L. LeGouet, J. L. Picque, F. Muilleumier, J. M. Bizau, P. Shez, P. Koch and D. L. Ederer, Phys. Rev. Lett., 48, 600-603 (1982).
17. J. Kumar, W. T. Silfvat and O. R. Wood II, J. Appl. Phys. 53, 218-222 (1982).
18. R. M. Measures and P. G. Cardinal, Physical Review A, 23, 804-815 (1981).
19. R. M. Measures, P. G. Cardinal, G. W. Schinn, J. Appl. Phys., 52, 1269-1277 (1981) and 52, 7459 (1981).
20. R. M. Measures, P. L. Wizinowich and P. G. Cardinal, J. Appl. Phyus., 51, 3622-3628 (1980).
21. C. H. Muller and K. H. Burrell, Phys. Rev. Lett., 47, 330-333 (1981).
22. J. D. Bradshaw, N. Omenetto, G. Zizak, J. N. Bower and J. D. Winefordner, Appl. Optics, 19, 2709-2716 (1980).
23. G. B. Boutilier, N. Omenetto and J. D. Winefordner, Appl. Optics, 19, 1838-1843 (1980).
24. R. M. Measures, N. Drewell and H. S. Kwong, Phys. Rev. A, 16, 1093-1097 (1977).
25. R. M. Measures and H. S. Kwong, Appl. Optics, 18, 281-286 (1979).
26. M. R. Arnfield and R. M. Measures, Phys. Rev. A, 24, 535-539 (1981).
27. W. Muller and I. V. Hertel, Appl. Phys., 24, 33-38 (1981).
28. J. Rice, "Plasma Generation in PBFA II", First International Laser Science Conference, Nov. 18-22, 1985, Dallas, Texas.

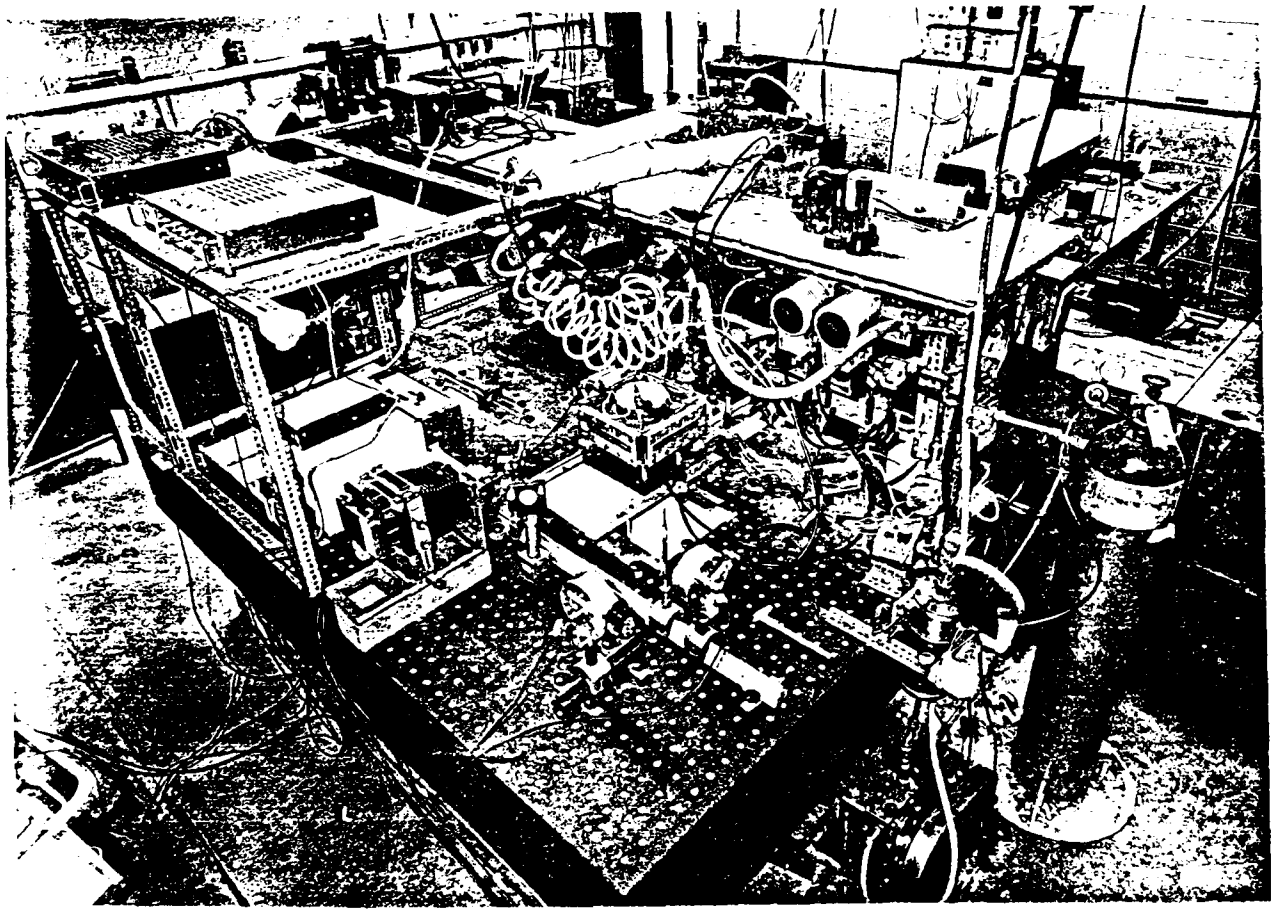

Fig. 1 Photograph of LIBORS Facility Showing the Heat Sandwich Oven and Photodetection System in the Foreground and the Nd-YAG Laser Pumped Dye Laser in the Background.

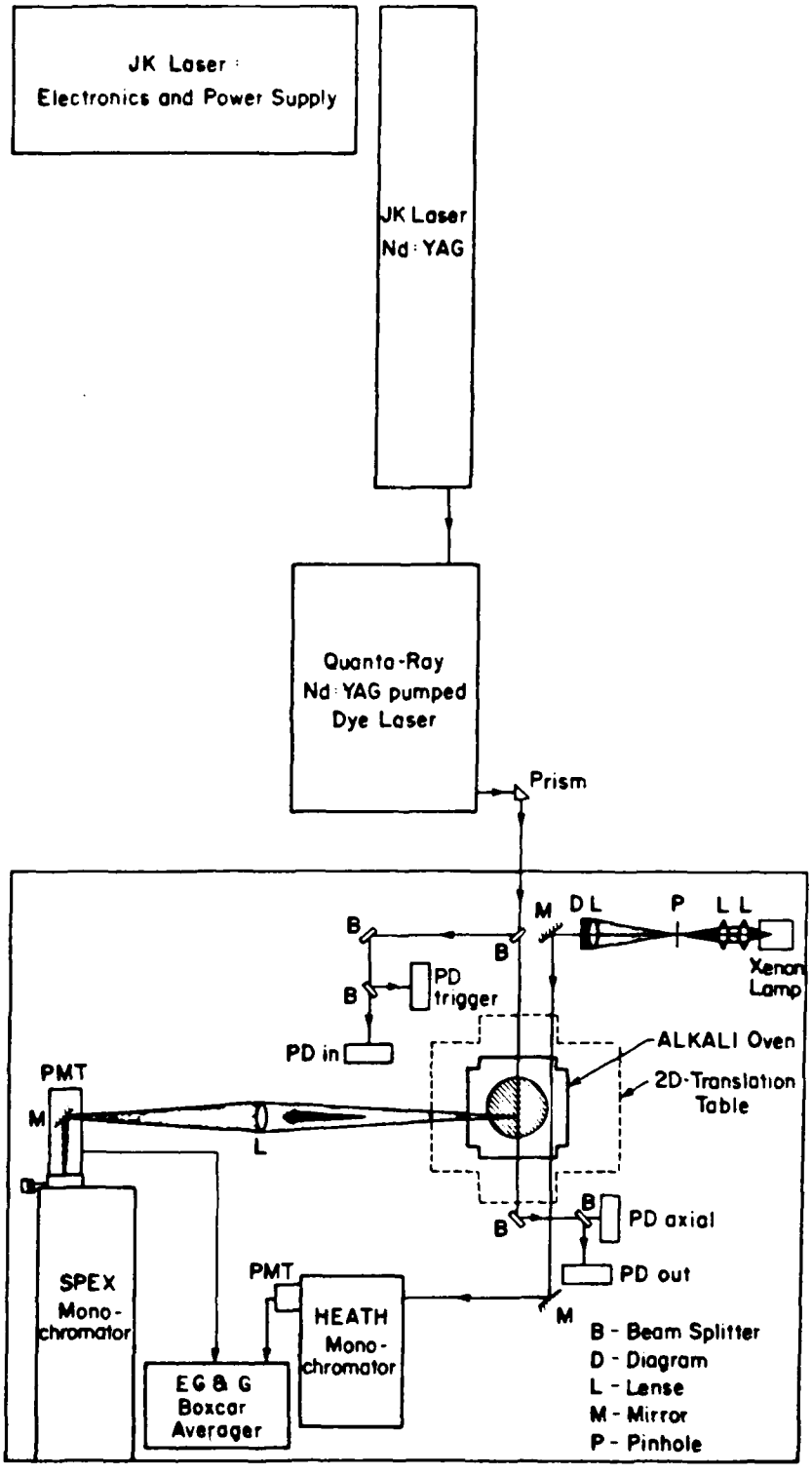


Figure 2. Schematic of LIBORS Experimental Facility.

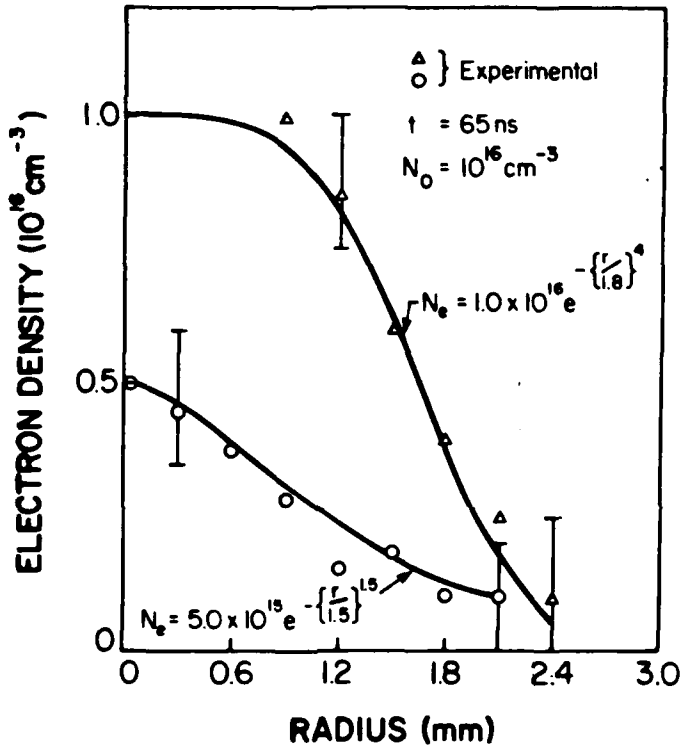


Figure 3. Free Electron Density Radial Profiles Attained at Z = -2 and 2 cm for $N_0 = 10^{16} cm^{-3}$ and t = 65ns, $E^{\ell}$=25mJ.

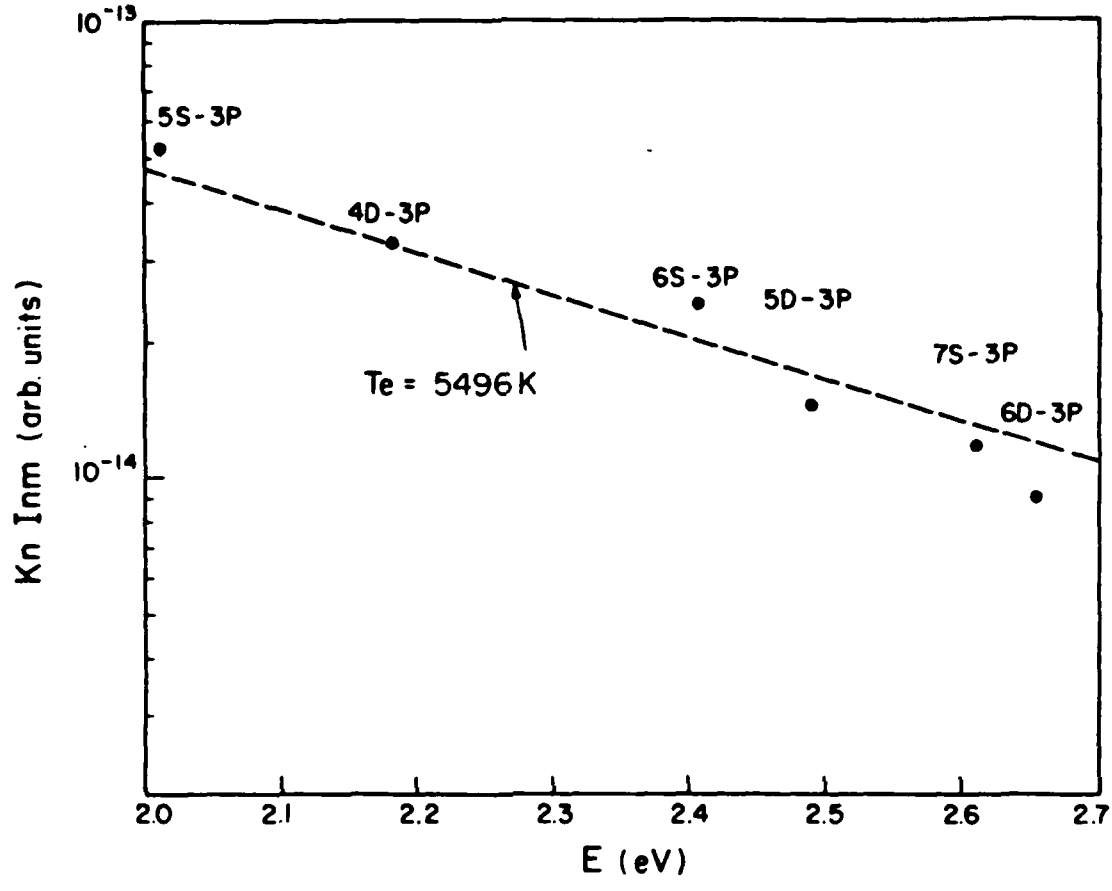


Fig. 4 Logarithmic variation of the observed emission intensity of several sodium multiplets with the energy of excitation. Also shown is the least square linear fit to the calculated data - the slope of this line gives an electron temperature of 5496 K.

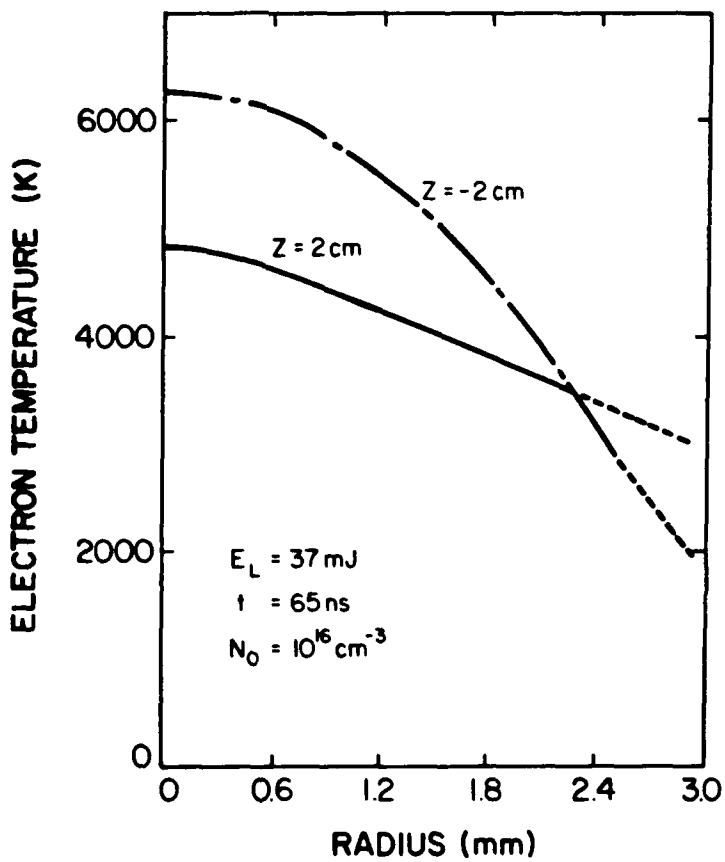


Fig. 5 Representative Free Electron Temperature Radial Profiles Deduced From the Measured Electron Density Radial Profiles Assuming LTE.

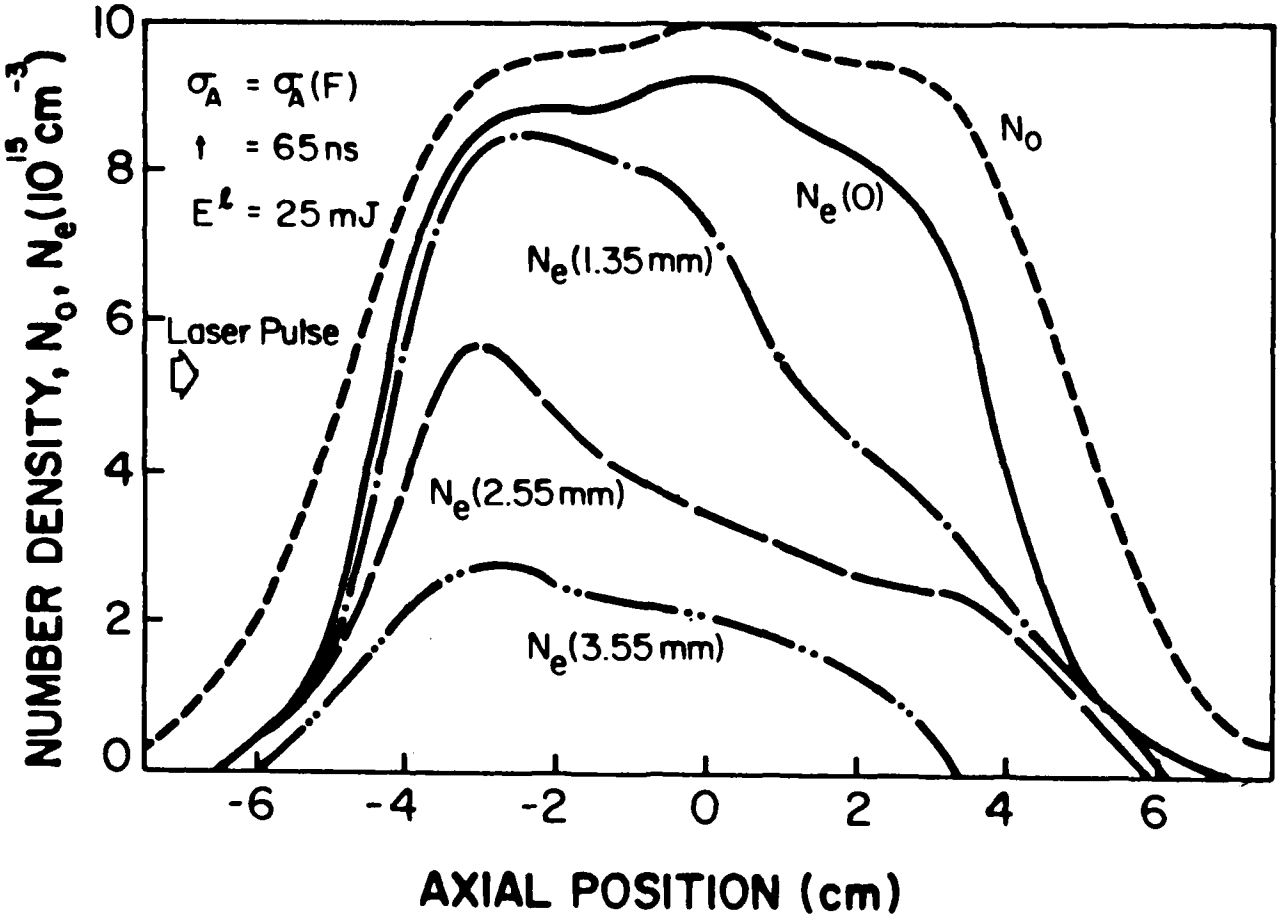


Fig. 6 Axial Variation of Free Electron Density Ne at Four Radial Positions (r = 0, 1.35, 2.55 and 3.55mm) predicted by LIBORS code at t = 65ns. Also shown is the Axial Sodium Atom Density Distribution $N_o(z)$ Used in the Computation.

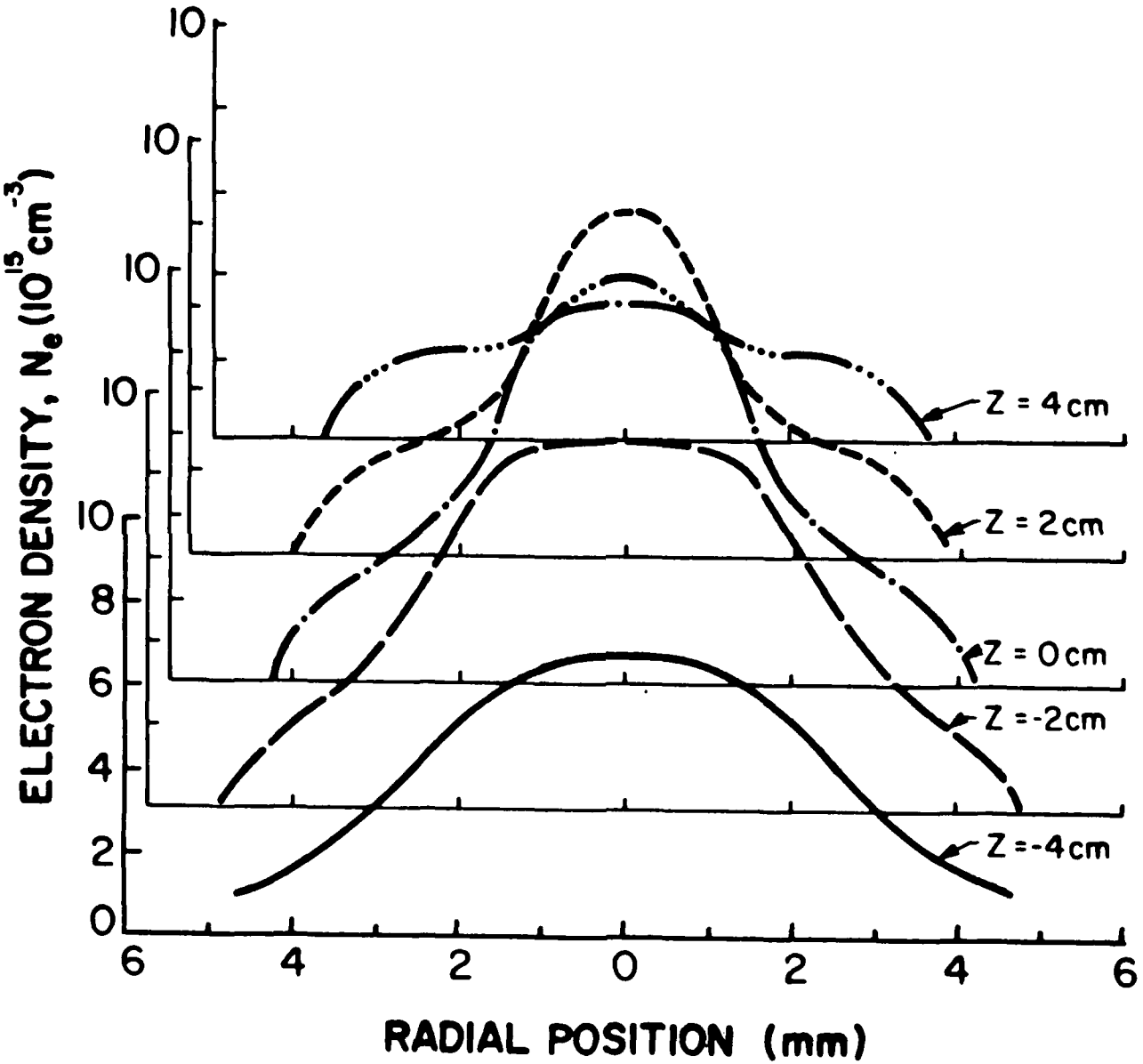


Fig. 7 Full Radial Profiles of the Free Electron Density Predicted at Five Axial Locations (Z = -4, -2, 0, 2, 4 cm) Along the Path of a 25mJ Laser Pulse, $N_O$=$10^{16}$$cm^{-3}$, t 65ns.

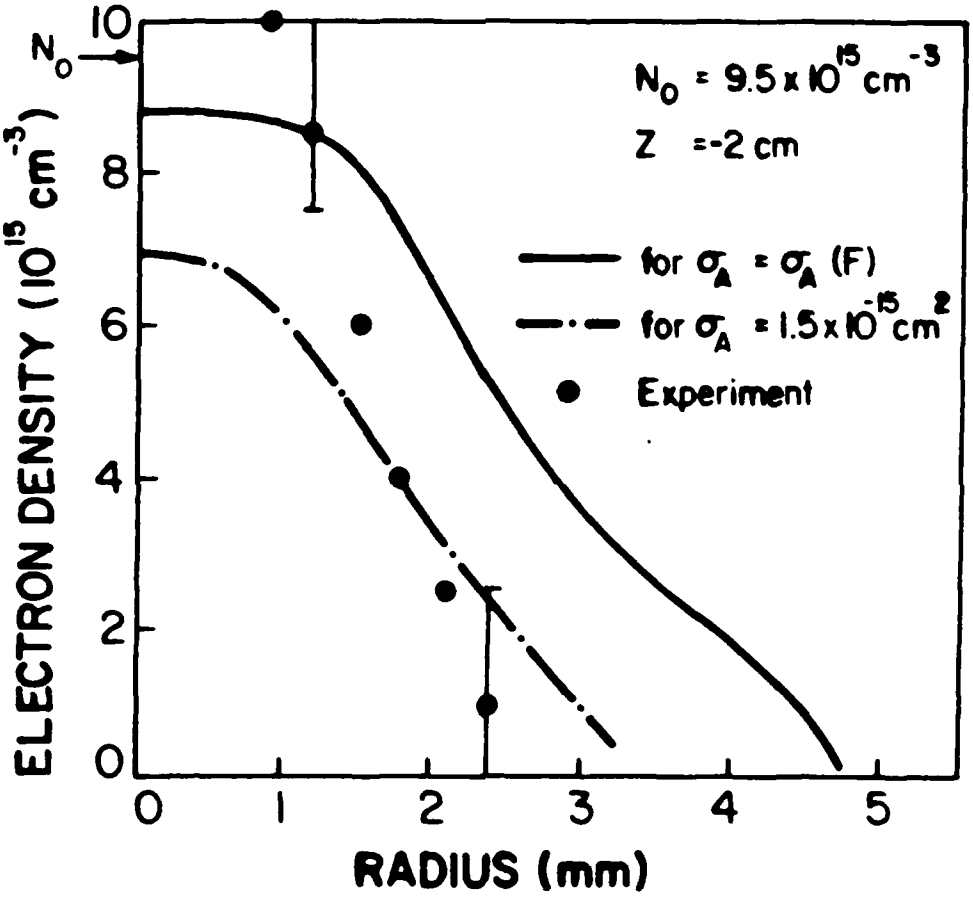


Fig. 8 Free Electron Density Radial Profile at Z = -2 cm where $N_o = 9.5 \times 10^{15}$ $cm^{-3}$ and t = 65ns as determined by: Experiment (●) and LIBORS computer code with $\sigma_A = \sigma_A(F)$ ———— and $\sigma_A = 1.5 \times 10^{-15} cm^2$ —— – ——.

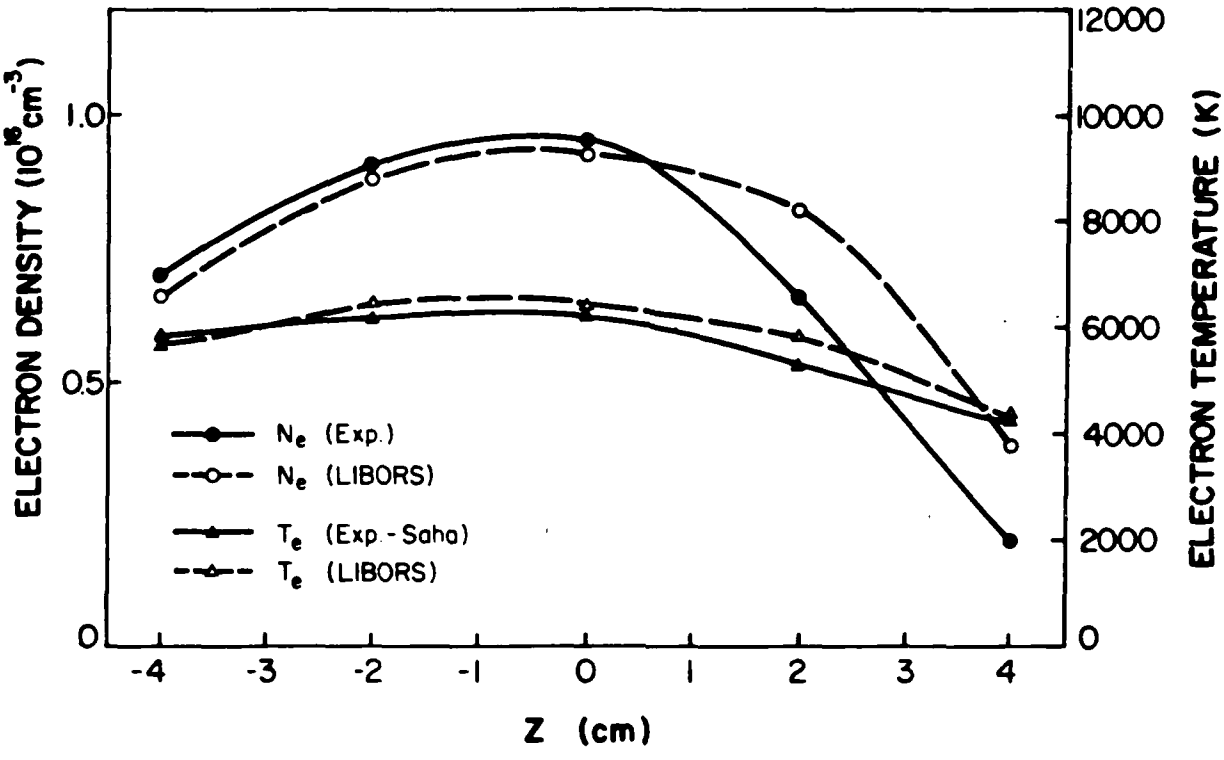


Fig. 9 Comparison of the axial variation (for r = 0) of the free electron density and temperature determined by experiment and predicted by our LIBORS computer code.

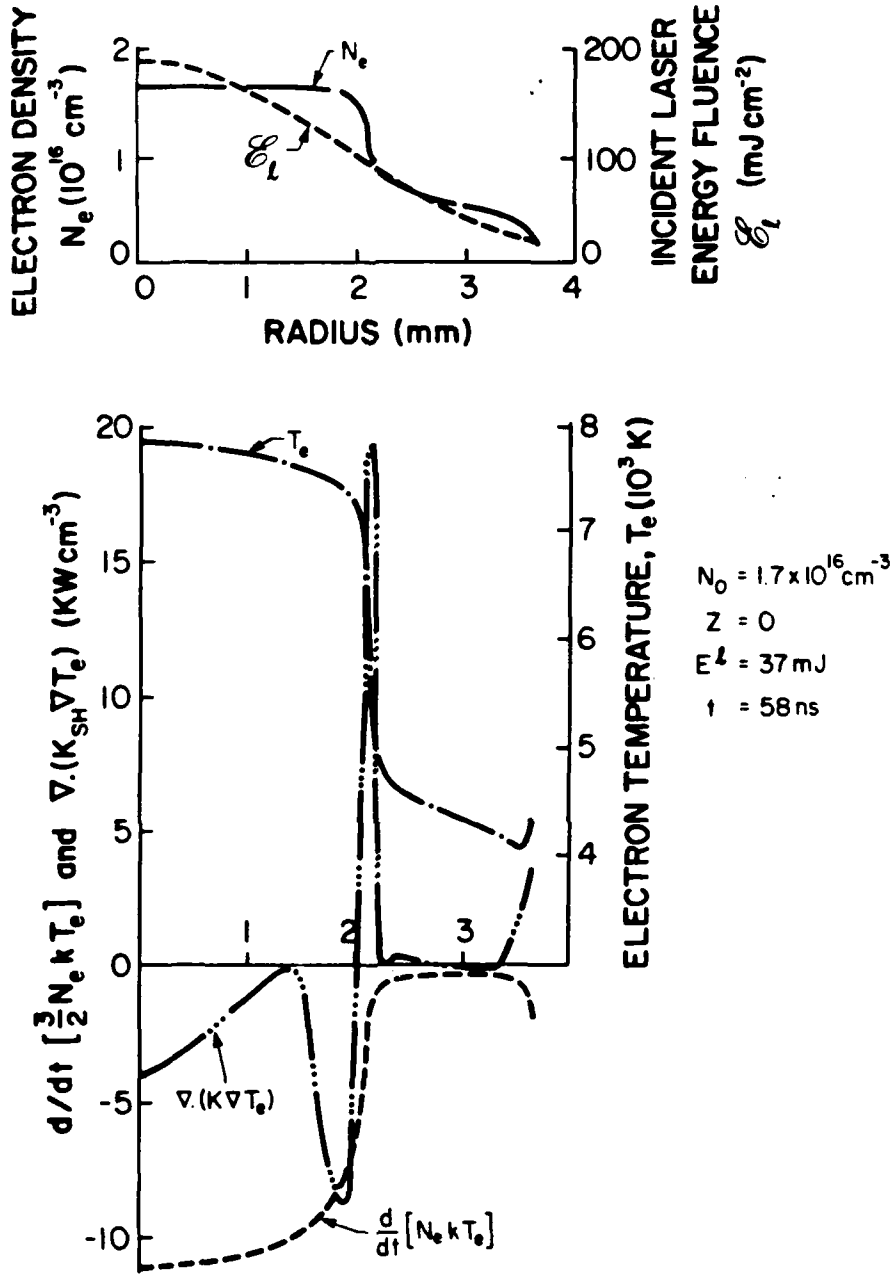


Fig. 10 LIBORS code predicted variation of the electron density, temperature, laser energy fluence, thermal conduction and rate of change of electron energy density with radius at z = 0 (where $N_0$ = $1.7 \times 10^{16} cm^{-3}$) and t = 58ns for an incident laser energy of 37mJ.

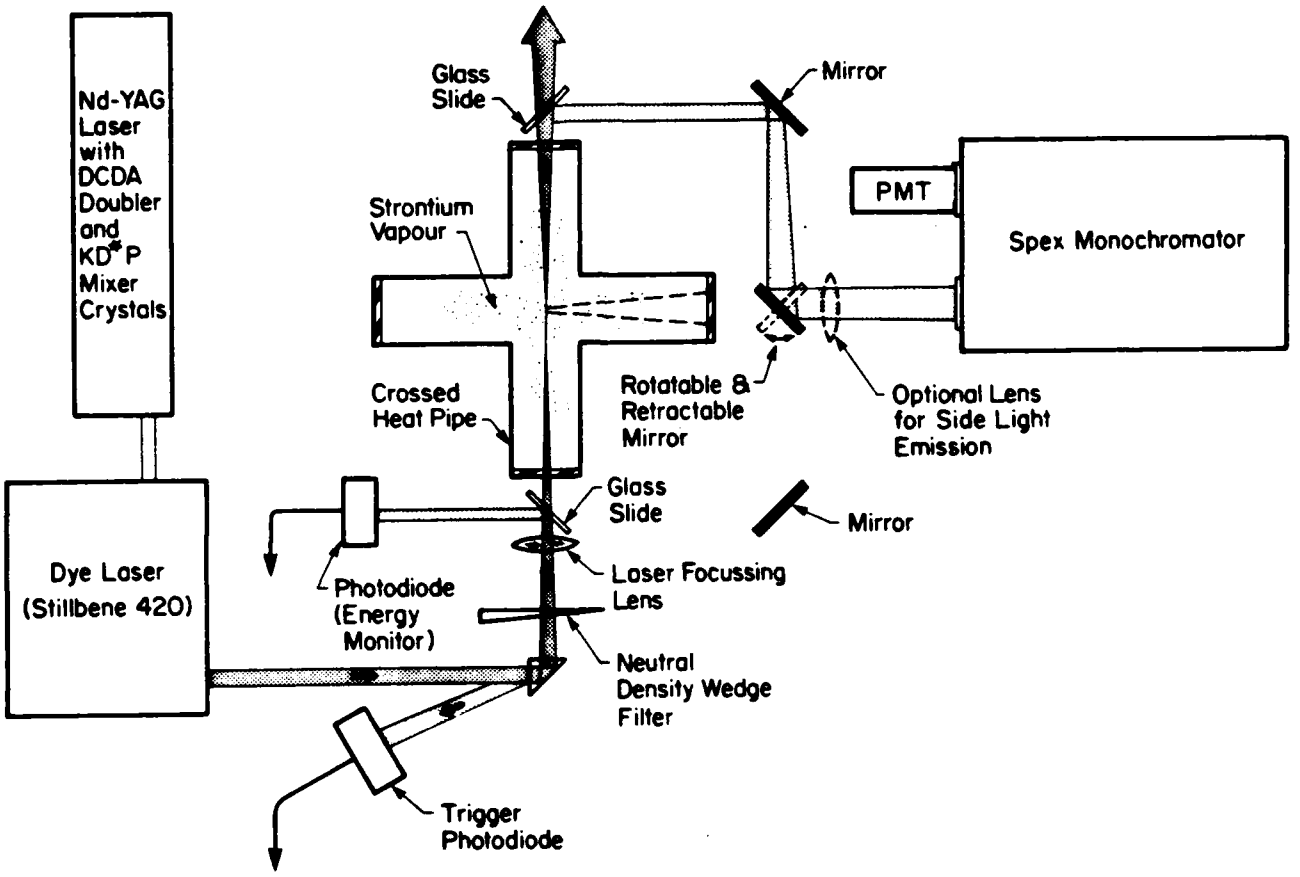


Fig. 11 Schematic View of the Strontium Multiphoton Interaction Facility.

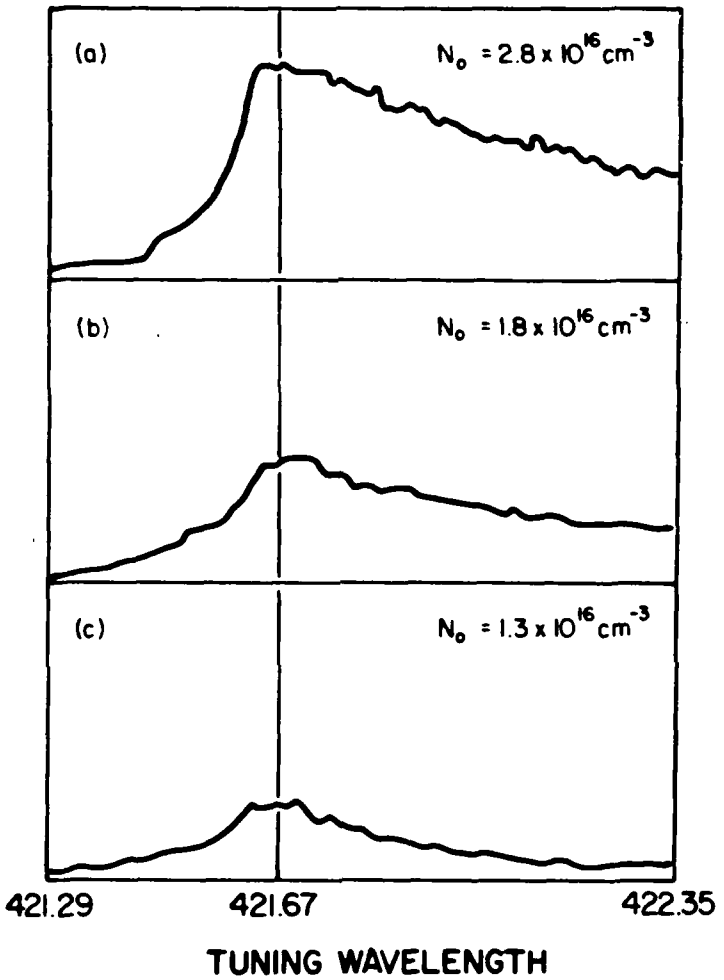


Fig. 12 Variation of Sr II ($5^2F_{5/2,7/2}$-$5^2D_{5/2}$) 565.20nm Emission from a Strontium Plasma as a Function of the Exciting Laser Wavelength for Three Values of the Initial Strontium Atom Density. Ion Resonance Line Wavelength at 421.67nm.

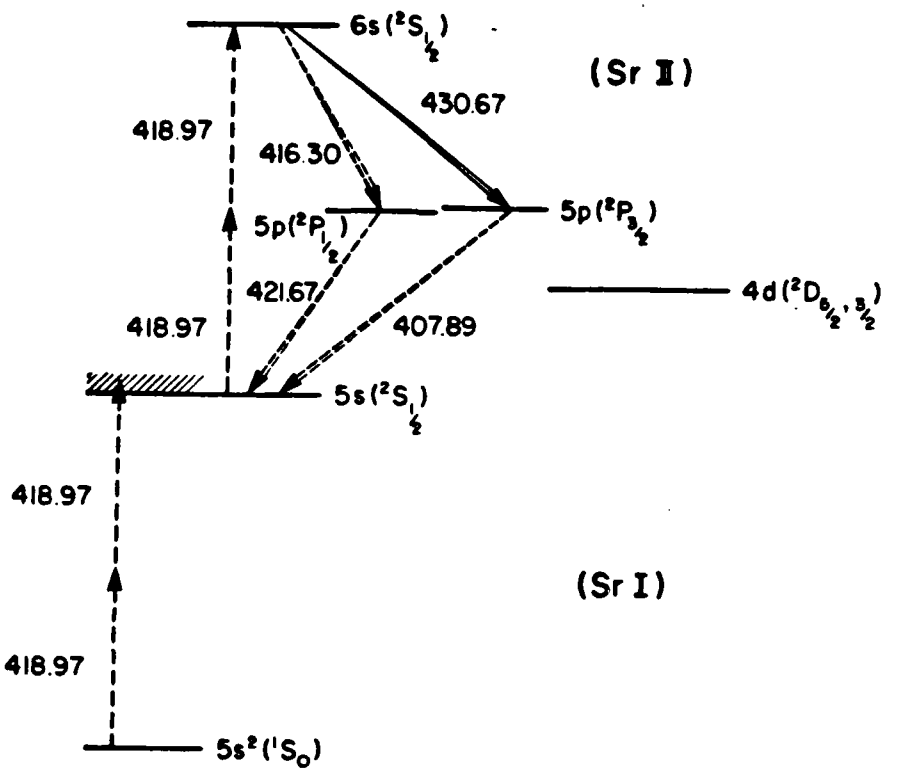


Fig. 13 Partial Grotrian energy level diagram of SrI and II.

APPENDIX A

# Sodium atom distribution within a heat sandwich oven

M. A. Cappelli, P. G. Cardinal, H. Herchen, and R. M. Measures

*Institute of Aerospace Studies, University of Toronto, 4925 Dufferin Street, Downsview, Ontario, M3H 5T6 Canada*

(Received 5 July 1985; accepted for publication 5 August 1985)

In a heat sandwich oven the metal vapor is confined to be disk shaped and is optically accessible through 360° in the plane of the disk. We have used this feature to optically measure the radial atom density distribution of sodium vapor within this type of oven, under a range of conditions. In particular, we have observed the formation of a donut-shaped atom density distribution when the heat sandwich oven is operated at high temperatures with an under pressure of the argon buffer gas.

## INTRODUCTION

Alkali metal vapors are highly reactive and, in the absense of adequate precautions, can quickly spoil the windows of any containment vessel built for optically studying them. One method of minimizing this degradation is to interpose a cooled inert buffer gas between the hot vapor and the windows. Vidal and Cooper[1] first demonstrated that a combination of the *heat pipe* concept with a buffer gas not only protected the windows but led to the formation of a well-defined column of the vapor.

The limited optical access of this system was overcome by Boyd *et al.*[2] who proposed a sandwich-like oven in which the vapor was trapped between two flat disk-shaped wire mesh wicks that were heated in their center and cooled around their periphery. This design leads to the creation of a disk-shaped region within the oven and to 360° optical access in the plane of the disk.

## I. HEAT SANDWICH OVEN

We have designed and built our own *heat sandwich oven* for undertaking experiments involving laser ionization of sodium vapor based on resonance saturation.[3–5] Our design differs from that of Boyd *et al.*[2] in two ways: We use a rectangular frame, which permits us to view the laser produced plasma channels through optically flat windows and we have introduced a circular thermal expansion buckle to relieve the radial stress in each of the heated plates. A cross-sectional view of one half of this heat sandwich oven is presented as Fig. 1. The axis of symmetry corresponds to the extreme right of Fig. 1. A photograph of the heat-sandwich oven illuminated by the ionizing laser pulse is shown as Fig. 2. The narrow sodium plasma channel created by this laser is clearly visible through the front window.

The basic frame of the system is constructed of stainless steel (type 304) and is held close to room temperature by circulating water through the cooling coils indicated in Fig. 1. The upper and lower wicks (required for heat pipe action) are made of three layers of stainless steel type 60 mesh (0.152-mm wires) and are secured to the heater plates (high-grade stainless steel–type 316) by a large number of small screws and to the cold lip by a ring. The rectangular viewports were each 20 cm × 3 cm in size and the heat sandwich walls had O-ring grooves cut into them in order to provide a seal for the windows.

Operation is commenced by pumping down the argon pressure until it is just below the sodium partial pressure required for a given experiment. The sodium is then heated

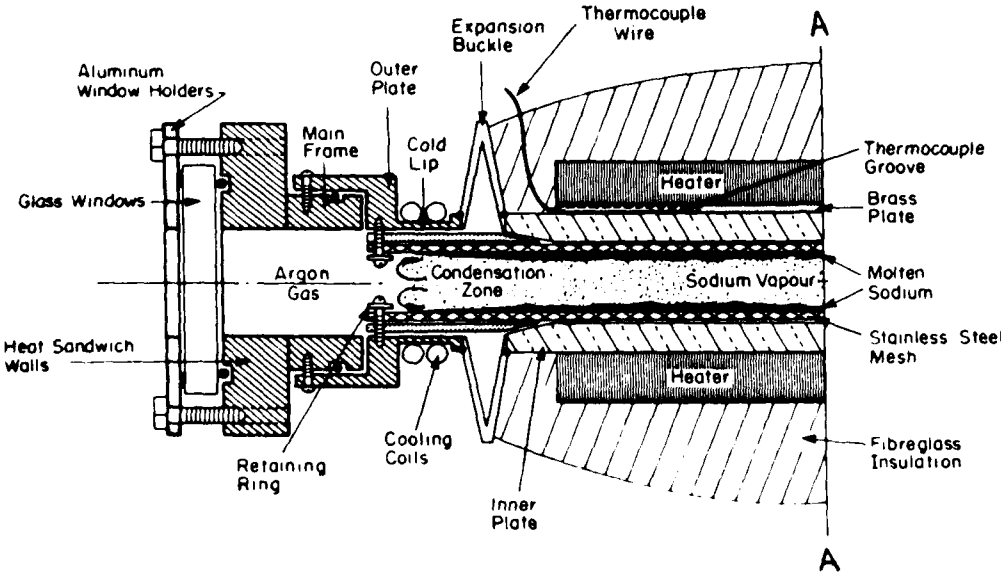


FIG. 1. Cross-sectional view of the Na heat sandwich oven (symmetric about A-A).

 0034-6748/85/112030-08$01.30  

FIG. 2. Photograph of sodium plasma created by laser resonance saturation within the heat sandwich oven.

until it melts, whereupon its vapor pressure increases and the resulting radial flow of the sodium atoms effectively pumps the argon into the cool outer region of the oven. An essential feature of this heat pipe action is the radially inward flow (from cold to hot) of the liquid sodium due to the capillary forces in the wicks. It should be noted that an overpressure of the buffer gas leads to an observed drop in the vapor pressure of the sodium for under these conditions the argon is able to permeate the hot core of the oven and thereby transfer energy from the hot vapor to the cool boundary region.

Although thermocouple temperature sensors were employed, it was felt that they could at best only provide a rough estimate of the sodium atom density using the empirical fit of Nesmeyanov,[6]

$$\log_{10} N = 29.84904 - 5619.4106/T - 2.04111 \log_{10} T + 3.45\times 10^{-6} T. \quad (1)$$

As one can see from Fig. 1, the thermocouple wires were placed just beneath the heaters. Temperature readings from the thermocouples may not necessarily reflect that of the liquid sodium within the heat sandwich wick, which actually determines the vapor pressure. In order to determine the sodium atom distribution across the oven we decided to employ the absorption measurement technique to be described below.

## II. SODIUM ATOM DENSITY MEASUREMENT TECHNIQUE

The spectral irradiance $I(\nu, l)$ of a well-collimated beam of radiation of frequency $\nu$ propagating in the $z$-direction through a vapor of length $l$ can be related to the incident spectral irradiance $I(\nu, 0)$ by the Beer–Lambert law.

$$I(\nu, l) = I(\nu, 0)\exp\left(-\int_0^l k(\nu, z)dz\right), \quad (2)$$

where $k(\nu, z)$ represents the volume absorption coefficient. In the event that $\nu$ is close to the resonance doublet $(3^2P - 3^2S)$ of sodium we can write

$$\kappa(\nu, z) = \frac{\lambda^2}{8\pi} N(J', z) \sum_{i=1}^{2} A(J_i, J') \mathcal{L}(J_i, J', \nu, z), \quad (3)$$

where $N(J', z)$ represents the population density (at a depth $z$ into the vapor) of the lower level having a total angular momentum quantum number $J'$ ($J' = 1/2$ for sodium), $A(J_i, J')$ represents the Einstein transition probability for the $J_i$ to $J'$ transition of the doublet (where $J_2 = 3/2$ and $J_1 = 1/2$ for the resonance doublet of sodium), $\mathcal{L}(J_i, J', \nu, z)$ is the corresponding line profile function, and $\lambda$ represents the mean wavelength of the doublet.

If we treat the absorption as arising from a single line with an "effective" line profile function, $\mathcal{L}(\nu, z)$ we can write

$$\kappa(\nu, z) = \frac{\lambda^2}{8\pi} N(J', z)[A(J_1, J') + A(J_2, J')]\mathcal{L}(\nu, z), \quad (4)$$

where

$$\mathcal{L}(\nu, z) = \zeta(J_1, J')\mathcal{L}(J_1, J', \nu, z) + \zeta(J_2, J')\mathcal{L}(J_2, J', \nu, z). \quad (5)$$

In this instance $\zeta(j_i, J')$ and $\mathcal{L}(J_i, J', \nu, z)$ represent the "fractional line strength" and "line profile function" of the $J_i$ to $J'$ transition of the doublet, respectively.

For the sake of brevity we introduce the simpler notation

$$\mathcal{L}_i(\nu) = \mathcal{L}(J_i, J', \nu, z)$$

and

$$A_i = A(J_i, J') \quad \text{for } i = 1 \text{ or } 2.$$

Also

$$N(z) = N(J', z).$$

It should be recognized that the use of Eq. (2) implies that the radiation is well below the saturated value[7] and that scattering is negligible.

At the 600–800 K temperature range corresponding to the $10^{15}$ to $10^{17}$ cm$^{-3}$ sodium atom density within the heat sandwich oven both Doppler and resonance broadening have to be considered. Under these circumstances the resultant resonance D-line absorption profile function is a convolution of the corresponding Gaussian (Doppler) and resonance broadened profiles, that is to say

$$\mathcal{L}_i(\nu) = \frac{1}{\beta_i \pi^{1/2}} \int_{-\infty}^{\infty} d\nu^* e^{-(\nu_i - \nu^*)^2/\beta_i^2} \mathcal{L}_i^R(\nu - \nu^*), \quad (6)$$

where $\nu_i$ represents the $i$th line center frequency, $\mathcal{L}_i^R(\nu)$ the resonance broadened atomic line profile, and $\beta_i$ the Gaussian width, given by the relation

$$\beta_i = (2kT\nu_i^2/mc^2)^{1/2}. \quad (7)$$

In this equation $k$ and $c$ have their usual meaning, $T$ is the translational temperature, and $m$ is the mass of the sodium atom.

### A. Resonance broadened line shape

The core of the resonance broadened atomic line profile, when calculated using the impact approximation (Appendix), can be described in the case of the sodium atom by a Lorentzian with half-width at half-maximum (HWHM)[8]

$$^{c}\Gamma_2 = (1.47e^2 f_2/4\pi\nu_2 m_e)(\mathrm{Hz}) \quad \text{for } (3^2S_{1/2} - 3^2P_{3/2})$$

and (8)

$$^{c}\Gamma_1 = (1.805e^2 f_1/4\pi\nu_1 m_e)(\mathrm{Hz}) \quad \text{for } (3^2S_{1/2} - 3^2P_{1/2}),$$

where $f_i$ and $\nu_i$ are the oscillator strength and line center frequency for the $i$th transition and $m_e$ and $e$ being the mass and charge of the electron, respectively.

Srivastava and Zaidi[9] have shown that the line wings of the resonance broadened profile can also be described by a Lorentzian with HWHM (when calculated using the quasi-static approximation)

$$^{w}\Gamma_i = \tfrac{2}{3}{}^{c}\Gamma_i , \tag{9}$$

where the superscripts $w$ and $c$ denote the line "wing" and line "core," respectively. The above two references assume that the broadening of the $3^2P$ state is dominated by the resonant dipole–dipole interaction with ground state sodium atoms.

We have chosen to use an empirical fit to the line profile of the form[10]

$$\mathcal{L}_i^R(\nu) = C_i\left(\frac{1}{\pi^{c}\Gamma_i}\frac{\exp\{-[(\nu-\nu_i)/{}^{c}\Gamma_i]^2\}}{1+[(\nu-\nu_i)/{}^{c}\Gamma_i]^2} + \frac{1}{\frac{2}{3}\pi^{c}\Gamma_i}\frac{1-\exp\{-[(\nu-\nu_i)/{}^{c}\Gamma_i]^2\}}{1+\frac{9}{4}[(\nu-\nu_i)/{}^{c}\Gamma_i]^2}\right), \tag{10}$$

which approaches the exact behavior in the core and wings [$\nu=\nu_i$ and $(\nu-\nu_i)/{}^{c}\Gamma_i \gg 1$, respectively] and resembles the numerical solution in the intermediate region.[9] $C_i$ is the normalization constant

$$C_i = 1.126/\pi , \tag{11}$$

which ensures

$$\int_{-\infty}^{\infty} \mathcal{L}_i^R(\nu)d\nu = 1 . \tag{12}$$

Upon substitution of Eq. (10) into Eq. (6), one obtains three integrals which all involve some form of the Voigt integral

$$W(u,\eta) = \frac{1}{\pi^{3/2}\eta}\int_{-\infty}^{\infty}\frac{e^{-(y^2/\eta^2)}}{1+(u-y)^2}dy . \tag{13}$$

We have chosen to use the approximation of Whiting[11] for $W(u,\eta)$,

$$W(u,\eta) = \left[\left(1-\frac{2}{w_i}\right)\exp\left(-2.772\frac{u^2}{w_i^2}\right) + \frac{2}{w_i}\frac{1}{(1+4u^2/w_i^2)}\right] \Big/ \left\{\frac{\sqrt{\pi}w_i}{2}\left[\left(1-\frac{2}{w_i}\right)\sqrt{\ln 2} + \frac{2\sqrt{\pi}}{w_i}\right]\right\}^{-1}, \tag{14}$$

with

$$w_i = 1 + (1+4\eta^2\ln 2)^{1/2} \tag{15}$$

and

$$\int_{-\infty}^{\infty} W(u,\eta)du = 1. \tag{16}$$

### B. Correction for finite instrument resolution

In our experiments a Heath scanning monochromator was employed to determine the spectral characteristics of the transmitted radiation. For this kind of monochromator, where the entrance and exit slits are comparable, the spectral transmission function $T(\nu_T-\nu)$ is well approximated by a Guassian profile and we can write

$$T(\nu_T-\nu) = (1/\gamma_T\pi^{1/2})e^{-(\nu-\nu_T)^2/\gamma_T^2}, \tag{17}$$

where $\nu_T$ is the frequency of peak transmission and

$$\gamma_T = \delta_T/(\ln 2)^{1/2}. \tag{18}$$

Here $\delta_T$ is the instrument's HWHM bandwidth corresponding to a given slit setting and can be expressed in terms of the slope $b_T$ and intercept $a_T$ of the linear relation between the observed HWHM bandwidth of an extremely narrow spectral line and the monochromator slit width $S_T$,

$$\delta_T = a_T + b_T S_T . \tag{19}$$

The observed spectral irradiance at frequency $\nu$ can thus be written in the form

$$\mathcal{S}(\nu,l) = \int_{-\infty}^{\infty} I(\nu^*,l)T(\nu-\nu^*)d\nu^* , \tag{20}$$

or using Eqs. (2) and (17) and assuming broadband incident radiation so that $I(\nu,0)\approx I(0)$, then the spectral profile

$$\mathcal{G}(\nu,l) \equiv \mathcal{S}\frac{(\nu,l)}{I(0)} = \frac{1}{\gamma_T\pi^{1/2}}\int_{-\infty}^{\infty}\exp\left(-\int_0^l k(\nu^*,z)dz - \frac{(\nu-\nu^*)^2}{\gamma_T^2}\right)d\nu^* \tag{21}$$

can be solved using Eqs. (4)–(6) and (10) with a quadrature routine. For our work, the slit width $S_T$ was 150 $\mu$m and the experimentally determined values for $a_T$ and $b_T$ are provided with other parameters of relevance in Table I.

To evaluate the atom density distribution it is necessary to undertake a series of measurements. The sodium vapor disk is assumed to be divided into a number of equally spaced rings of constant density (see Fig. 3) and the absorption is evaluated for a series of chords that intercept an increasing number of these rings. Reference to Fig. 3 reveals that the element of path length

TABLE I. Parameters of relevance in sodium atom density measurement

| | |
|---|---|
| $\nu_2 = 5.093\times10^{14}\ \mathrm{s}^{-1}$, | $\lambda_2 = 589.0$ nm |
| $\nu_1 = 5.088\times10^{14}\ \mathrm{s}^{-1}$, | $\lambda_1 = 589.6$ nm |
| $A_2 = 6.30\times10^{7}\ \mathrm{s}^{-1}$ | |
| $A_1 = 6.28\times10^{7}\ \mathrm{s}^{-1}$ | |
| $\xi_2 = 2/3$ | |
| $\xi_1 = 1/3$ | |
| $^{c}\Gamma_2$ | $3.81\times10^{-8} N_1(\mathrm{cm}^{-3})\ \mathrm{Hz}$ |
| $^{c}\Gamma_1$ | $2.34\times10^{-8} N_1(\mathrm{cm}^{-3})\ \mathrm{Hz}$ |
| $a_T$ | $3.44\times10^{8}\ \mathrm{s}^{-1}$ |
| $b_T$ | $4.45\times10^{8}\ \mathrm{s}^{-1}\mu\mathrm{m}^{-1}$ |

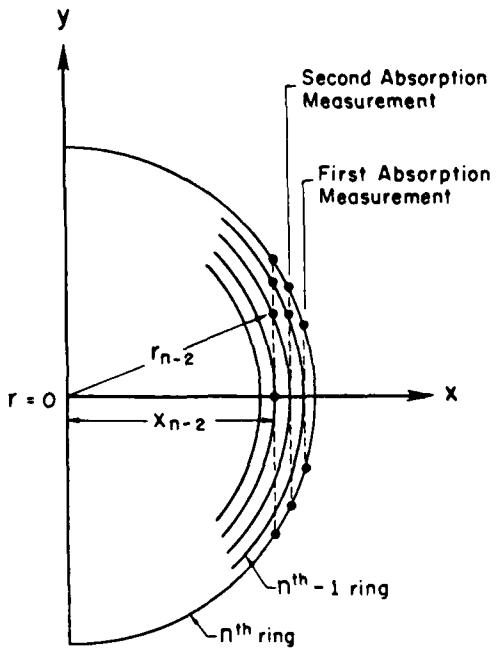


FIG. 3. Schematic diagram illustrating the rings of constant density into which the sodium vapor disk is divided for the purpose of determining the radial density distribution.

$$l_{mn} = (r_{n+1}^2 - x_m^2)^{1/2} - (r_n^2 - x_m^2)^{1/2}, \tag{22}$$

where $x_m$ is the $x$ displacement of the $m$th-measurement chord and $r_n$ the radius of the $n$th-density ring. The total optical depth for the $m$th-chord

$$\tau(\nu^*, x_m) = 2 \sum_{n=1}^{n=n_{max}} \kappa_n(\nu^*) l_{mn}, \tag{23}$$

where

$$\kappa_n(\nu^*) = (\lambda^2/8\pi)\, N(r_n)(A_1 + A_2)\mathcal{L}^n(\nu^*) \tag{24}$$

represents the absorption coefficient for the $n$th ring of atom density $N(r_n)$ and $\mathcal{L}^n(\nu^*)$ the relevant total absorption profile for the sodium D doublet, as given by Eq. (5). In order to evaluate the Doppler contribution to $\mathcal{L}^n(\nu^*)$ for each ring the temperature is assumed to be related to the atom density $N(r_n)$ of that ring through the equilibrium relation given earlier as Eq. (1).

The density for the $n$th ring is then guessed and the appropriate absorption spectrum calculated; this is then compared with the corresponding experimentally determined spectrum. The assumed density is then adjusted until reasonable agreement is obtained. The average density of the $n$th ring is then approximately known and is used in conjunction with a slightly higher density for the two segments of the next ring required to compute the absorption spectrum expected for the second chord. The density of this second ring is then adjusted until reasonable agreement is obtained between the calculated spectrum and that measured. This series of calculations and comparisons with the measurements is continued towards the center of the heat sandwich oven leading to an effective radial density profile for the sodium vapor.

Reasonable agreement is obtained when the full-width at half-maximum (FWHM) of the predicted absorption spectrum closely matches that measured well within the limit of instrument resolution (see top inset of Fig. 5). When the sodium doublet is clearly resolvable (usually for $x \gtrsim 5$ cm), we used the absorption at line center of the $3^2P_{3/2} - 3^2S_{1/2}$ transition as our matching condition (see lower inset of Fig. 5). It should be noted that best results were obtained when preliminary smoothing of the data was performed. The FWHM of the absorption spectrum was fit to a polynomial in position $x$ of the form

$$P(x) = (\alpha_1 + \alpha_2 x^2 + \alpha_3 x^4) \exp(-\alpha_4 x^2), \tag{25}$$

where $\alpha_i$ $(i = 1\text{–}4)$ represents the various fitting parameters. The variation of the transmission at line center of the $D_2$ line with position $x$ was approximated by a straight line. Data from these two curves were then directly used in the density reconstruction routine.

## III. EXPERIMENTAL ARRANGEMENT AND RESULTS

The facility for measuring the sodium atom distribution comprised a broadband xenon light source, an aperture and collimating optics, the heat sandwich oven, a Heath model EU-700 scanning grating (1180 lines/mm, $f/6.8$, 35-cm focal length) monochromator, and an RCA type 1P28 photomultiplier. A schematic of the optical arrangement is presented as Fig. 4. The diameter of the probe beam of continuum radiation was set to about 0.3 cm by the stop S.

An example of the variation of the FWHM and $D_2$ line center transmission with position $x$ is presented as Fig. 5. The two insets display two representative absorption pro-

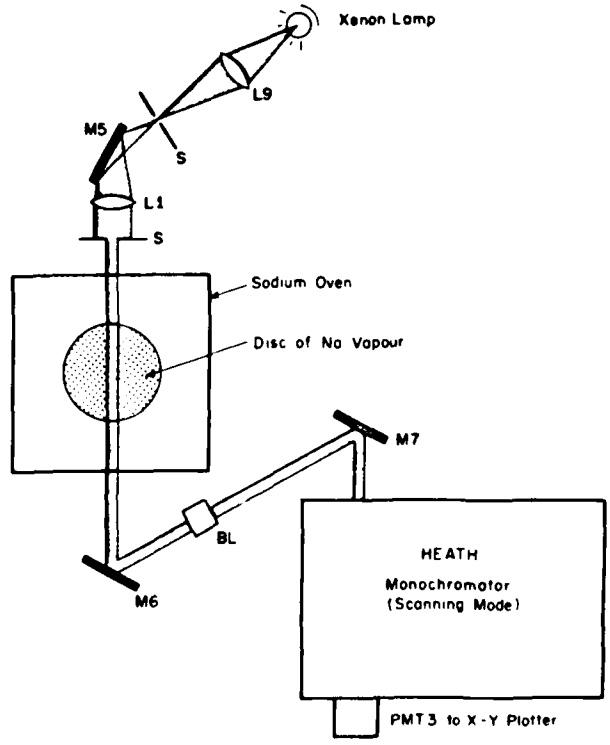


FIG. 4. Facility for determining the sodium vapor density by means of measuring the absorption spectrum. The lenses are designated L, aperture S, pinhole PH, and mirrors M.

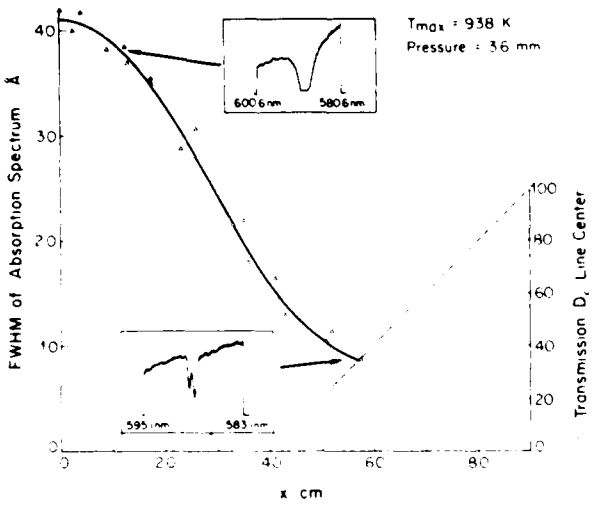


FIG. 5. Variation of the full-width half-maximum (solid line) and $D_2$ line center transmission (dashed line) with position X. In this run the argon pressure was about 3.6 mm of mercury and the maximum temperature was 938 K. The two insets display examples of the absorption spectrum measured for a chord passing through the core of the vapor disk and one passing through the low-density rim.

files, one corresponding to a path close to the center of the oven the other in the low-density rim of the vapor disk. In the latter the absorption arising from the two sodium D lines is evident, while in the former the optical depth is so great that only one wide spectral hole is apparent. The corresponding radial density distribution of sodium atoms within the heat sandwich oven is presented as Fig. 6. This distribution was determined from a series of absorption measurements in accordance with the technique described earlier. The maximum temperature registered by the thermocouple near the oven center was 938 K, which would suggest a peak density considerably larger than that measured. Mechanical equilibrium between the argon buffer gas and sodium vapor was ensured by continuously monitoring and adjusting the buffer gas pressure to match the sodium vapor pressure at the center of the heat sandwich oven.

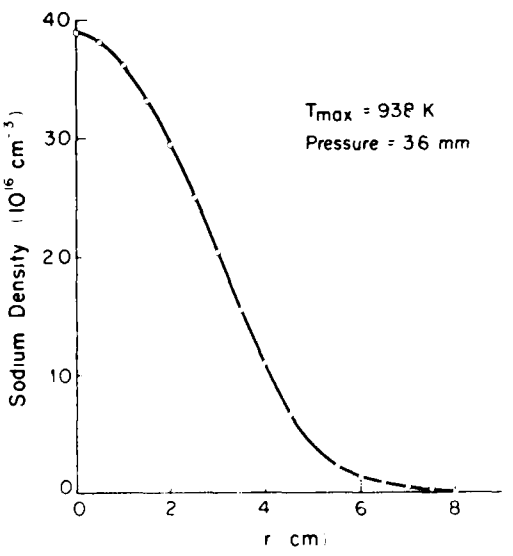


FIG. 6. Sodium atom density distribution within the heat sandwich oven (corresponding to the data of Fig. 5) determined by absorption and the deconvolution technique described in the text.

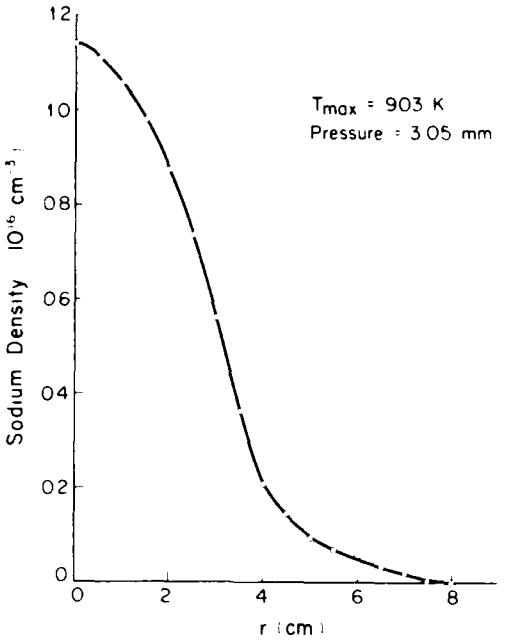


FIG. 7. The sodium atom distribution measured within the heat sandwich oven for an argon pressure of 3.05 mm of mercury and a maximum temperature of about 903 K.

An important observation to be drawn from this density profile is that the radial atom distribution proceeds to fall by an order of magnitude over the first 4 cm of radius. A similar result was obtained when the oven was operated at a lower temperature such that the peak sodium density was about a factor of 3 less than indicated for the case shown in Fig. 6. The atom density distribution in this instance is presented in Fig. 7.

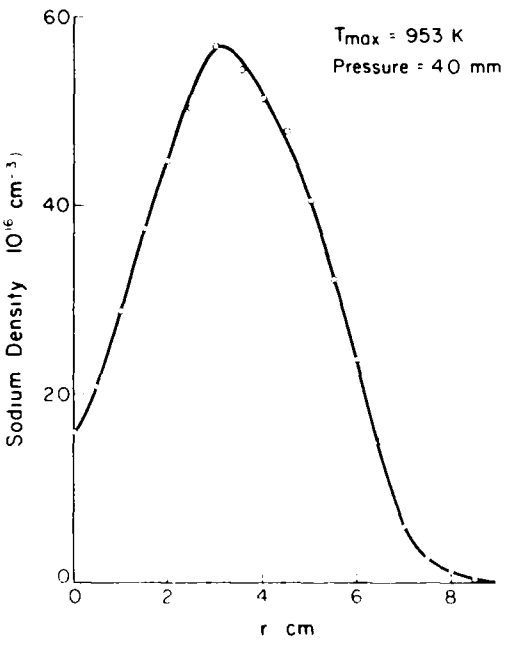


FIG. 8. The sodium atom distribution measured within the heat sandwich oven for an argon pressure of 4.0 mm of mercury and a maximum temperature of about 953 K.

These results are to some extent in keeping with the analysis of Vidal[12] and Boyd and Dodd[13] who suggests that substantial variations of density are possible in heat-pipe systems as a result of the large flow velocities that can be established.

We have found that operation of the heat sandwich oven for an extensive period of time ($\gtrsim 10$ h) at relatively high temperatures, with an underpressure of argon gas, leads to a "donut"-shaped distribution of sodium vapor. Figure 8 displays such a distribution. We believe that this arises from too great a heater power combined with too low a buffer gas pressure. Under these conditions, large radial flow velocities were established and the sodium was found to condense and solidify beyond the region of the wick, resulting in a loss of sodium and a gradual reduction in the amount available to fill the heated volume. In time, the center of the wick dries out and any liquid sodium which migrates inwards from the condensation zone as a result of the capillary action would evaporate before reaching the oven center. We assume that under these circumstances a pressure balance is maintained by the formation of an argon bubble in the center of the heat sandwich oven.

These surprising results suggest that operation of the oven in a heat pipe mode requires a continuous monitoring of both the vapor density distribution and buffer gas pressure. Periodic adjustment of the buffer gas pressure may be necessary to avoid the creation of this donut-like distribution.

We estimate the accuracy of the atom density measurements presented here to be within $\pm 20\%$. This is primarily determined by the uncertainty in the half-width of the resonance broadened atomic absorption profile. The theoretical values by Carrington *et al.*[8] used here agree fairly well with the experimental measurements of Huennekens and Gallagher[14] which were estimated to have an error of no more than $\pm 15\%$. We have found that in the density regions of interest, there is at most a direct relationship between the percentage change in the half-width of the atomic absorption profile and the percentage change in the peak atom density evaluated.

Secondary sources of error are contributions to the atomic line profile due to van der Waals interactions (Appendix), as well as fluctuations in the oven temperature ($\pm 5$ K leading to $\approx 10\%$ density variation) during the series of measurements. There was no noticeable change in the output of the xenon lamp between each scan. Currently we are attempting to reduce the uncertainty as a result of temperature fluctuations by making these density measurements in a much shorter time.

## ACKNOWLEDGMENTS

Financial support for this research was provided by the United States Air Force Office of Scientific Research under Grant No. 85-0020 and the Natural Science and Engineering Research Council of Canada.

## APPENDIX

If absorption of a photon by an atom takes place during a collision of that atom with another atom (perturber), then the transition can be thought of as occuring between two quasimolecular states formed as a result of the interaction between the wavefunctions of the colliding partners. The resulting energy shifts of the excited and ground states are a function of the interatomic separation and depend on the type of interaction. The curves depicting the potential energy of these quasimolecular states as a function of internuclear separation $r$ are referred to as the ground or excited state potentials.

For the case of sodium perturbed by another sodium atom, the $3^2P$ states of the absorbing atom split up into four potential curves[15] (neglecting spin-orbit and spin-spin interactions) situated symmetrically about the atomic $3^2P$ state, at large internuclear separations (long range). At long range, the splitting of the $3^2P$ state primarily determines the shape of the atomic absorption profile and is dominated by the long-range resonant dipole–dipole interaction.[16] The magnitude of the energy shift has the form

$$\bar{h}\Delta\omega = C_3/r^3 , \tag{A1}$$

where $C_3/\bar{h}$ is the resonant dipole–dipole interaction constant, $\Delta\omega = \omega - \omega_0$, $\omega$ the frequency of the absorbed photon, $\omega_0$ that in the absence of a perturber, and $r$ is the internuclear separation. At very large internuclear separations, where the duration of the collision

$$\tau_d = R_c/v \tag{A2}$$

(here $R_c$ is the impact parameter and $v$ the relative velocity) is much less than the correlation time describing the phase relationship between two points in time of the amplitude of the electron treated as a classical oscillator,[17] i.e.,

$$\tau_d \ll 1/(\omega - \omega_0), \tag{A3}$$

then the effect of the collision can be treated as a sudden disruption of phase in the amplitude of the oscillator. Treated under this "impact" approximation, the absorption profile is Lorentzian in shape

$$\mathcal{I}(\omega) = \frac{\gamma}{2\pi} \frac{1}{(\omega - \omega_0)^2 + \gamma^2/4} \tag{A4}$$

with full-width half-maximum (FWHM) $\gamma$ varying linearly with perturber density $N$. The value $\gamma/N$ is often referred to as the resonance broadening parameter.[15]

In the other extreme, where

$$\tau_d \gg 1/(\omega - \omega_0) , \tag{A5}$$

the field experienced by the absorber as a result of a neighboring perturber a distance $r_I$ away is assumed constant in time, and the line shape is proportional to the probability of finding the nearest particle a distance $r$ from the absorber. Assuming that the nearest perturber is much closer than the average separation between atoms (nearest neighbor or binary approximation), yet sufficiently far apart such that the interaction does not significantly alter the distribution of atoms about the absorber, then we can describe the probability $P(r)dr$ of the nearest perturber being within a distance $r$ and $r + dr$ from the absorbing atom[16]

$$P(r)dr = 4\pi r^2 N \exp[-(4\pi/3)Nr^3]dr . \tag{A6}$$

According to the statistical theory, the line shape

$$\mathcal{I}(\omega)d\omega \propto P(r)dr \tag{A7}$$

and substituting (A1) into (A6), we arrive at

$$\mathscr{L}(\omega)d\omega \propto \frac{4\pi NC_3}{3\Delta\omega^2}\exp\left(-\frac{\Delta\omega_0}{\Delta\omega}\right)d\omega\,, \tag{A8}$$

where we have defined

$$\bar{h}\Delta\omega_0 = C_3/r_0^3 \tag{A9}$$

with $r_0$ representing the mean internuclear separation, i.e.,

$$r_0 = (3/4\pi N)^{1/3}\,. \tag{A10}$$

Applying the conditions that

$$\int_0^\infty \mathscr{L}(\omega)d\omega = \tfrac{1}{2} \tag{A11}$$

[since the splitting is in the form of $\pm C_3/r^3$ (Ref. 15) and that we are only considering one side of the line profile] and assume that $\Delta\omega_0 \ll \Delta\omega$ (or $r \ll r_0$, i.e., nearest-neighbor approximation), then

$$\mathscr{L}(\omega) = (2\pi/3)NC_3(\Delta\omega)^{-2} \tag{A12}$$

and the wings of the profile are also Lorentzian in shape.

Of course, this "quasistatic" approximation is inapplicable to the line core as one can see that it would violate the conditions described by (A5). In the line core, the shape is described by Eq. (A4) which conversely is inapplicable to the line wings.

Detailed calculations of the resonance broadened line profile describing the line wings, core, and the intermediate regions where $\tau_d \simeq 1/(\omega - \omega_0)$, have been performed by Srivastava and Zaidi.[9] They have found that the effective FWHM of the Lorentzian describing the quasistatic wings is two-thirds that of the profile describing the line core

$${}^w\gamma = \tfrac{2}{3}\,{}^c\gamma\,, \tag{A13}$$

where the superscripts $c$ and $w$ refer to the core and wings, respectively.

Under the range of conditions expected for our experiments, with maximum sodium density $N_{\max} = 5\times10^{16}$ cm$^{-3}$, the average internuclear separation

$$r_0 = (3/4\pi N_{\max})^{1/2} \simeq 168\ \text{Å}\,. \tag{A14}$$

The binary approximation describing the distribution of the nearest perturber is valid for $r \ll r_0$. At an interatomic separation of $r_0/10$, it remains to check the frequency range imposed by the criteria for applicability of the quasistatic approximation [Eq. (A5)]

$$\Delta\omega \gg 10v/r_0\,. \tag{A15}$$

For relative velocities of approximately $10^5$ cm/s, we arrive at

$$\Delta\omega \gg 7\times10^{11}\ \text{rad/s}\,, \tag{A16}$$

which, for the sodium resonance lines, corresponds to

$$\Delta\lambda \gg 1\ \text{Å}\,. \tag{A17}$$

Generally, when passing the broadband radiation through the oven center spectral holes of greater than 25 Å were observed. For such measurements, the sodium density is estimated from the absorption at approximately 10 Å from line center, thereby satisfying the criterion imposed by (A17).

Where the broadband radiation passes through regions of low density and short optical path (i.e., an outer chord of the vapor disk), the density is estimated from the absorption at line center of the $3^2S_{1/2} - 3^2P_{3/2}$ transition. The line center of course satisfies the criteria of (A3), thereby permitting the use of the impact approximation to describe the shape of the line core.

At shorter interatomic separations ($\sim r_0/10$) one should be cautious to check that the van der Waals dipole–dipole interaction plays a negligible role in the perturbation of the $3^2P$ state. This interaction leads to an energy shift of the state

$$\bar{h}\Delta\omega = C_6/r^6\,. \tag{A18}$$

We have estimated the $C_6$ contribution to the excited state $A\,{}^1\Sigma_u^+$ van der Waals potential by fitting the numerically tabulated potentials by Kaminsky[18] to

$$\bar{h}\Delta\omega = -\frac{C_3}{r^3} - \frac{C_6}{r^6} - \frac{C_8}{r^8}\,, \tag{A19}$$

where we have also included the quadrupole-quadrupole $C_8r^{-8}$ interaction term. Using the value of $C_3$ experimentally determined by Niemax and Pichler [15c]

$$C_3/\bar{h} = 5\times10^{-8}\ \text{cm}^3\,\text{s}^{-1}\,, \tag{A20}$$

we arrive at

$$C_6/\bar{h} = 5\times10^{-29}\ \text{cm}^6\,\text{s}^{-1}, \quad C_8/\bar{h} = 10^{-43}\ \text{cm}^8\,\text{s}^{-1}\,. \tag{A21}$$

The shift of energy state due to the resonance and van der Waals interaction becomes comparable at interatomic separations

$$r = (C_6/C_3)^{1/3} = 10\ \text{Å}\,. \tag{A22}$$

Using Eqs. (A19)–(A21) with $r = 10^{-7}$ cm (10 Å), then

$$(\omega - \omega_0) = 1.1\times10^{14}\ \text{rad}\,\text{s}^{-1} \tag{A23}$$

or

$$(\lambda - \lambda_0) = 202\ \text{Å}, \tag{A24}$$

at which one can no longer exclude the van der Waals interaction in determining the shape of the extreme line wings. If we limit our measurements to approximately $\pm 20$ Å ($\omega - \omega_0 = 1.1\times10^{13}$ rad s$^{-1}$) from either resonance line center, then Eq. (A19) leads to

$$r \simeq 18\ \text{Å} \tag{A25}$$

and at such internuclear separations, the contribution to the potential due to the van der Waals interaction is about 15% that due to the resonant dipole–dipole interaction. This would translate to a 15% change in the absorption coefficient which we have found to alter the peak sodium density measured by approximately the same amount. Only in few cases however have we operated the oven at such high densities and have measured such large spectral holes.

### van der Waals broadening due to a foreign gas

At some internuclear separation $r$, the contribution to the potential due to the van der Waals interaction with a foreign gas as a perturber would be

$$\bar{h}\Delta\omega = C_6^f/r^6\,, \tag{A26}$$

where $C_6^f/\bar{h}$ is the van der Waals interaction constant estimated by Keilkopf[19] for argon, to be

$$C_6^f/\bar{h} \simeq 5\times10^{-30}\ \text{cm}^6\,\text{s}^{-1}\,, \tag{A27}$$

which, for internuclear separations of approximately 18 Å, leads to

$$(\omega - \omega_0) = 1.5 \times 10^{11} \text{ rad s}^{-1}, \quad \text{(A28)}$$

which is orders of magnitude less than that resulting from the resonant dipole–dipole interaction. At argon pressures comparable to the sodium vapor pressure, we could safely ignore the broadening of the atomic absorption profile due to argon present as a buffer gas.


[1]C. R. Vidal and J. Cooper, J. Appl. Phys. **40**, 3370 (1969).
[2](a) R. W. Boyd, J. G. Dodd, J. Krasinski, and C. R. Stroud, Jr., Opt. Lett. **5**, 117 (1980); (b) R. W. Boyd and D. J. Harter, Appl. Opt. **9**, 2660 (1980).
[3](a) R. M. Measures and P. G. Cardinal, Phys. Rev. A **23**, 804 (1981); (b) R. M. Measures, P. G. Cardinal, and G. W. Schinn, J. Appl. Phys. **52**, 1269 (1981).
[4]M. A. Cappelli and R. M. Measures, Appl. Opt. **23**, 2107 (1984).
[5]R. M. Measures, in *Proceedings of the International Conference on LASERS '82*, New Orleans (STS, McLean, VA, 1982), pp. 101–114.
[6]An. N. Nesmeyanov, in *Vapor Pressures of the Elements* (Academic, New York, 1963), p. 443.
[7]R. M. Measures and H. Herchen, J. Quant. Spectrosc. Radiat. Transfer **29**, 9 (1982).
[8]C. G. Carrington, D. N. Stacey, and J. Cooper, J. Phys. B **6**, 417 (1973).
[9]R. P. Srivastava and H. R. Zaidi, Can. J. Phys. **53**, 84 (1975).
[10]M. A. Cappelli, Ph.D. thesis, University of Toronto, 1986.
[11]C. E. Whiting, J. Quant. Spectrosc. Radiat. Transfer **8**, 1379 (1969).
[12]C. R. Vidal, J. Appl. Phys. **44**, 2225 (1973).
[13]R. W. Boyd and J. G. Dodd, J. Appl. Phys. **51**, 6058 (1980).
[14]J. Huennekens and A. Gallagher, Phys. Rev. A **27**, 1851 (1983).
[15](a) K. Niemax and G. Pichler, J. Phys. B **7**, 1204 (1974); (b) K. Niemax and G. Pichler, J. Phys. B **7**, 2355 (1974); (c) K. Niemax and G. Pichler, J. Phys. B **8**, 179 (1975).
[16]I. I. Sobelman, L. A. Vainshtein, and E. A. Yukov, *Excitation of Atoms and Broadening of Spectral Lines* (Springer, New York, 1981).
[17]J. Cooper, in *Laser Physics; Proceedings of the 2nd New Zealand Summer School in Laser Physics* (Academic, New York, 1981), p. 241.
[18](a) M. E. Kaminsky, J. Chem. Phys. **66**, 4951 (1977); (b) M. E. Kaminsky, J. Chem. Phys. **73**, 3520 (1980).
[19]J. F. Keilkopf, J. Chem. Phys. **61**, 4733 (1974).

APPENDIX B

# ELECTRON DENSITY RADIAL PROFILES DERIVED FROM STARK BROADENING IN A SODIUM PLASMA PRODUCED BY LASER RESONANCE SATURATION

M. A. Cappelli and R. M. Measures

University of Toronto, Institute for Aerospace Studies
4925 Dufferin Street
Downsview, Ontario, Canada
M3H 5T6

## Abstract

The first free electron density radial profiles of a sodium plasma created by laser resonance saturation are reported. The measurements were based on Stark broadening of the $4^2D$-$3^2P$ multiplet and reveal that strong absorption of the laser pulse leads to formation of a conically shaped plasma along the path of the laser pulse.

## INTRODUCTION

Electron density measurements from the Stark broadening of spectral emission lines has developed into a useful and common diagnostic tool since the formulation of reliable Stark broadening theories.[1-4] The most attractive feature of this technique is that it is noninvasive and has been widely used in applications where plasma ionization probes either directly interfere with the processes studied, or are easiy contaminated by highly reactive constituents of the plasma. The viability of the technique was clearly demonstrated by Agnew and Reichelt[5] in determining the electron density in a cesium plasma diode, and afterwards in wall stabilized arcs[6-10] where cylindrical symmetry and plasma stability permitted the Abel inversion of lateral intensity measurements to obtain the local emission coefficient, and hence the radial variation in electron density. Concurrently, Stark broadening has been widely investigated and employed as a diagnostic tool in transient plasmas produced in shock tubes,[11-14] laser ablation of solid targets,[15,16] low induction vacuum sparks[17,18] and in plasmas produced by laser resonance saturation.[19-21] Most of these, however, were spatially and/or temporally averaged, depending on the nature or reproducibility of the source. In some cases, multishot averaging has been performed.[20,21]

The question of multishot averaging in highly nonlinear systems, such as a plasma column produced by laser resonance pumping, has been addressed in a numerical simulation of the spectral emission of a sodium plasma and is described elsewhere.[22]

In this paper, we report on the measurement of the radial variation of the electron density in a sodium plasma column produced by laser saturation of one of the $3^2S$-$3^2P$ resonance transitions. This process has been found to lead to high degrees of ionization in both alkali[19-21,23-25] and alkaline earth[26,27] metal vapors in the atom density range of $10^{15}$-$10^{17}$ $cm^{-3}$. At comparable electron densities, lines of the $n^2D$-$3^2P$ series in sodium suffer significant electron Stark broadening. We have elected to use Stark broadening of the $4^2D$-$3^2P$ transition in sodium to measure the electron density. The broadening of this transition and its equivalent in potassium has been studied extensively,[6,28-30] providing us with a fair degree of confidence in using the tabulated values for the electron Stark widths and shifts of Griem[4] and Dimitrijević and Sahal-Bréchot.[31] The electron densities are derived from the local emission coefficients which in turn are obtained from the Abel inversion of the lateral spectral radiances measured perpendicular to the direction of laser propagation into sodium vapor confined within a specially designed heat sandwich oven.[32]

In the case of sodium the visible wavelength spectral lines of interest either terminate on the ground or resonance states. Unfortunately, spectral lines terminating on the ground state will always suffer severe radiation trapping and are of minimal use for spectroscopic measurements. Furthermore, under conditions of laser resonance saturation the lines terminating on either of the $3^2P$ levels can be influenced by the intense radiation field of the laser and suffer radiation trapping due to the large population of atoms excited into the resonance state by the laser field. This appears to preclude measurements of the free electron density $N_e$ during the period of laser radiation. However, this limitation might be avoided if infrared spectral lines terminating on the $4^2S$ level are employed.

Lines that terminate on the 3p-levels can provide meaningful data after the laser field has sufficiently diminished and the excess 3p-resonance state population has had adequate time to decay by means of spontaneous emission and electron collision quenching. Since the electron density and the temperature will vary considerably across the plasma column created by



the laser pulse it is necessary to undertake an elaborate series of measurements across the plasma column, then perform an appropriate inversion in order to ascertain the radial variation of $N_e$. This inversion was made much simpler by our assumption of azimuthal symmetry.

## Theory of the Measurement

The spectral radiance at wavelength $\lambda$, arising from the nm-transition and observed in the x-direction at some height y above the axis of a cylindrical plasma column of radius $r_0$, see figure 1, can be expressed in the form

$$J_{nm}(\nu,y) = \int_{-\sqrt{(r_0^2-y^2)}}^{\sqrt{(r_0^2-y^2)}} \varepsilon_{nm}(\lambda,x,y)\exp\left\{-\int_x^{\sqrt{(r_0^2-y^2)}} \frac{\varepsilon_{nm}(\lambda,x^*,y)dx^*}{P(\lambda,x^*,y)}\right\}dx \quad (1)$$

where

$$\varepsilon_{nm}(\lambda,x,y) = \frac{hc}{4\pi\lambda} N_n(x,y)A_{nm}L_{nm}(\lambda,x,y) \quad (2)$$

represents the volume emission coefficient with $N_n(x,y)$ the upper state population density at $(x,y)$, $A_{nm}$ the Einstein spontaneous emission probability and $L_{nm}(\lambda,x,y)$ is the associated line profile function at $(x,y)$ the shape of which is determined by the many line broadening mechanisms. If the plasma is assumed to be in local thermodynamic equilibrium, we may write

$$P_{mn}(\lambda,x,y) = \frac{2hc^2}{\lambda^5}\left\{\exp\{hc/\lambda kT_e(x,y)\} - 1\right\}^{-1} \quad (3)$$

which is the Blackbody spectral radiance (or Planck function) and $T_e(x,y)$ the free electron temperature at $(x,y)$.

If the plasma can be regarded as optically thin at this frequency and azimuthally symmetric we can write

$$J_{nm}(\lambda,y) = 2\int_0^{r_0} \frac{\varepsilon_{nm}(\lambda,r)rdr}{\sqrt{(r^2-y^2)}} \quad (4)$$

by introducing $r^2 = x^2+y^2$. If the plasma emission is imaged onto the entrance slit of a monochromator with the slit aligned in the direction parallel to the cylinder's axis, then we can express the output current signal (Watts) of a photomultiplier tube positioned at the exit slit in the form

$$I_{nm}(\lambda,y) = S_{nm} \int_{y-\Delta y/2}^{y+\Delta y/2} \int_{z-\Delta z/2}^{z+\Delta z/2} \int_{-\infty}^{\infty} J_{nm}(\lambda',y)T(\lambda'-\lambda)d\lambda'dzdy \qquad (5)$$

where, for long focal lengths and 1:1 imaging, $\Delta y$ represents the entrance slit width and $\Delta z$ the slit height. $S_{nm}$ is the photomultiplier sensitivity (Amps/Watts) in the vicinity of the wavelength of the nm-transition (a slowly varying function of $\lambda$ over the range of the line spectra) and $T(\lambda'-\lambda)$ is the transmission function of the monochromator and input optics, generally described by a Gaussian function

$$T(\lambda'-\lambda) = \frac{K}{\gamma}\left\{\frac{\ell n2}{\pi}\right\}^{1/2} \exp\left[-\left(\frac{\lambda'-\lambda}{\gamma}\right)^2 \ell n2\right] \qquad (6)$$

with $\gamma$ the instrument half-width half maximum (HWHM) spectral width and K, the filter function, defined by the relation

$$K \equiv \int_{-\infty}^{\infty} T(\lambda'-\lambda)d\lambda \qquad (7)$$

since $T(\lambda'-\lambda)$ is independent of r, then equation (5) can be expressed as

$$I_{nm}(\lambda,y) = S_{nm} \int_y \int_z |2 \int_o^{r_0} \frac{\epsilon_{nm}(\lambda,r)*T(\lambda)rdr}{\sqrt{(r^2-y^2)}}\Big| dzdy \qquad (8)$$

where * denotes the convolution operation, i.e.,

$$\epsilon_{nm}(\lambda,r)*T(\lambda) = \int_{-\infty}^{\infty} \epsilon_{nm}(\lambda',y)T(\lambda'-\lambda)d\lambda \qquad (9)$$



The Abel transformation can then be used to provide the corresponding radial distribution of the volume emission coefficient convoluted with $T(\lambda)$:

$$\xi(\lambda,r) = \epsilon_{nm}(\lambda,r)*T(\lambda) = \frac{-1}{S_{nm}\Delta y\Delta z}\left(\frac{1}{\pi}\right) \int_o^{r_0} \left\{\frac{dI_{nm}(\lambda,y)}{dy}\right\} \frac{dy}{\sqrt{(r^2-y^2)}} \qquad (10)$$

Equation (2) implies that $\epsilon_{nm}(\lambda,r)$ is directly proportional to the atomic line profile function $L_{nm}(\lambda,r)$. For our experimental conditions, Doppler, resonance and Van der Waals broadening of the $4^2D$-$3^2P$ multiplet transition were negligible in comparison to electron Stark broadening.[33] The contribution to the broadening of the lines by the quasi-static field of the ions is evident as an enhanced red shift which can lead under our conditions, at most, to a 25% increase in the linewidth.[33] If we ignore the effects of the ions, the Stark profile is Lorentzian in shape with a half-width half maximum of w and a shift of d, both linearly dependent on the free electron density $N_e$. $N_e(r)$ can be evaluated by suitably fitting a Lorentzian function convoluted with a Gaussian [to represent the instrument function, in accordance with equation (10)] to the Abel inverted radial emission coefficient $\epsilon_{nm}(\lambda,r)$.

Semi-classical calculations of w and d for isolated neutral lines of sodium have been performed by Griem[1,4] and independently by Dimitrijević and Sahal-Bréchot.[31]

The results for the $4^2D$-$3^2P$ multiplet transitions over a wide range of electron temperatures $T_e$ are given in Table 1.

Table 1

| | d* | | w* | |
|---|---|---|---|---|
| $T_e$ (K) | Griem[4] | D-SB[31] | Griem[4] | D-SB[31] |
| 2500 | | 0.809 | | 1.125 |
| 5000 | 0.920 | 0.773 | 1.44 | 1.105 |
| 10000 | 0.805 | 0.672 | 1.35 | 1.055 |
| 20000 | 0.647 | 0.552 | 1.23 | 0.985 |

*The units of d and w are °A (or $10^{-8}$m) at the values we quoted for $N_e = 10^{16}$ cm$^{-3}$.

A spectral line is considered isolated if the linewidth (2w) is much narrower than separation between either of the upper or lower level (having orbital momentum quantum number $\ell$) involved in the transition and its nearest interacting level[4] with orbital angular momentum quantum number $\ell \pm 1$. This describes a critical electron density[31] $N_e^*$, above which w and d listed in Table 1 cannot be used. For the $4^2D$-$3^2P$ transition in sodium, $N_e^* = 6\times10^{16}$ cm$^{-3}$.

The Abel inversion is performed using the procedure proposed by Deutsch.[34] The lateral distribution of the line of sight spectral radiance from a plasma of non-dimensionalized radius, unity, can be approximated by the product of a polynomial and an exponential function, viz.,

$$I_{nm}(\lambda,Y) = \left\{\sum_{k=0}^{N} a_k Y^{2k}\right\} \exp(-\alpha Y^2) \qquad (11)$$

where we define the non-dimensionalized variables; $Y = y/r_0$ and $R = r/r_0$. Under these conditions direct integration enables us to write

$$\varepsilon_{nm}(\lambda,R) = -\frac{1}{\pi}\sum_{k=0}^{N} b_k f_k(R) \qquad (12)$$



where

$$b_k = \begin{cases} 2(k+1)a_{k+1} - 2\alpha a_k, & \text{for } 0 \le k \le N-1 \qquad (13) \\ -2\alpha a_k, & \text{for } k = N \qquad (14) \end{cases}$$

and

$$f_k(R) = \sum_{p=0}^{K} \frac{k!}{(k-p)!p!} R^{2p}\left[(2\alpha)^{p-k-1}(\alpha\pi)^{1/2}\exp(-\alpha R^2)\operatorname{erf}\left\{\alpha(1-R^2)\right\}^{1/2} - \exp(-\alpha)\sum_{s=1}^{k-p}(2\alpha)^s(1-R^2)^{k-p-s+\frac{1}{2}}\right] \qquad (15)$$

where the last sum vanishes for $p=k$, and erf denotes the Error function. Although equation (15) is fairly complicated, it is not too difficult to evaluate numerically since in most practical situations four or five terms are adequate.[33] Indeed, in our analysis we have found that we can represent the lateral emission profiles by a function of the form[33]

$$I(y) = \left\{a_0 + a_1 y^2 + a_2 y^4\right\}\exp(-\alpha y^2) \qquad (16)$$

where the fitting parameters: $a_0$, $a_1$, $a_2$ and $\alpha$ are chosen to minimize the residual sum of the squares of the deviations from the actual data.

## EXPERIMENTAL FACILITY AND RESULTS

At the heart of our "laser ionization based on resonance saturation" (LIBORS) facility is a Nd-YAG (JK-HY750) laser, the second harmonic of which pumps a dye laser (Quanta-Ray PDL-1). The sodium vapor is confined to a disc-like distribution within a specially designed "heat sandwich oven" that provides 360° optical access. A detailed description of this novel oven and the method of measuring the sodium atom density distribution is provided elsewhere.[32]

The electron density measurements were undertaken using a sideways mounted SPEX 1700 II monochromator. This enables the entrance slit of the monochromator to sample a thin horizontal slab of the plasma emission at a height y (scanned by adjusting the input optics) above the axis of the laser beam. The magnification of the optics was 1:1 with the SPEX entrance slit

at 1 cm × 40 μm. A photograph of the facility is shown in figure 2, while a schematic overview is present as figure 3.

The signal from the RCA C31034 photomultiplier mounted on the SPEX monochromator was processed by an EG&G 4420 Signal Averager that was typically gated to sample the emission in a 2 ns interval, some 65 ns after the start of the laser pulse. Since the laser pulse duration was less than 40 ns, the influence of the laser field (through the dynamic Stark effect) should be minimal and spontaneous and electron collision induced decay of the resonance state population should minimize optical depth effects.

In order to evaluate the radial profile of the free electron density $N_e(r)$, spectral scans of the $4^2D$-$3^2P$ multiplet were taken for 15 positions across the plasma column. The spectral resolution was estimated to be 0.05 nm (FWHM) with 16 laser shots being averaged to constitute one intensity measurement (at a given wavelength) and 128 such measurements comprise one spectral scan. A set of representative spectral scans of the $4^2D$-$3^2P$ multiplet recorded 65 ns after the start of the laser pulse at $z = -2$ cm and $z = 2$ cm (laser pulse enters from $z = -\infty$) are presented as figure 4. The emission arising for small lateral displacements are seen to suffer a much greater Stark broadening and red shift than the emission originating from the more weakly ionized rim of the plasma column. The difference in broadening between $z = -2$ cm and $z = 2$ cm indicates that the electron density of the plasma is decreasing along the path of the laser pulse. The laser in this run was tuned to the 589.6 nm resonance line and the energy incident on the sodium vapor was about 25 mJ. The peak sodium atom density occurs at $z = 0$ and was estimated to be about $1.5\times10^{16}$ cm$^{-3}$.

Two representative inverted ($4^2D$ - $3^2P$) multiplet spectra for $z = -2$ cm and $r = .2$ mm, and $z = 2$ cm and $r = 0.3$ mm are displayed as "o" data points in figure 5. Each inverted multiplet spectra was then fitted by three theoretically computed Stark electron impact broadened profiles that have been convoluted with a Gaussian function having a 0.05 nm FWHM (curves). This permits us to ascertain both the most likely value for the free electron density and the spread in this value for each radial position. For the curves depicted in figure 5, we have used the Stark widths and shifts of Griem,[4] and the temperature of the free electrons was assumed to be 5000 K. Fortunately, these profiles are quite insensitive to the changes in electron temperature (see Table 1) for the present range of conditions. Use of the



Stark widths and shifts calculated by Dimitrijevic' and Sahal-Bréchot[31] would systematically increase our measurements by roughly 20%.

In figures 6 and 7, we present four inverted multiplet spectra with the theoretically computed Stark broadened profiles for the most likely free electron density. These figures reaffirm the qualitative interpretation of the raw spectral data presented in figure 5 — that is to say the density and radius of the plasma is decreasing along the path of the laser pulse. This deduction is even more graphically illustrated in figure 8 where we have evaluated the free electron density radial profiles at $z = -2$ cm (Δ data) and $z = 2$ cm (o data). Also shown are two empirical curves for $N_e(r)$ that represent this data quite well.

These results indicate that although the sodium atom density is roughly the same at these two axial positions ($z = -2$ and 2 cm) the radius and the peak density of the free electrons is dramatically different. This can be understood in terms of absorption of the laser pulse as it propagates through the sodium vapor. A comparison between these experimentally evaluated free electron density radial profiles and those predicted on the basis of a computational model of LIBORS is presented elsewhere.[35]

As a check on the consistency of our measurements we have computed the optically thin [equation (4)] and optically thick [equation (1)] multiplet spectrum that would be observed at $z = -2$ cm and $y = 1.125$ mm corresponding to the free electron density radial profile at $z = -2$ cm (see figure 8) and compared these spectra with the measured multiplet spectrum (+) at $z = -2$ cm and $y = 1.125$ mm.

The computed multiplet spectra were obtained by first deriving the radial profile of the free electron temperature at $z = -2$ cm using the Saha equation, the analytical fit to the free electron density radial distribution and the initial sodium atom density. This temperature distribution, combined with the assumption of LTE allowed us to ascertain the radial profiles of the $4^2D$ and $3^2P$ population densities. The multiplet spectrum observed at any given lateral (y) position was then determined by solving the radiative transfer equation assuming that either the $3^2P$ population was zero everywhere (optically thin solution) or as determined above under LTE conditions (optically thick solution).[33]

This comparison is presented as figure 9 and suggests that the

distortion to the profiles due to optical depth is within experimental uncertainty and can be neglected. Both of the computed spectra are in excellent agreement with the experimental data.

As a further check on our measurements we have compared the computed $4^2D$ population density radial profiles at z = -2 cm and 2 cm (curves) with the normalized (at r = 0) $4^2D$ population density radial profiles (data points Δ and o) derived by inverting the spectrally integrated experimental lateral emission profiles. This comparison is presented as figure 10, and indicates a general, but not exact, agreement.

## CONCLUSIONS

Sodium vapor, confined within a specially designed heat sandwich oven, has been ionized by a pulse of laser radiation tuned to saturate one of the resonance lines. We have undertaken the first experimental evaluation of the plasma's free electron density radial profile at several locations along the path of the laser pulse. These measurements were based on matching the radially inverted ($4^2D$-$3^2P$) multiplet spectral data with the convoluted Stark (electron impact) and instrumental broadened profiles. The results clearly reveal that the plasma formed by this interaction is strongly conical in nature due to severe absorption of laser energy. This is in keeping with the predictions of our computational analysis[35] which has also indicated that the free electron temperature can be quite low ($\lesssim$ 4000K) after the laser pulse has appreciably penetrated the sodium vapor. These findings could account for the lack of ionization noted by Bowen and Thorpe[36] and the low electron temperature observed by Landen et al,[21] as neither set of authors seemed to have appreciated the degree of laser absorption arising in their experiments.

## ACKNOWLEDGEMENTS

This work was supported by the U.S. Air Force Office of Scientific Research (under grant number AFOSR 85-0020) and the Natural Science and Engineering Research Council of Canada.

## REFERENCES

1. M. Baranger, in Atomic and Molecular Processes, D. R. Bates, Ed. (Academic, New York, 1962).
2. H. R. Griem, Plasma Spectroscopy (McGraw-Hill, Toronto, 1964).
3. S. Sahal-Bréchot, Astron. Astrophys. 1, 91 (1969).
4. H. R. Griem, Spectral Line Broadening by Plasmas (Academic, New York, 1974).
5. L. Agnew and W. H. Kelchelt, J. Appl. Phys. 39, 3149 (1968).
6. J. Gumbery, G. Coulaud, and Nguyen-Hoe, Phys. Lett. 57A, 227 (1976).
7. V. Helbig, D. E. Kelleher, and W. L. Wiese, Phys. Rev. A 14, 1082 (1976).
8. J. H. Waszink and H. J. Flinsenberg, J. Appl. Phys. 49, 3792 (1978).
9. D. E. Kelleher, J. Quant. Spectrosc. Radiat. Transfer 25, 191 (1981).
10. C. Goldbach, G. Nollez, P. Plomdeur, and J. P. Zimmermann, Phys. Rev. A 25, 2596 (1982).
11. M. Neiger and H. R. Griem, Phys. Rev. A 14, 291 (1976).
12. J. F. Bauer and J. Cooper, J. Quant. Spectrosc. Radiat. Transfer 17, 311 (1977).
13. W. T. Chiang, D. P. Murphy, Y. G. Chen, and H. R. Griem, Z. Naturforsch. 32a, 818 (1977).
14. P. H. M. Vaessen, J. M. L. Van Engelen, and J. J. Bleize, J. Quant. Spectrosc. Radiat. Transfer 33, 51 (1985).
15. S. Hashimoto and N. Yamaguchi, Phys. Lett. 96A, 299 (1983).
16. R. W. Lee, J. D. Kilkenny, R. L. Kauffman, and D. L. Matthews, J. Quant. Spectrosc. Radiat. Transfer 31, 83 (1984).
17. R. U. Datla and H. R. Griem, Phys. Fluids 21, 505 (1978).
18. R. U. Datla and H. R. Griem, Phys. Fluids 22, 1415 (1979).
19. M. A. Cappelli and R. M. Measures, Appl. Opt. 23, 2107 (1984).
20. D. J. Krebs and L. D. Schearer, J. Chem. Phys. 76, 2925 (1982).
21. O. L. Landen, R. J. Winfield, D. D. Burgess, J. D. Kilkenny, and R. W. Lee, Phys. Rev. A 32, 2963 (1985).
22. R. S. Kissack, M. A. Cappelli, and R. M. Measures, "Computer Modelling of the Multishot Average Spectral Emission from a Laser Created Sodium Plasma" (in preparation).
23. (a) T. B. Lucatorto and T. J. McIlrath, Phys. Rev. Lett. 37, 428 (1976); (b) T. J. McIlrath and T. B. Lucatorto, Phys. Rev. Lett. 38, 1390 (1977).

24. T. Stacewicz, Opt. Commun. 35, 239 (1980).
25. F. Roussel, P. Breger, G. Spiess, C. Manus, and S. Geltman, J. Phys. B 13, L631 (1980).
26. L. Janreiss and M. C. E. Huber, Phys. Rev. A 28, 3382 (1983).
27. C. H. Skinner, J. Phys. B 13, 55 (1980).
28. P. E. Oettinger and J. Cooper, J. Quant. Spectrosc. Radiat. Transfer 9, 591 (1969).
29. J. P. Hohlmer, Phys. Rev. A 30, 1449 (1984); 32, 676 (1985).
30. N. Konjevic, Phys. Rev. A 32, 673 (1985).
31. M. S. Dimitrijevic and S. Sahal-Bréchot, J. Quant. Spectrosc. Radiat. Transfer 34, 149 (1985).
32. M. A. Cappelli, P. G. Cardinal, H. Herchen, and R. M. Measures, Rev. Sci. Instrum. 56, 2030 (1985).
33. M. A. Cappelli, UTIAS Report No. 306 (1986).
34. M. Deutsch, Appl. Phys. Lett. 42, 237 (1983).
35. R. S. Krissack, S. K. Wong, M. A. Cappelli, and R. M. Measures, "Plasma Channel Formation Based on Laser Resonance Saturation" (in preparation).
36. J. L. Bowen and A. P. Thorne, J. Phys. B: At. Mol. Phys. 18, 35-50 (1985).

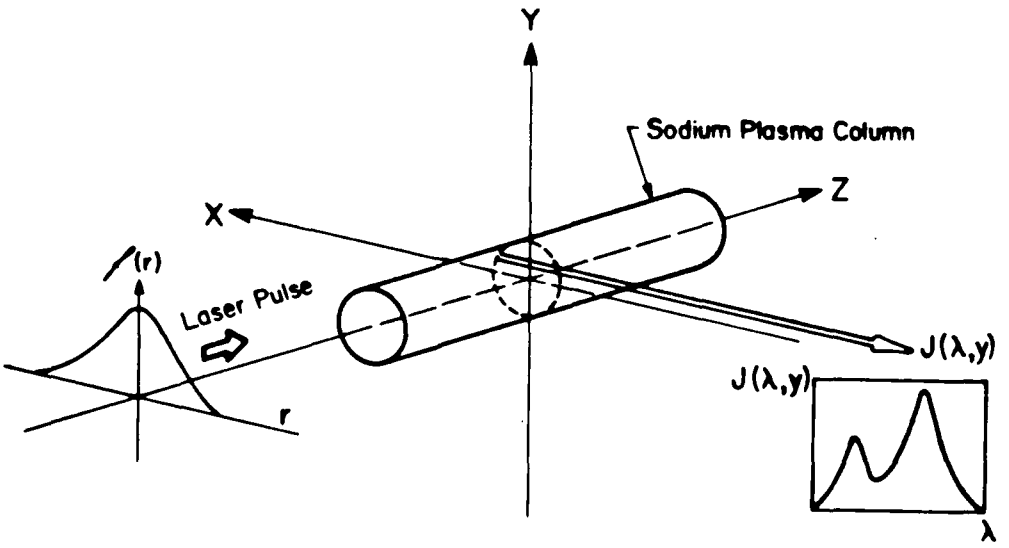


Fig. 1 Geometrical Configuration for Spectral Measurements of Sodium Plasma Created by Laser Resonance Saturation.

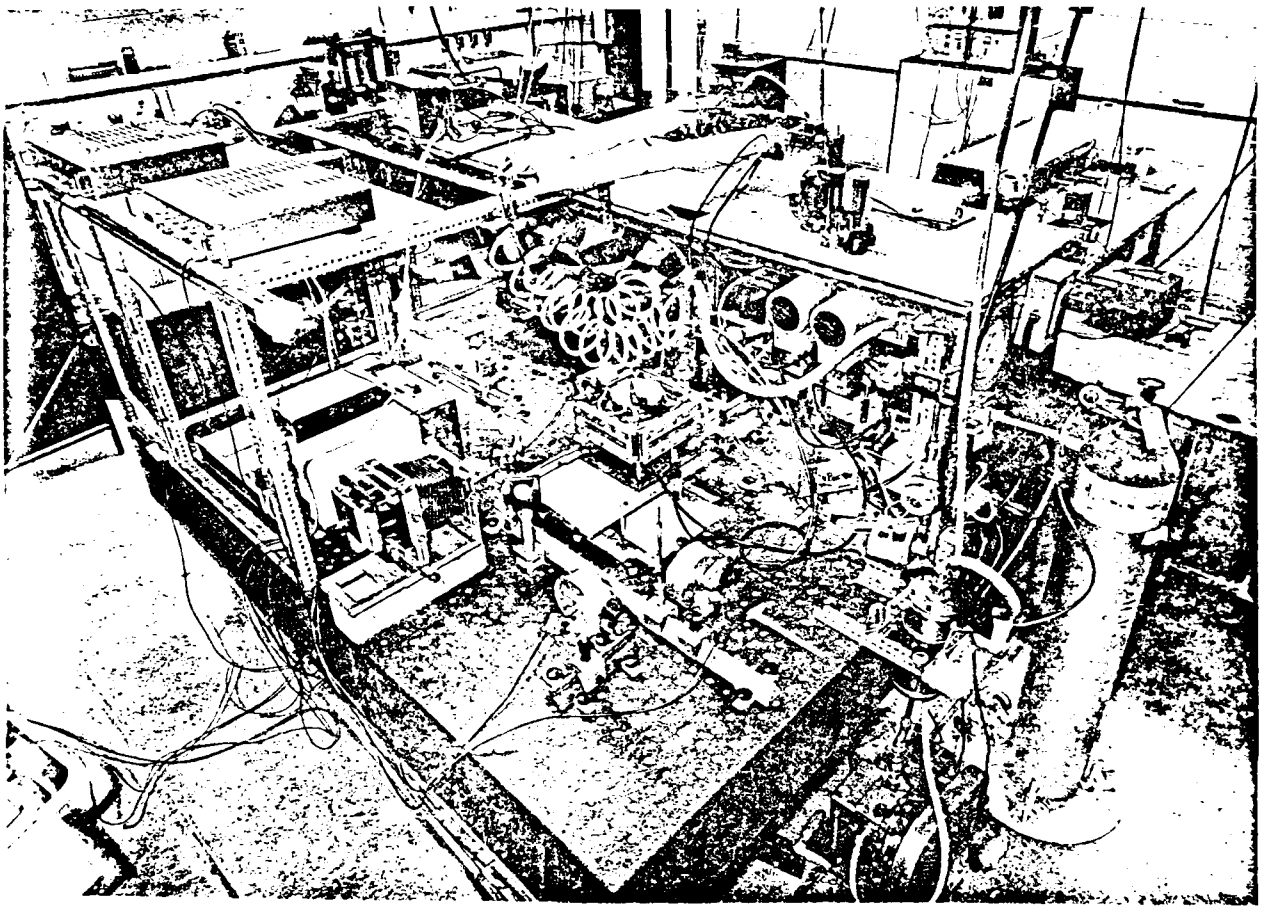

Fig. 2 Photograph of LIBORS Facility Showing the Heat Sandwich Oven and Photodetection System in the Foreground and the Nd-YAG Laser Pumped Dye Laser in the Background.

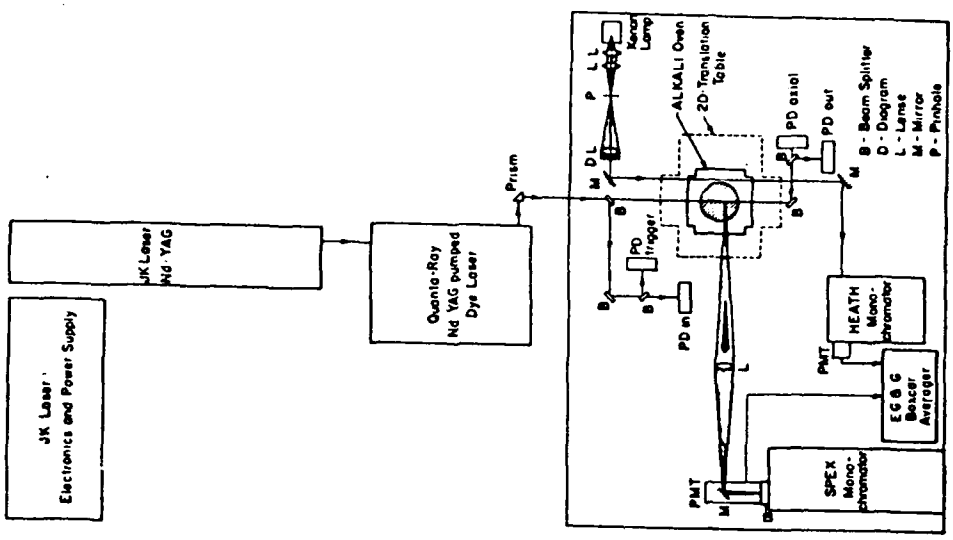


Fig. 3 Schematic Overview of LIBORS Facility.

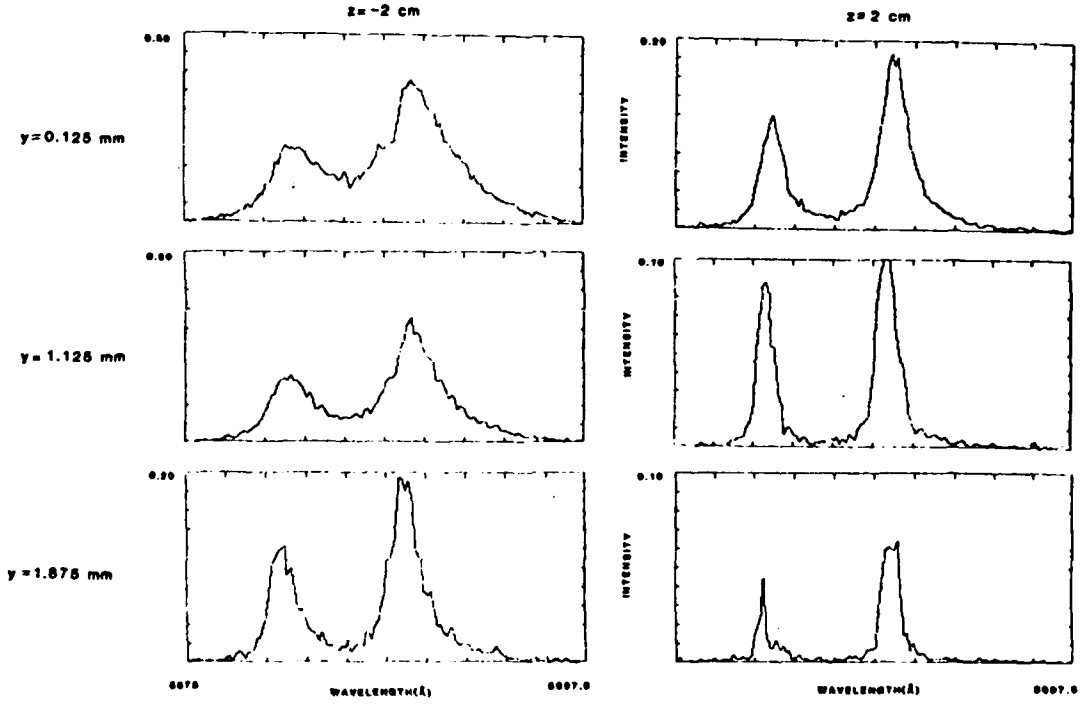


Fig. 4 Set of $4^2D$-$3^2P$ Sodium Multiplet Spectra Recorded at Three y-positions and Z = -2 and 2cm.

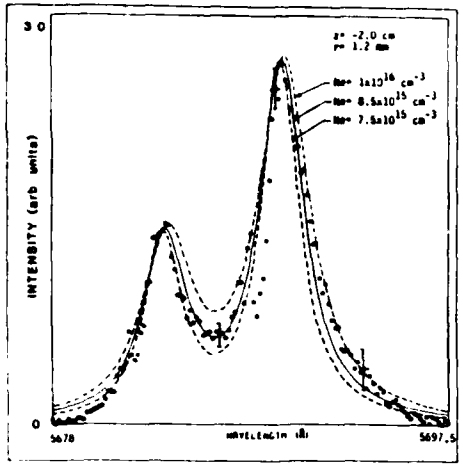


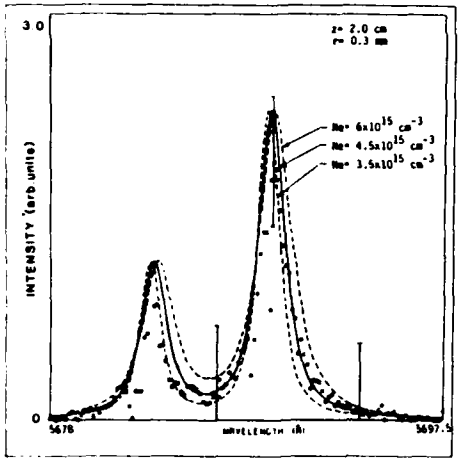


Fig. 5 Fitting of Stark and Instrument Profiles to the Experimental Spatially Inverted $4^2D$-$3^2P$ Sodium Multiplet Spectra at (a) Z = -2cm, r = 1.2mm, and (b) Z = 2cm, r = 0.3mm.

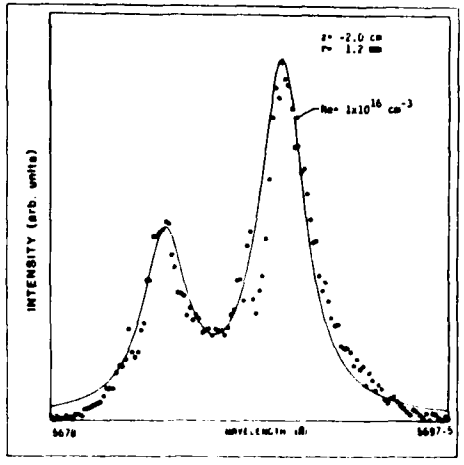


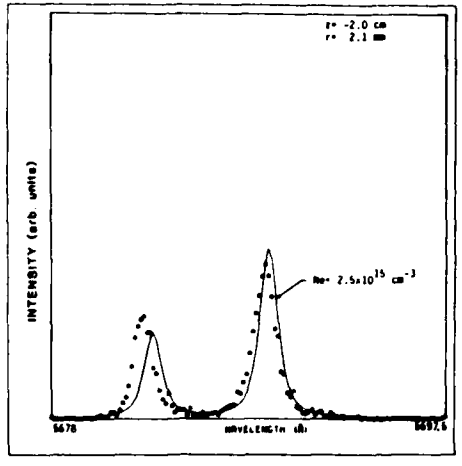


Fig. 6 Best Fit of Stark and Instrument Profiles to the Experimental Spatially Inverted $4^2D$-$3^2P$ Sodium Multiplet Spectra at (a) Z = -2cm, r = 1.2mm, and (b) Z = -2cm, r = 2.1mm.

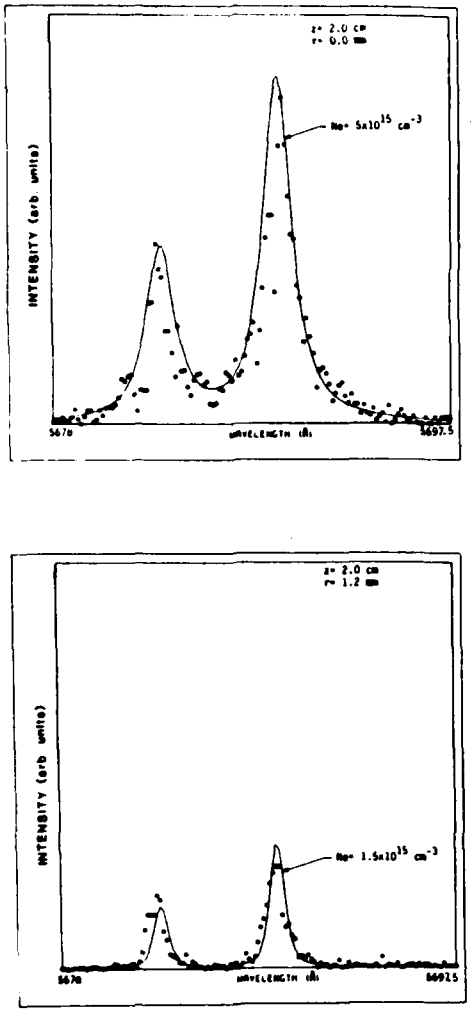


Fig. 7 Best Fit of Stark and Instrument Profiles to the Experimental Spatially Inverted $4^2D - 3^2P$ Sodium Multiplet Spectra at (a) Z = 2cm, r = 0mm, and (b) Z = 2cm, r = 1.2mm.

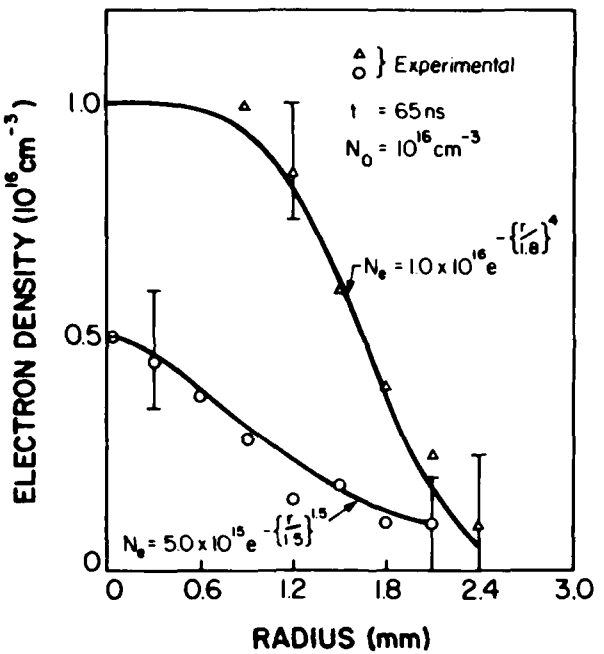


Fig. 8 Experimentally Determined Electron Density Radial Profiles at Z = -2 and 2cm in a Sodium Plasma Created by Laser Resonance Saturation. Also Shown are Analytical Fits to the Experimental Data.

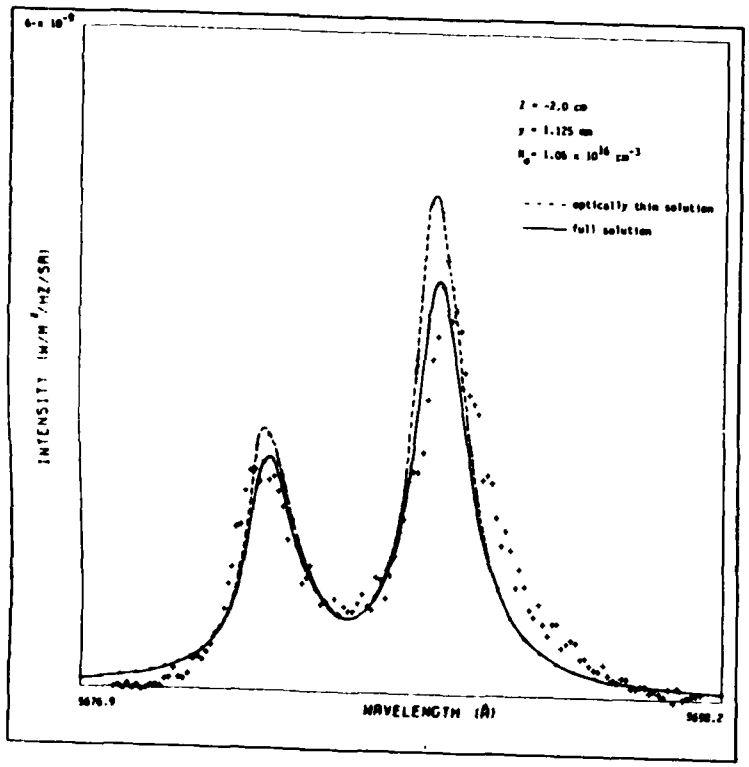


Fig. 9 Comparison of Computer Generated Optically Thin and Optically Thick Spectra Derived from the Measured Radial Electron Density Profile (Assuming LTE) with the Experimental Spectrum (Data Points) at Z = -2cm, y = 1.125mm.

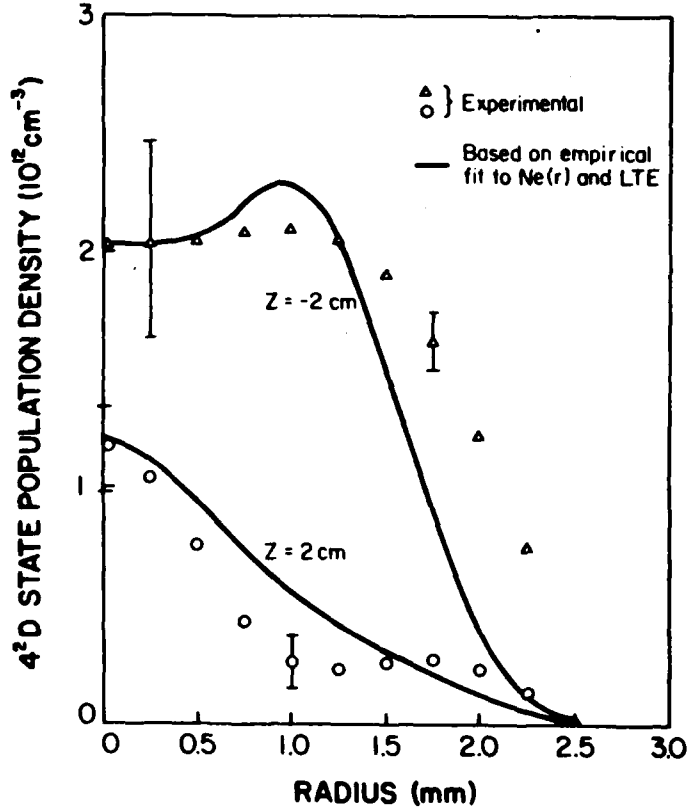


Fig. 10 Comparison of the Radial Distribution of $4^2D$ Population of Sodium Atoms Derived from the Empirical Fit to $N_e(r)$ (assuming LTE) and the Radially Inverted $4^2D - 3^2P$ Emission (Normalized at r = 0) for Z = -2 and 2cm.

APPENDIX C

# EFFECTS OF INHOMOGENEITIES, OPTICAL DEPTH AND FINITE BANDWIDTH ON ELECTRON TEMPERATURE MEASUREMENTS IN A CYLINDRICAL SODIUM PLASMA

M. A. Cappelli and R. M. Measures

University of Toronto
Institute for Aerospace Studies
4925 Dufferin Street
Downsview, Ontario, Canada
M3H 5T6

## Abstract

A computational study of the effects of: inhomogeneities, self-absorption and finite detection bandwidth on the electron temperatures deduced from Boltzmann plots of line intensities from sodium plasmas in LTE has been undertaken and the results compared with an experiment.

## INTRODUCTION

The measurements of the electron temperatures from the relative intensities of spectral lines[1-4] is a common approach in plasmas where either an absolute measurement of line intensity is not possible, or the recombination radiation is weak and where limited spectral resolution prevents the measurement of the shift to width ratio of Stark broadened emission lines.[5-7] The applicability of a "Boltzmann plot", the slope of which can be used to evaluate the free electron temperature, $T_e$, in an LTE plasma and the simplicity of the technique, rests on the assumptions that the plasma is homogeneous and that the spectral lines suffer negligible self-absorption.

The first assumption is rarely justified and even in the case of cylindrical symmetry, a more detailed analysis is required, involving the solution of the Abel transform[8] to reconstruct the radial volume emission coefficients from lateral intensity measurements.[9] The latter assumption is generally valild for lines with high lying upper states whose terminating state is any state other than the ground state. Such lines have relatively weak oscillator strengths and are usually optically thin. These same lines,

however, are quite weak under LTE conditions and may appear to be very diffuse as a result of Stark broadening for electron densities, $N_e$, greater than $10^{15}$ cm$^{-3}$.

The latter assumption of negligible self absorption is likely to be invalid under conditions where the terminating state population density is significantly influenced by mechanisms other than electron collisions. Such may be the case for plasmas produced in alkali and alkaline earth metal vapors by laser resonance saturation.[10-14] Measurements of the electron temperature in such sodium plasmas have been undertaken by analysing the emission of several lines terminating on the resonantly pumped $3^2P$ state.[15-17]

We present in this paper, the results of an analysis aimed at elucidating some of the problems and limitations likely to be encountered in measurements of this nature. Our investigation is based on the solution of the one dimensional radiative transfer equation and allows us to examine the effects of: (i) a radial variation in the free electron temperature, (ii) optical depth, (iii) limited range of spectral integration, and (iv) different observation geometries. Consideration is also given to a situation where LTE, although extending down to the $3^2P$ resonance state, may not encompass the $3^2S$ ground state as a result of radiative pumping either directly from the laser field or as a result of strong imprisonment of the spontaneous emission.[18] Results are presented, of an experiment where sodium vapor ([Na] = $1.5\times10^{16}$ cm$^{-3}$) is irradiated with a laser beam of modest power ($10^6$-$10^7$ W cm$^{-2}$) tuned to one of the $3^2S$ - $3^2P$ resonance transitions.

## RADIATIVE TRANSFER THEORY

The steady state solution to the one dimensional radiative transfer equation enables the spectral radiance $J_{nm}(\nu,y)$ arising from the n-m transition emitted in the x direction from a cylindrically symmetric plasma column of radius R at some height y from the column axis (see figure 1) to be written in the form

$$J_{nm}(\nu,y) = \int_{-\sqrt{(R^2-y^2)}}^{\sqrt{(R^2-y^2)}} \varepsilon_{nm}(\nu,x,y)\, \exp\left[-\int_{x}^{\sqrt{(R^2-y^2)}} \frac{\varepsilon_{nm}(\nu,x^*y)dx^*}{P(\nu_{nm},x^*,y)}\right]dx \qquad (1)$$



where

$$\varepsilon_{nm}(\nu,x,y) = \frac{h\nu_{nm}}{4\pi} N_n(x,y) A_{nm} L_{nm}(\nu,x,y) \qquad (2)$$

represents the volume emission coefficient, $N_n(x,y)$ the upper state population density at position (x,y), $A_{nm}$ the Einstein spontaneous emission probability and $L_{nm}(\nu,x,y)$ the atomic line profile for the nm transition.

The shape of the atomic line profile is determined by several line broadening mechanisms. We have incuded the effects of electron Stark broadening,[5] resonance broadening,[1,19] foreign gas broadening due to sodium atom collisions with argon as a buffer gas,[20] and Doppler broadening as a result of the atom's thermal motion. The first three mechanisms produce a Lorentzian line shape when treated in the impact regime. The latter, namely Doppler broadening, has a Gaussian form and must be convoluted with the Lorentzians giving rise to a Voigt line shape.[21]

If the plasma is in LTE, then the source function

$$P(\nu_{nm},x,y) = \frac{2h\nu_{nm}}{c^2}\left[\exp\left\{-\frac{h\nu_{nm}}{kT_e(x,y)}\right\} - 1\right]^{-1} \qquad (3)$$

which is the Planck function, $h\nu_{nm}$ being the n to m transition photon energy, $T_e(x,y)$ the free electron temperature at (x,y), and h, Planck's constant.

Experimentally, the radiance $J_{nm}(x,y)$ can be measured by collecting the spectral line emission over a finite bandwidth $\Delta\nu_I$ centred about the unperturbed line centre frequency $\nu_{nm}$. Spectrally integrating equation (1) yields the radiance emitted at y, i.e.,

$$J_{nm}(y) = \int_{\nu_{nm}-\frac{\Delta\nu_I}{2}}^{\nu_{nm}+\frac{\Delta\nu_I}{2}} J_{nm}(\nu,y)d\nu \qquad (4)$$

For a typical experimental configuration, with the monochromator slit aligned in the direction parallel and its field of view centred about the cylinder axis at y = 0 [configuration A, see figure 2(a)], the photodetector

signal $I^{(A)}_{nm}(z)$ at a distance z along the column axis,

$$I^{(A)}_{nm}(z) = S_{nm} \int_{z-\Delta z/2}^{z+\Delta z/2} \int_{-\Delta y/2}^{\Delta y/2} J_{nm}(y^*,z^*)dy^*dz^* \qquad (5)$$

where, for long focal lengths and 1:1 imaging, $\Delta y$ represents the slit width and $\Delta z$ the slit height. $S_{nm}$ represents the instrument factor incorporating the transmission efficiency of the monochromator and input optics, and the response of the photomultiplier (Amps/Watt) in the spectral range of interest. If we assume that spatial variations in the plasma are small over the range defined by $\Delta z$ and $\Delta y$, then

$$I^{(A)}_{nm}(z) = S_{nm} J_{nm}(0,z) \Delta y \ \Delta z \qquad (6)$$

A second configuration frequently used: Configuration B, see figure 2(b), involves aligning the monochromator slit such that it views a slab of plasma that is perpendicular to, and centred about the cylinder axis. The photodetector signal $I^{(B)}_{nm}(z)$ under these circumstances is given by

$$I^{(B)}_{nm}(z) = S_{nm} \int_{z-\Delta z/2}^{z+\Delta z/2} \int_{-\infty}^{\infty} J_{nm}(y^*, z^*)dy^* \ dz^* \qquad (7)$$

where in this instance we have taken $\Delta z$ to represent the slit width, and the slit height $\Delta y >> 2R$. For uniform conditions over $\Delta z$,

$$I^{(B)}_{nm}(z) = S_{nm} \Delta z \int_{-\infty}^{\infty} J_{nm}(y^*, z)dy \qquad (8)$$

If significant differences in electron temperatures are measured using configurations A and B, from Boltzmann plots of the intensity of several optically thin spectral lines, this suggests strong variation in the



electron temperature and the need for a more detailed analysis based on the Abel inversion of the lateral intensity distribution.

## NUMERICAL SIMULATION

We have applied the above formulation to the $n^2D$-$3^2P$ (n = 4, 5, 6) and $n^2S$-$3^2P$ (n = 5, 6, 7) spectral series of a cylindrically symmetric sodium plasma with a preassigned radial variation in the electron temperature. The assumption of: LTE, Saha equilibrium for the free electron density $N_e(r)$, and continuity,[21]

$$N_e + \sum_{n-1}^{\infty} N_n = N_o \qquad (9)$$

where $N_o$ represents the total neutral sodium density, allows us to model the individual excited state population densities as functions of the radial position. Numerical integration of equation (1) is then performed on a Perkin-Elmer 3250 computer.

We have chosen to investigate plasma conditions [namely $N_e(r)$, $T_e(r)$] which encompass the range expected in our experimental study of Laser Ionization Based On Resonance Saturation (LIBORS).

(A) Homogeneous electron temperature, complete spectral integration and configurtion A, y = 0

Equation (1) was integrated for configuration A, with a neutral density $[N_a] = 2.0\times10^{16}$ cm$^{-3}$ and plasma column radius R = 5 mm. We have first considered two electron temperatures, $T_e$ = 5000K and $T_e$ = 10,000K taken to be constant over the plasma radial domain and assume that the monochromator exit slit width has been selected so that complete spectral integration takes place. The 'optically thin solutions' [equation (1) solved with $\epsilon_{nm}/P_{nm} = 0$] for the six transitions indicated earlier, as expected, lie on the straight line of a Boltzmann plot (see figure 3), the slope of which should retrieve the assumed temperature. Any deviation from the assumed 5000K and 10000K temperatures reflects numerical error in the integration routine.

In addition to the optically thin solution the full solutions of equation (1) for the six transitions are also plotted. Clearly, for $T_e$ = 10000K, all transitions appear to be optically thin as the neutral species

is efficiently ionized ($N_e = 1.993\times10^{16}$ cm$^{-3}$). For $T_e$ = 5000K, only transitions from states above the $6^2S$ state appear to be optically thin, suggesting that in similar experimental situations, only these transitions should be conidered for determining the equilibrium electron temperature, even if LTE exists all the way down to the ground state. The validity of LTE down to lower states should always be checked by an independent measurement of the electron density.[1]

(B) Gaussian electron temperature radial distribution, complete spectral integration and configuration A, y = 0

With the same conditions of neutral density, plasma radius and observation geometries, the radiances for the following electron temperature distributions:

$$T_e(r) = 2000 + 8000\ e^{-(r^2/r_0^2)}$$ [inset to figure 4(a)]

$$T_e(r) = 2000 + 3000\ e^{-(r^2/r_0^2)}$$ [inset to figure 4(b)]

with $r_0$ = 2.5 mm, were calculated. The results are depicted in figure 4(a) and 4(b) respectively. For the case illustrated in figure 4(a), as expected, transitions from states above the $6^2S$ state suffer little attenuation due to self-absorption. More important, however, is the observation that the optically thin emission from these transitions fit with reasonable accuracy to a straight line on the Boltzmann plot. The slope of this line tends to reflect the electron temperature of the region where the excited state population density is a maximum. This could be understood by reference to figure 5, where the radial variation of the $4^2D$ population density is displayed and it is apparent that an intense ring of emission is expected for r = 2.0 mm. Similar results are obtained for the case illustrated in figure 4(b), but in this instance the excited state population density peaks at r = 0, where the electron temperature $T_e$ = 5000K. One important conclusion to be drawn from this is that measurements of this nature do not necessarily reflect the peak electron temperature, but rather, the electron temperature of the region of the plasma containing the maximum emitter density.

(C) Gaussian electron temperature radial distribution, 3 nm bandwidth and configuration A, y = 0

As discussed earlier, a common mode of measurement is one in which the exit slit of the monochromator is centred about the unshifted line centre



and opened to integrate the emission over a finite spectral interval. In an experiment, an estimate of the contribution to the signal due to the continuum background is made by detuning the monochromator off line centre to the point where there is virtually no contribution to the signal from line emission yet not so far that the background level changes appreciably. If the bandwidth is much greater than the width of the emission line (which may be significantly Stark broadened) there is the potential problem of low signal to noise levels due to background continuum emission. If, however, the bandwidth is comparable to the width of the emission line, then a contribution to the signal from the emission line wings is lost. Figure 6 depicts, superimposed onto the results of figure 4(b), the solutions to equation (4) for the six transitions assuming a monochromator bandwidth of 3 nm. Clearly, for the transitions with higher lying $^2D$ upper states, the effect is quite pronounced as they are more vulnerable to Stark broadening in the electron impact regime, than the $4^2D$ state or any of the $^2S$ states considered.[5] This feature adds further complications and restrictions in choosing spectral lines for analysis using a Boltzmann plot.

(D) Comparison between configurations A and B

The spectral radiance $J_{nm}(\nu,y)$ is calculated for a number of y positions. These values are then fitted using a linear least squares routine, to a function of the form

$$J_{nm}(\nu,y) = [c_1 + c_2y^2 + c_3y^4]\exp(-\alpha y^2) \qquad (10)$$

where $c_1$, $c_2$ and $c_3$ are the polynomial coefficients and $\alpha$ is chosen to minimize the residual of the least squares. Equation (8) can then be integrated in closed form,[24] thereby simulating the signal that would be observed with experimental configuration B. Figures 7(a) and 7(b) illustrate the Boltzmann plots that would subsequently be obtained with the vertical slit arrangement, for the two previously described electron temperature radial distributions. Comparison of figures 7 and 4 demonstrate quite similar effects due to optical depth and limited bandwidth. Not surprising is the fact that one obtains again a linear relationship between the optically thin lines that are fully spectrally integrated. However, the slopes and therefore the predicted temperatures differ somewhat between the two configurations (by roughly 10%). Where the temperature gradients are

more severe [figure 7(a)], the difference between the measurements made using the two configurations clearly become more pronounced.

(E) Collisional-radiative coupling between ground and resonance level

A collisional-radiative model has been formulated,[21] to include stimulated absorption and emission of resonance radiation as a mechanism of populating the resonance state. We now assume that LTE exists down to the resonance level which is also taken to be in Saha equilibrium with the free electron density, and that the continuity relation takes the form,

$$N_e + N_1 + N_2 + \sum_{n\geq 3}^{\infty} N_n = N_o \qquad (11)$$

$N_1$ and $N_2$ represent the ground and resonance population densities and are principally determined by: stimulated and spontaneous decay of the resonance state atoms, stimulated absorption of resonance radiation by atoms in the ground state and by electron excitation and de-excitation collisions between atoms in the ground and resonance states,

$$N_2 = \frac{R_{12} + N_e K_{12}}{R_{21} + N_e K_2 + A_{21}} N_1 \qquad (12)$$

where $R_{12}$ and $R_{21}$ are the respective rates of stimulated absorption and emission. $K_{12}$ and $K_{21}$ represent the electron excitation and de-excitation collisional rate coefficients, respectively. With $T_e(r)$, $N_o$ and $R_{21}/A_{21}$ specified, $N_e(r)$, $N_n(r)$ and $J_{nm}(\nu,y)$ can be computed. For times during or shortly after the laser pulse, $R_{21}$ may be comparable to $A_{21}$. We investigated the case where $R_{21}/A_{21} = 0.1$, with $T_e(r)$ and $N_o$ equal to that used to generate figure 4(a). The resulting Boltzmann plot is illustrated in figure 8. Comparing figure 4(a) to figure 8, one notices an enhancement in the scatter of the full solution, i.e., an increase in the optical depth resulting from a "halo" of atoms in their resonance state surrounding the plasma core. Further evidence of such a halo is the self-reversal in the computed spectrum of the $4^2D$-$3^2P$ transition for $y = 0$, that is not evident in the corresponding spectrum when LTE down to the $3^2S$ state is assumed, i.e., $R_{21}/A_{21} = 0$ (figure 9).



EXPERIMENTAL RESULTS AND DISCUSSION

A facility has been developed to study Laser Ionization Based on Resonance Saturation (see figure 10). The facility utilizes a Nd:YAG laser (JK HY750) pumped dye laser (Quanta Ray PDL-1) operating at 10 Hz repetition rate and tuned to the $3^2S$-$3^2P$ transition in sodium at $\lambda$ = 589.0 nm. The laser beam is directed into a specially designed heat sandwich oven[22] containing molten sodium in equilibrium with its vapor at a peak density of about $2.0\times10^{16}$ cm$^{-3}$. A scanning monochromator (SPEX Model 1700 II) in conjunction with a photomultiplier tube (RCA model 7265) served to measure the spectral radiance from the $n^2D$-$3^2P$ (n = 4, 5, 6) and $n^2S$-$3^2P$ (n = 5, 6, 7) transitions emitted perpendicular to the direction of the ionizing laser beam. The SPEX monochromator was rotated by 90° so that the field of view of its entrance slit is parallel to the axis of the laser beam (configuration A of figure 1). With the magnification of the optics at 1:1, the entrance slit height (1.0 cm) and width (40 μm) defined the cross section of the slab of observation. Data acquisition and processing was achieved by using a boxcar averager (EG&G-PARC model 4420), a gated integrator (model 4421) and an Apple II Plus microcomputer.

When viewing the spectral emission, the signal averager was triggered and gated to sample a window 2 ns wide, 60 ns after the onset of the laser pulse. The laser beam had a cross section of roughly 0.5 cm in diameter and the estimated energy entering the vapor was 37 mJ. The 60 ns delay on the sample time was chosen to minimize the effect of the laser field (having a pulse duration of about 30 ns), on the $3^2P$ state (through the dynamic Stark effect) as well as to give the $3^2P$ state enough time to decay through spontaneous emission and approach thermal equilibrium with the ground state.

An independent measurement[21] of the radial variation in the electron density using the Stark broadening of the $4^2D$-$3^2P$ multiplet spectrum was undertaken and the corresponding Saha based electron temperature radial profile is presented in figure 11. Using the model derived earlier and assuming that LTE extends down to the ground state, we can compute the observed radiance from the six transitions of interest. In this experiment, spectral integration was performed over a range of 4 nm, centred about the unshifted line centre, with corrections to the signal to compensate for background radiation.

In order to test the validity of setting $R_{21}/A_{21} = 0$ in our computational model we have measured the $4^2D$-$3^2P$ multiplet spectrum, shown as (o) data in figure 12, and found it free of self-reversal. This suggests that there is no excessive resonance state population remaining at the time of observation and setting $R_{21}/A_{21} = 0$ was justified. Figure 13 depicts the Boltzmann plot of the measured spectrally integrated intensity (normalized to the theoretically calculated intensity of the $4^2D$-$3^2P$ transition) along with that predicted using the temperature distribution of figure 11.

It can be seen that the agreement is fairly good. The scatter of the data from a straight line demonstrates that a Boltzmann plot can only be used to provide an approximate indication of the electron temperature within a plasma having strong radial variation.

## CONCLUSIONS

A computational study has been undertaken of various real effects such as radial inhomogeneity, self-absorption and finite deteection bandwidth on the Boltzmann plot based measurement of the free electron temperature in a sodium plasma in LTE. Inhomogeneous plasmas are shown to give rise to apparent temperatures that reflect regions of maximum upper state population density. Self-absorption is found to be responsible for strong scatter in the line emission data on a Boltzmann plot. This effect is even more pronounced when the population of the terminating state for the emission lines is enhanced by either a laser field or radiation trapping. Limited spectral integration has also been found to cause significant deviations from linearity in highly ionized plasmas where Stark broadening is significant. Comparison of experimental results with numerical calculations show similar trends in the scatter of emission line intensity on a Boltzmann plot for several sodium transitions from a plasma produced by laser resonance saturation.

## REFERENCES


1. H. R. Griem, Plasma Spectroscopy, McGraw-Hill, Toronto (1964).
2. R. H. Huddlestone and S. L. Leonard, Plasma Diagnostic Techniques, Chap. 5, Academic Press, New York (1965).
3. T. L. Eddy, JQSRT 3, 197 (1985).
4. M. Gersten, J. E. Rauch, W. Clark R. D. Richardson, and G. M. Wilkinson, Appl. Phys. Lett. 39(2), 148 (1981).
5. H. R. Griem, Spectral Line Broadening by Plasmas, Academic Press, New York (1974).
6. D. D. Burgess and J. Cooper, J. Sci. Instruments 42, 829 (1965).
7. D. D. Burgess and J. Cooper, Proc. Phys. Soc. 86 1333 (1965)
8. H. Jeffreys and B. S. Jeffreys, Methods of Mathematical Physics, Cambridge University Press, London (1962).
9. M. A. Cappelli and R. M. Measures, "Electron Density Radial Profiles Derived from Stark Broadening in a Sodium Plasma Produced by Laser Resonance Saturation" submitted for publication).
10. (a) T. B. Lucatorto and T. J. McIlrath, Phys. Rev. Lett. 37, 428 (1976).
    (b) T. J. McIlrath and T. B. Lucatorto, Phys. Rev. Lett. 38, 1390 (1977).
11. L. Jahreiss and M. C. E. Huber, Phys. Rev. A28, 3382 (1983).
12. R. M. Measures and P. G. Cardinal, Phys. Rev. A 23, 804 (1981).
13. M. A. Cappelli and R. M. Measures, Appl. Optics 23, 2107 (1984).
14. R. S. Kissack, S. K. Wong, M. A. Cappelli and R. M. Measures, "Plasma Channel Formation Based on Laser Resonance Saturation" (submitted for publication).
15. P. G. Cardinal, UTIAS Report No. 299 (1985).
16. O. L. Landen, R. J. Windfield, D. D. Burgess, J. D. Kilkenny, and R. W. Lee, Phys. Rev. A 32, 2963 (1985).
17. D. J. Krebs and L. D. Schearer, J. Chem. Phys. 76, 2925 (1982).
18. (a) T. Holstein, Phys. Rev. 72, 1212 (1947).
    (b) T. Holstein, Phys. Rev. 83, 1159 (1951).
19. C. G. Carrington, D. N. Stacey, and J. Cooper, J. Phys. B 6, 417 (1973).
20. J. F. Keilkopf, J. Chem. Phys. 61, 4733 (1974).
21. M. A. Cappelli, UTIAS Report No. 306 (1986).
22. M. A. Cappelli, P. G. Cardinal, H. Herchen, and R. M. Measures, Rev. Sci. Instrum. 56, 2030 (1985).

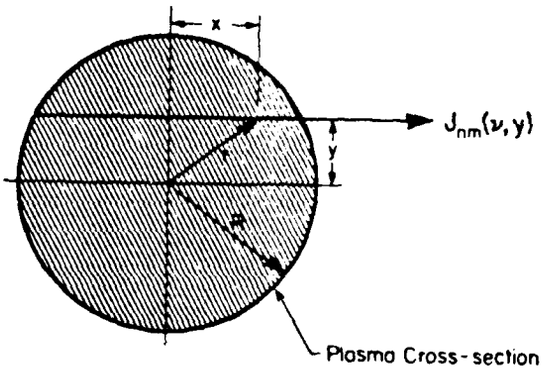


Fig. 1 Geometrical Representation of the Spectral Radiance, $J_{nm}(\nu,y)$, Emitted from the nm-Transition in the x-Direction at a Lateral Displacement y from the z-axis.

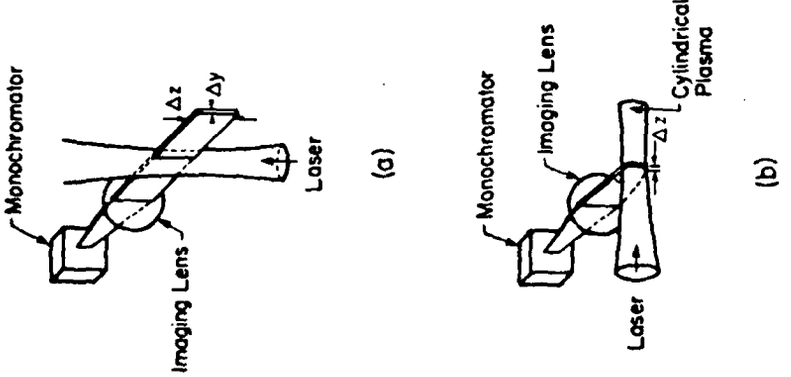


Fig. 2 Two Configurations for Sampling the Emission from a Thin Slab of Plasma: (a) Oriented Parallel to the z-Axis, Configuration A, (b) Oriented Perpendicular to the z-Axis, Configuration B.

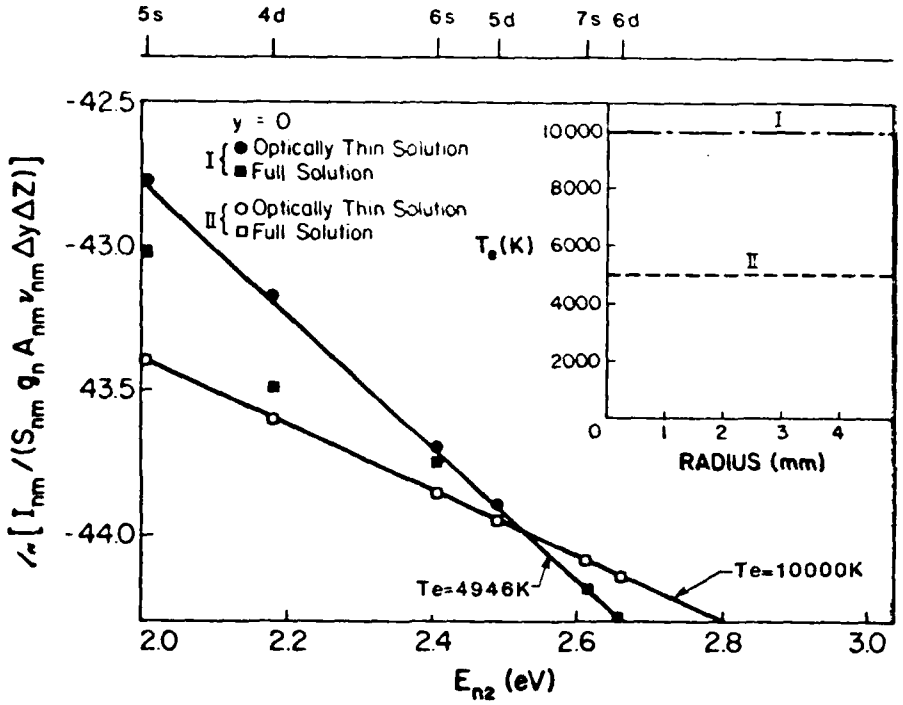


Fig. 3 Computed Boltzmann Plots for Several Transitions in a Sodium Plasma with Flat Radial Distributions of Electron Temperature Corresponding to: (I) 10,000K and (II) 5,000K (Shown in the Small Inset).

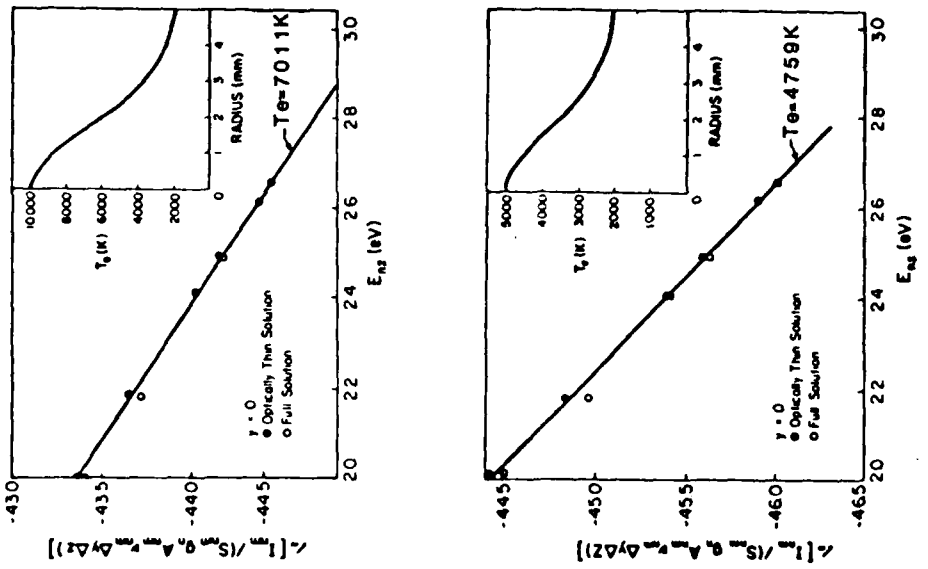


Fig. 4 Boltzmann Plots for Several Transitions Expected from Configuration (A) for a Sodium Plasma Assumed to have a Radial Electron Temperature Distribution of the Form (a) $T_e(r) = [2+8e^{-r^2/r_0^2}]\times10^4$K and (b) $T_e(r) = [2+3e^{-r^2/r_0^2}]\times10^4$K (with $r_0$ = 0.6mm as unknown in the small inset). Although Both Optically Thin and Full Solutions (see text) are Presented, the Lines Represent the Least Squares Fit to the Optically Thin Solutions.

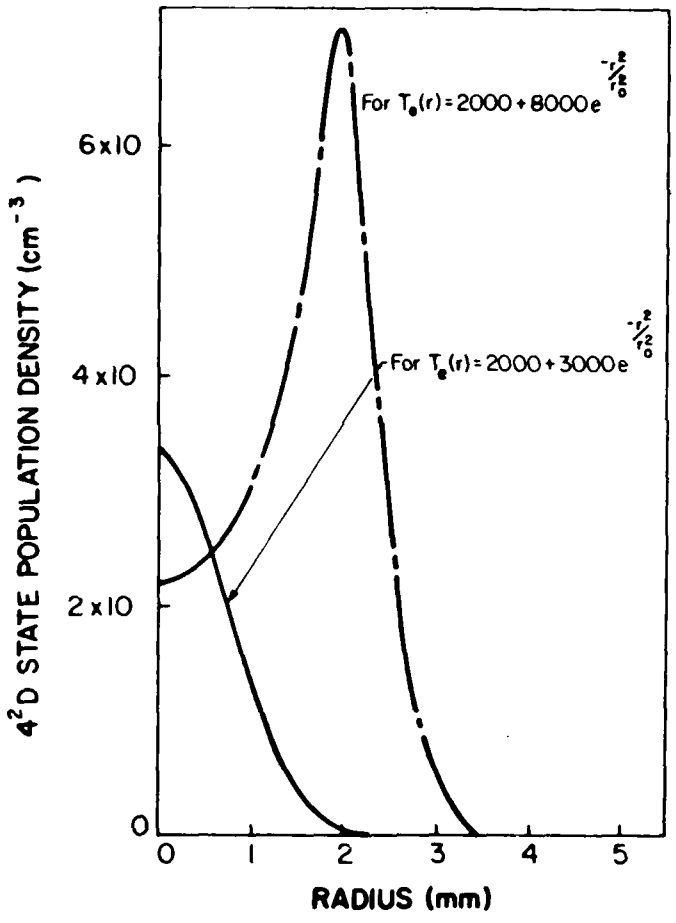


Fig. 5 Radial Distributions of 4D Population in a Sodium Plasma Corresponding to the Two Radial Electron Temperature Profiles Shown.

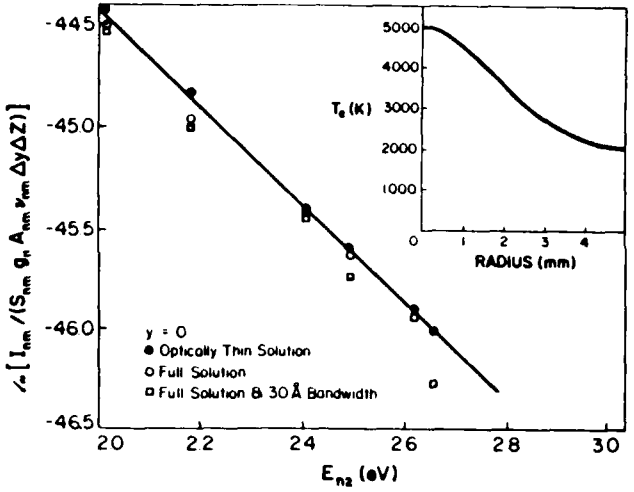


Fig. 6 Emission Data, Corresponding to the Full Solution of Figure 4(b) Observed with a 3nm Detection Bandwidth, are Added to Figure 4(b).

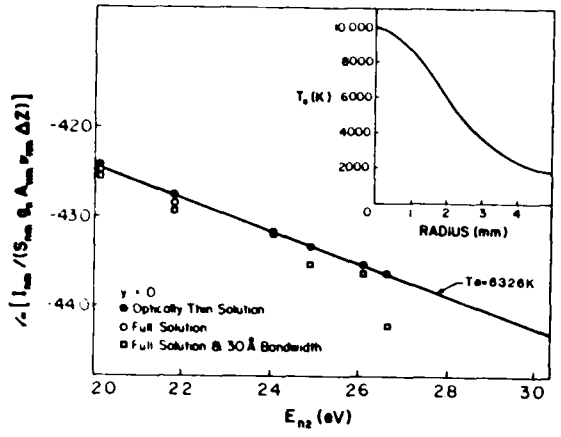


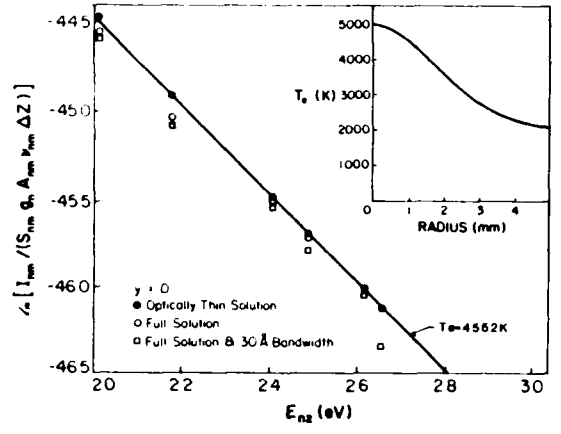


Fig. 7 Boltzmann Plots for Several Transitions Expected from Configuration B for a Sodium Plasma Assumed to have the Two Temperature Distributions Indicated in Figure 4 (a) and (b). Both Optically Thin and Full Solution Data are Presented. Solutions Corresponding to Observation with a 3nm Detection Bandwidth are also Presented.

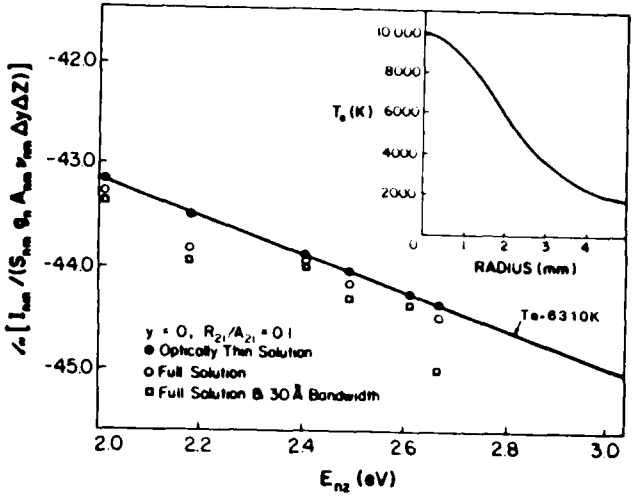


Fig. 8 Boltzmann Plot for Several Transitions Expected from Configuration A for a Sodium Plasma with a Radial Electron Temperature Distribution: $T_e(r) = (2+8e^{-r^2/r_0^2}) \times 10^3$k, $r_0$ = 2.5mm (See Inset) Assuming $R_{21}/A_{21}$ = 0.1.

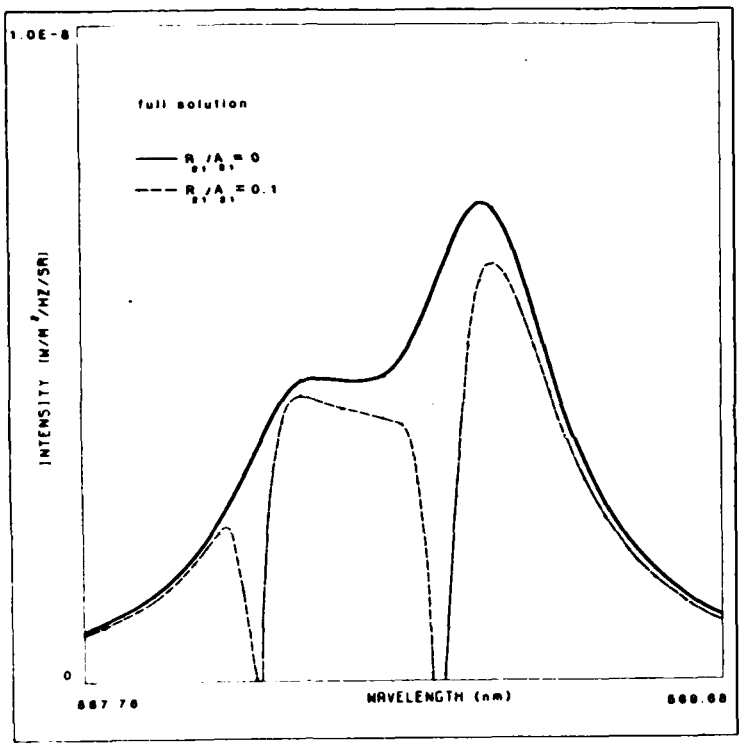


Fig. 9 Comparison of Computer Predicted $4^2D - 3^2P$ Multiplet Spectra for a Sodium Plasma with a Radial Electron Temperature Distribution. $T_e(r) = (2+8e^{-r^2/r_o^2}) \times 10^3 K$, $r_o$=2.5mm, Assuming $R_{21}/A_{21}$ = 0 (————), or 0.1 (--------).

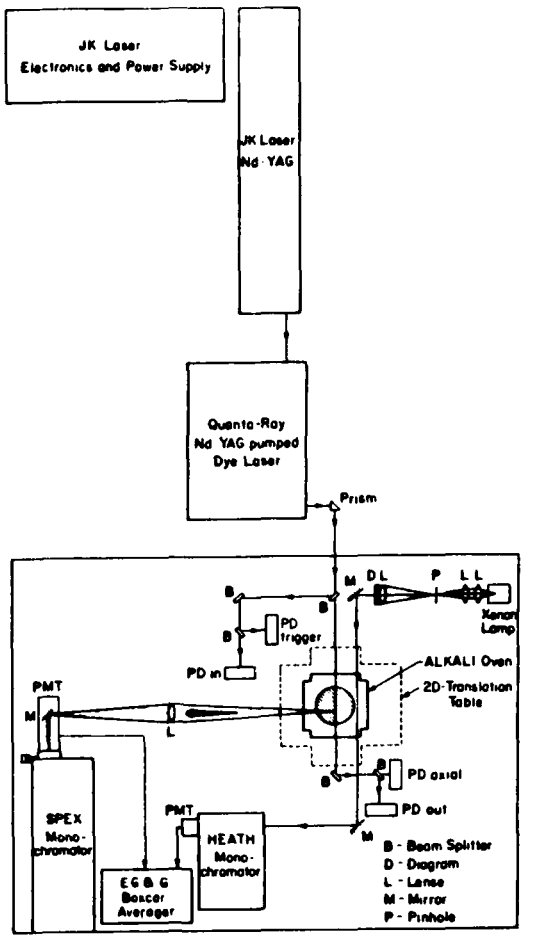


Fig. 10 Schematic of Experimental Facility for Creating Sodium Plasma By Laser Resonance Saturation.

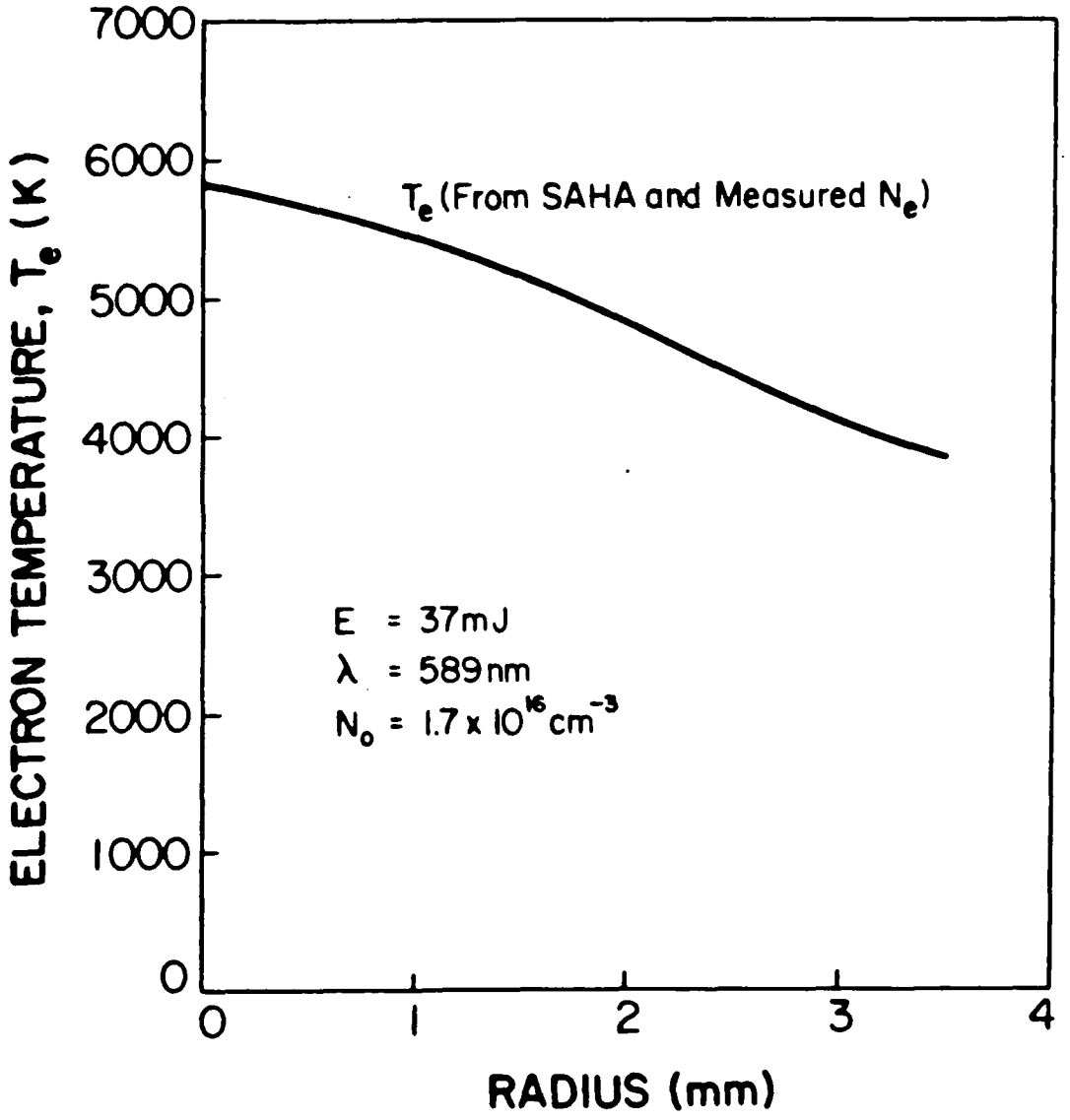


Fig. 11 Representative Free Electron Temperature Radial Profile Deduced From the Measured Electron Density Radial Profile Assuming LTE.

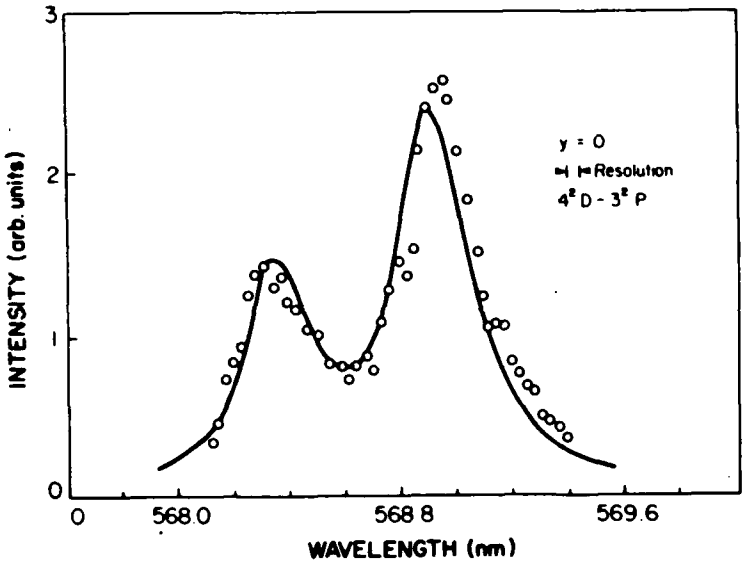


Fig. 12 Comparison of Measured $4^2D$-$3^2P$ Sodium Multiplet Spectrum with that Computed from the Electron Temperature Radial Profile Deduced from the Same Experiment.

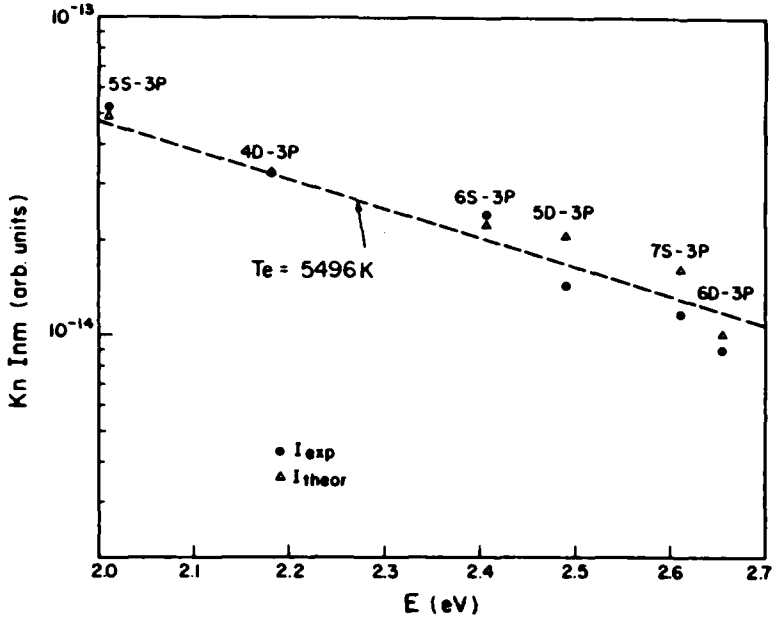


Fig. 13 Boltzmann Plot of the Experimental Data and Corresponding Computer Model.

APPENDIX D

# COMPUTER MODELING OF THE MULTISHOT AVERAGED SPECTRAL EMISSION FROM A LASER CREATED SODIUM PLASMA

R. S. Kissack, M. A. Cappelli and R. M. Measures

University of Toronto
Institute for Aerospace Studies
4925 Dufferin Street
Downsview, Ontario, Canada
M3H 5T6

## Abstract

The suitability of assuming a Gaussian radial profile for the incident laser pulse used in a computational model of a highly nonlinear interaction (laser resonance ionization of sodium vapor) is addressed when the predictions of this model are to be compared with the multishot average results of an experiment using radially noisy incident laser pulses.

## INTRODUCTION

The experimental measurements of spatial distributions of quantities such as electron density and temperature in a plasma are frequently derived from an analysis of the spatially integrated spectral radiances arising from high lying atomic or ionic transitions. In many pulsed experiments the spectral distribution of the emission is determined from a series of measurements at different wavelengths. If the shot-to-shot reproducibility is poor, or the signal is weak, the emission recorded in each spectral interval is an average of several shots. When the results of such experiments are to be compared with those predicted by a theoretical model, difficulties can arise if the shot-to-shot variation of the interaction responsible for the observed emission is appreciable and the dependence is highly nonlinear.

This situation is well illustrated in the case of plasmas created by laser resonance saturation. The ionization capability of resonantly tuned laser radiation was experimentally discovered by Lucatorto and McIlrath[1,2] and theoretically accounted for by Measures and his coworkers.[3,5] However, the strong attenuation of the laser pulse and the highly nonlinear

nature of the interaction may not have been fully appreciated by some experimenters.[6,7]

In this paper we have attempted to clarify the situation by reference to our own comparison of experiments and theoretical modeling. In essence, a laser pulse is fired through sodium vapor that is confined within a specially designed heat sandwich oven.[8] The wavelength of the laser pulse is tuned to closely coincide with the 589.6 nm sodium D-resonance line and its fluence is sufficient to saturate and subsequently ionize the vapor along its path. In most instances the laser pulse was axisymmetric but had some radial (noisy) structure.

In order to measure the electron density and temperature distributions within the resulting plasma column, the lateral spectral emission from several high lying transitions was monitored as a function of vertical (or y) displacement for a number of axial (or z) locations, see figure 1. The emission recorded in each spectral interval was averaged over a number of shots and the resultant signal variation with y for a given wavelength was inverted using the Abel transform[9] to yield the emission spectrum of the multiplets corresponding to various radial positions. The free electron density was then evaluated from these spectra using a knowledge of the Stark broadening of the various lines.[10] The electron temperature was determined from the relative intensities of several spectral lines.[11]

We have also developed a collisional-radiative computer code for modeling this new method of laser ionization.[5] This code uses a 5-level model of the sodium atom and predicts the temporal variation of the free electron density, electron temperature and other dynamic variables along the path of the laser pulse for a given incident laser pulse and an experimentally measured sodium atom distribution, taking into account absorption of the laser radiation. An example of the predicted variation of the free electron density $N_e$ and temperature $T_e$ produced along the path of a laser pulse with an energy fluence of 65 mJ cm$^{-2}$ is displayed as figure 2. The experimentally based sodium atom distribution $N_o(z)$ employed in this calculation is also indicated in figure 2.

To illustrate the highly nonlinear nature of the interaction we present in figure 3 the predicted variation of the free electron density, temperature and the $4^2D$ level population density $N_{4D}$, with incident laser energy fluence at the centre of the heat sandwich oven ($z = 0$) where the



peak sodium atom density is $1.7\times10^{16}$ cm$^{-3}$, at 58 ns from the start of a laser pulse having a 40 ns duration. These computational results clearly indicate that full ionization should be attained at this location (about 9 cm from where the laser pulse first enters the vapor) provided the incident laser energy fluence is greater than about 100 mJ cm$^{-2}$. However, both the free electron density and the free electron temperature are predicted to fall rapidly as the laser energy fluence drops below 100 mJ cm$^{-2}$. This suggests that a variation of about 10% around a mean value of 90 mJ cm$^{-2}$ for the laser energy fluence would lead to much greater fluctuations in the state of the plasma created at this location.

The real (experimental) situation is further complicated by the radial variation of the incident laser pulse. To model the three dimensional nature of the interaction we use the data from a series of computer runs at various laser fluences for a given sodium atom distribution, to synthesize the radial variation of the plasma properties ($N_e$, $T_e$, etc) at the z-location of interest.[5] For example, figure 4(a) displays the predicted free electron density and temperature radial profiles at 58 ns from the start of the laser pulse at the $z = 0$ axial location corresponding to the incident laser pulse radial profile also shown. The radial variation of this laser pulse is an extreme representation of the radial fluctuations observed in the experimental laser pulses. In figure 4(b), we present the radial profile of the resulting sodium $4^2D$ population corresponding to the same incident laser pulse since the Stark broadening measurements of $N_e$ are based on the emission from the ($4^2D$ - $3^2P$) multiplet.

In the experiments these variations in the radial distribution of the incident laser pulse led to a shot-to-shot fluctuation in the emission and necessitated the averaging of the emission detected in each spectral interval of a scan to ascertain the multiplet emission spectrum.

In our computational modeling of this laser ionization process we were forced to consider whether the use of a Gaussian radial profile for the laser pulse was adequate in light of the noisy radial distributions of the laser pulses used in the experiments and the strong nonlinearity of the interaction.

## MULTISHOT AVERAGE SPECTRUM DEFINITIONS

Generally speaking, the incident laser pulse is characterized by a given distribution and a number of defining parameters (e.g., peak fluence $E_p$, characteristic radius $r_c$, horizontal and vertical displacements of the axis of symmetry of the pulse $\delta_x$ and $\delta_y$, spectral bandwidth $\beta_\ell$, etc) which may vary from shot to shot. With this in mind, we introduce three different definitions of "multishot average spectrum" in an attempt to address the question posed at the end of the last section.

### Type 1 Average Spectrum

The characteristic parameters of the incident laser pulse assume their mean values. The multishot average ($4^2D$-$3^2P$) multiplet spectrum is then generated from a computer program[9] which solves the one dimensional radiative transfer equation using the radial distribution of the dynamical variables predicted by our LIBORS computer code[5] for the average incident laser pulse described above.

For purposes of this computational experiment the spatial profile of the pulse is assumed to be Gaussian with mean values $\bar{E}_p$ = 90 mJ cm$^{-2}$, $\bar{r}_c$ = 2.5 mm, $\bar{\delta}_x = \bar{\delta}_y = 0$, $\bar{\beta}_\ell$ (spectral analog of $\bar{r}_c$) = 0.015 nm. The line-centre wavelength of the laser is assumed to be 589.7 nm. It should be noted that in our comparisons with experiment to date, it is this Gaussian shaped laser pulse which we have used in our computer simulation of this interaction. It is the merit of this practice that we are addressing in this paper.

### Type 2 Average Spectrum

The incident laser pulse for the LIBORS code is the arithmetical mean of a finite (or possibly, in principle, infinite) number of shots. The corresponding multishot average multiplet spectrum is constructed as above.

In this computational experiment, however, some simplifying assumptions have been made. First, those parameters which characterize the spectral and temporal behaviour of the pulse are assumed to be constant from shot to shot in order to keep the computer costs within reasonable limits. Second, $\delta_x$ and $\delta_y$ were both assumed to be zero for each shot so that the average input laser pulse and the generated dynamical distributions are azimuthally symmetric.



### Type 3 Average Spectrum

Each noisy laser pulse (with a random displacement of its centre relative to the z-axis) is used to determine the radial distribution of excited states from which the lateral emission in the various spectral intervals is computed. The average value (over a given number of shots) of this spectral radiance is then computed and used to generate the Multishot Average ($4^2D$ - $3^2P$) Multiplet Spectrum.

This Type 3 - Average Spectrum is used to simulate the experimentally derived Multishot Average ($4^2D$ - $3^2P$) Multiplet Spectrum in order to answer the question posed earlier. That is to say, can a Gaussian shaped laser pulse be used to model the experiment with a reasonable number of shots? To rigorously test our simulation we deliberately chose the range of incident laser energy fluence to encompass the greatest rate of change of the free electron density.

To conclude this section, we point out that neither all of the characteristic spatial parameters which describe the incident laser pulse nor their associated probability distributions are known. This, coupled with the fact that any given pulse has a somewhat noisy spatial distribution experimentally, suggests that the radial profile for each "computational" shot needs to be constructed in a special manner. We now outline a method for doing this.

## COMPARISON OF COMPUTATIONAL AVERAGE SPECTRA

The "noiseless" incident radial energy fluence function

$$E(r) = E_p \exp\left[-\frac{r^2}{r_c^2}\right] \qquad (1)$$

is assumed to be Gaussian with a peak value $E_p$ and a characteristic (exponential) radius $r_c$. Laser pulses with a "noisy" radial distribution are produced in the following manner: the energy fluence at the $r_n$ ($n$ = 1, 2,...,10) radial position, $E(r_n)$, is regarded as a random variable with an associated Gaussian probability distribution characterized by the mean energy fluence

$$E_n = E_p \exp\left[-\frac{r_n^4}{r_c^4}\right] \qquad (2)$$

and by a standard deviation $\sigma_n$. In order to produce an appreciable noise level we set $\sigma_n = 0.25\ E_n$. $E(r_n)$ is selected via a random number generator and weighted according to the above Gaussian distribution. To allow for the possible jumping around of the laser pulse with respect to the z-axis (the centre of the field of view) we set the standard deviation in this displacement of the centre of the energy fluence profile to be 20% of $r_c$. In addition the computer spectrum corresponded to that which would have been observed at y = 1.5 mm in order to accentuate the sensitivity of the measurement to lateral displacement of the laser beam axis relative to the field of view.

In the numerical simulations we have chosen to model the ($4^2D$ - $3^2P$) multiplet spectrum created at z = 0, for a sodium atom distribution that is symmetrical about z = 0 and has its maximum value of $1.7\times10^{16}$ cm$^{-3}$. The time of observation is set at 58 ns from the start of the 30 ns duration laser pulse in order that the plasma be close to LTE. The mean value of the peak energy fluence (at r = 0), $E_p$ = 90 mJ cm$^{-2}$, was chosen so that much of the incident radial energy fluence distribution would lie in the 80-100 mJ cm$^{-2}$ range where the most rapid nonlinear change of $N_e$ and $r_e$ occurs, see figure 2. The exponential radius, $r_c$ = 2.5 mm, corresponds to the value in an actual experiment.

The comparison of Type 1 and Type 2 Average ($4^2D$ - $3^2P$) Spectra can be gauged by reference to figures 5(a) and 5(b). The Type 2 Average Spectrum is derived from 4 shots in the former case and 16 shots in the latter case. It is quite apparent that a considerable difference exists when only 4 shots are considered — indeed, a 20% difference in the free electron density would be predicted on the basis of this comparison. In contrast the Type 2 Average Spectrum derived from 16 shots appears to agree very closely with the Type 1 Average Spectrum which is the norm used in theoretical modeling and assumes the incident laser pulse to have a Gaussian radial distribution. This indicates that little difference would be expected in the computed spectrum if we used either a Gaussian radial profile or the actual averaged



radial profile for the laser pulse, provided we averaged over at least 16 shots.

In figures 5(c) and 5(d) we present a comparison of Type 2 and Type 3 Average ($4^2D$ - $3^2P$) Spectra for 4 and 16 shots respectively. It is again clear that while there is a significant difference between the spectra based on the 4 shot average, the spectra based on the 16 shot average agree quite well. This implies that computer modeling based on a 16 shot average laser pulse radial profile for laser pulses with a representative amount of noise in their radial profile can be expected to generate a spectra that is in good agreement with that measured in an actual experiment where the spectra is averaged over 16 shots. However, since we have shown in figures 5(a) and 5(b) that the spectra predicted on the basis of a 16 shot average of the actual laser pulse radial profile is in excellent agreement with that derived from a Gaussian laser radial profile, we can deduce that the Gaussian approximation is valid in the computer modeling provided the experimental data with which it is being compared is based on at least a 16 shot average.

## CONCLUSIONS

We are now in a position to answer the question posed earlier, that is to say, can a laser pulse with a Gaussian radial profile be used in computational modeling of a highly nonlinear interaction (such as laser ionization based on resonance saturation) when the experimental laser pulse has a noisy radial profile. From the analysis we have undertaken we can conclude that for our work computer modeling based on a Gaussian radial profile is acceptable provided the experimental results are averaged over about 16 shots.

## ACKNOWLEDGEMENTS

This work was supported by the U.S. Air Force Office of Scientific Research (under grant number AFOSR 85-0020) and the Natural Science and Engineering Research Council of Canada.

1. T. B. Lucatorto and T. J. McIlrath, Phys. Rev. Letters, 37, 428-431 (1976).
2. T. J. McIlrath and T. B. Lucatorto, Phys. Rev. Letters, 38, 1390-1393 (1977).
3. R. M. Measures and P. G. Cardinal, Physical Review A, 23, 8904-815 (1981).
4. R. M. Measures, P. G. Cardinal, G. W. Schinn, J. Appl. Phys., 52, 1269-1277 (1981) and 52, 7459 (1981).
5. R. Kissack, S. Wong, M. A. Cappelli and R. M. Measures, "Plasma Channel Formation Based on Laser Resonance Saturation" (submitted for publication in Phys. Rev. A).
6. D. J. Krebs and L. D. Shearer, J. Chem. Phys. 76, 2925 (1982).
7. O. L. Landen, R. J. Windfield, D. D. Burgess, J. D. Kilkenney and R. W. Lee, Physical Rev. A, 32, 2963 (1982).
8. M. A. Cappelli, P. G. Cardinal, H. Herchen and R. M. Measures, Rev. Sci. Instrum. 56, 2030-2037 (1985).
9. M. A. Cappelli and R. M. Measures, "Electron Density Radial Profiles Derived from Stark Broadening in a Sodium Plasma Created by Laser Resonance Saturation" (submitted for publication in JQRST).
10. H. R. Griem, "Spectral Line Broadening by Plasmas", Academic Press, N.Y. (1974).
11. M. A. Cappelli and R. M. Measures, "Effects of Inhomogeneities, Optical Depth and Finite Bandwidth on Electron Temperature Measurements in Cylindrically Symmetric Plasmas in LTE" (submitted for publication in J. of Optical Sensors).

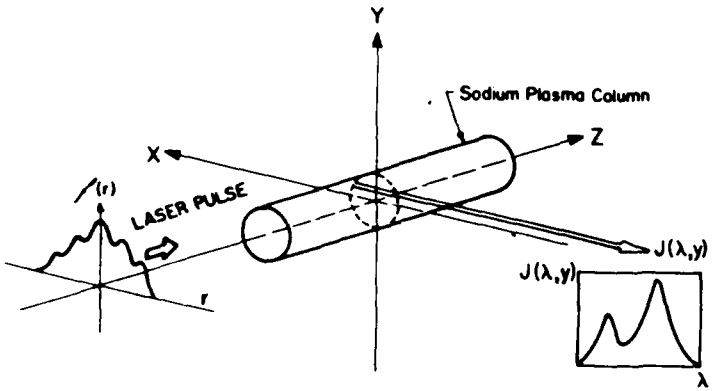


Figure 1. Schematic Configuration Showing the Incident Laser Pulse with Noisy Radial Profile and the Observed Spectrum Corresponding to a Line of Sight of Lateral Displacment-y.

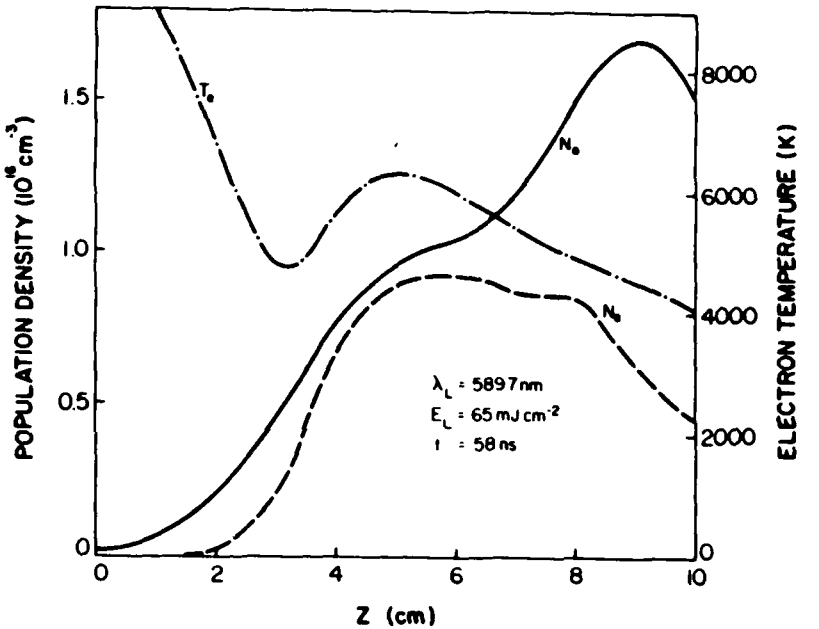


Figure 2. Computer Predicted Variation of the Free Electron Density and Temperature at t=58ns Along the Path of a (65mJcm$^{-2}$) Laser Pulse Tuned to 589.7nm. The Sodium Atom Number Density Distribution $N_0(z)$ is also shown.

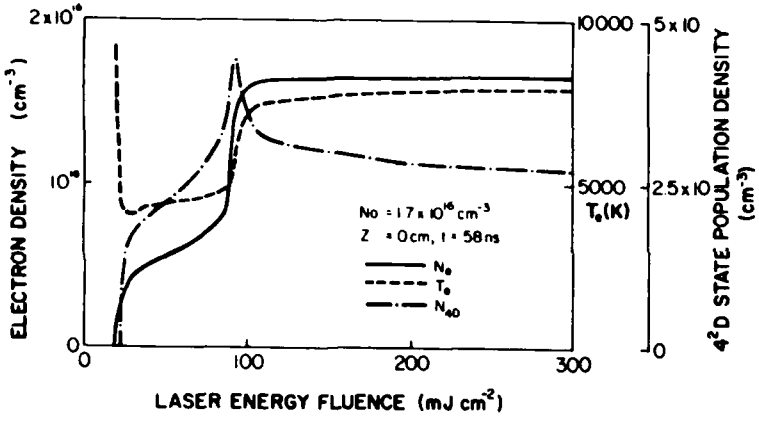


Figure 3. Dependence of the Free Electron Density, Temperature and the 4D Population Density on the Laser Energy Fluence.

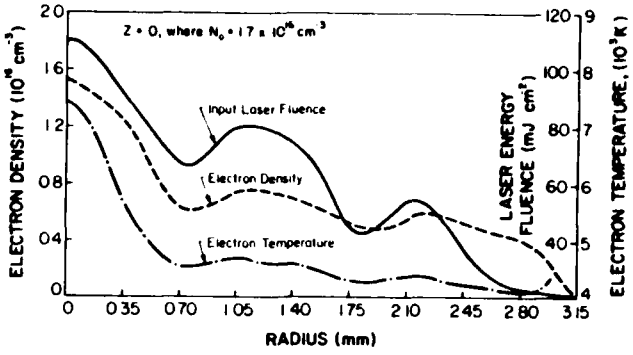


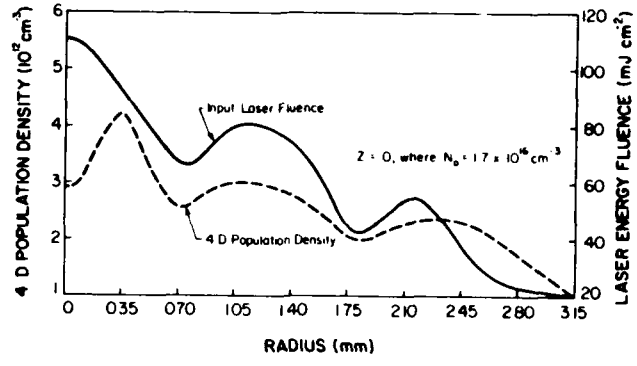


Figure 4. Computer Predicted Radial Variation of (a) Free Electron Density and Temperature, (b) 4D Population Density at t=58ns and Z=0. Also shown is the Noisy Radial Profile of the Incident Laser Pulse Used in the Computation.

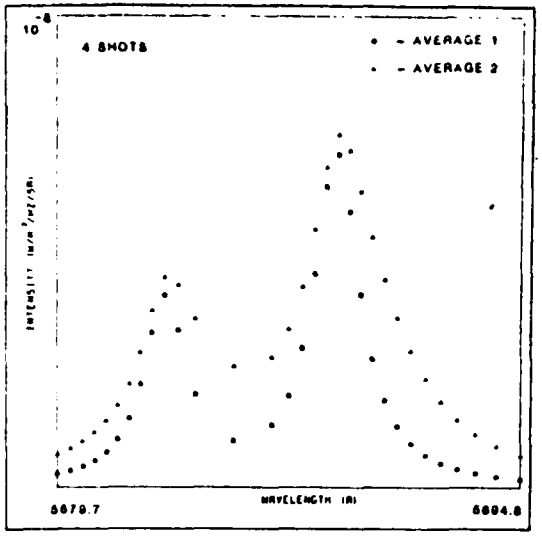


6 a)

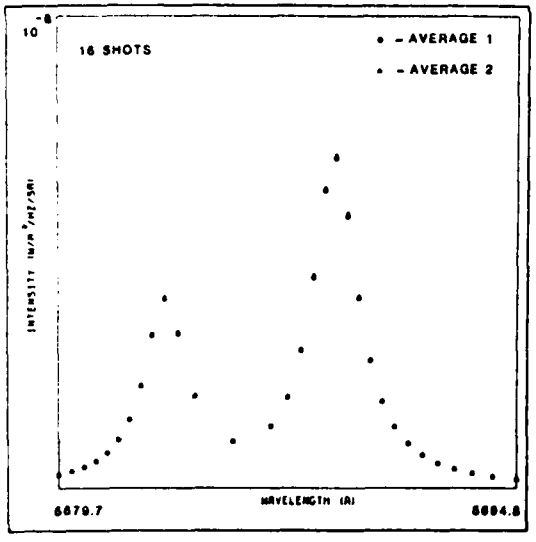


6 b)

Figure 5. (a) Comparison of Computer Generated 4-Shot Type 1 and Type 2 Average ($4^2D$-$3^2P$) Multiplet Spectra.
(b) Comparison of Computer Generated 16-Shot Type 1 and Type 2 Average ($4^2D$-$3^2P$) Multiplet Spectra.

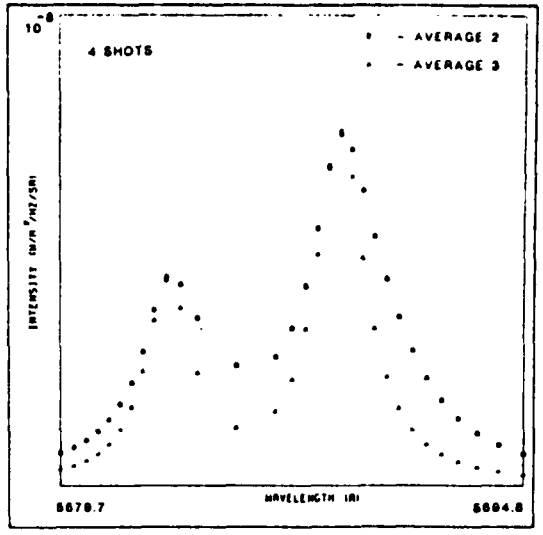


6 c)

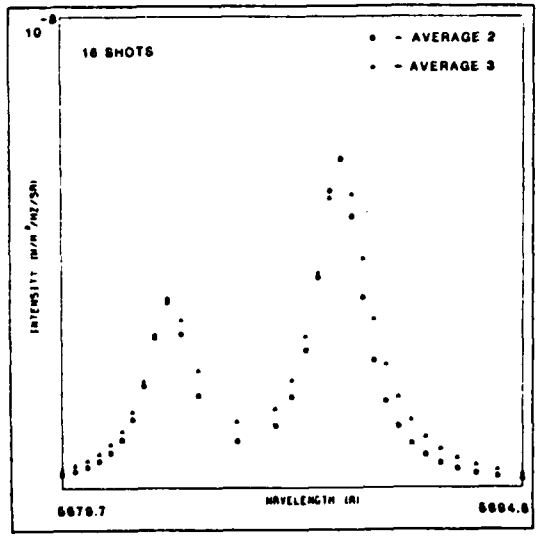


6 d)

Figure 5. (c) Comparison of Computer Generated 4-Shot Type 2 and Type 3 Average ($4^2D$-$3^2P$) Multiplet Spectra.
(d) Comparison of Computer Generated 16-Shot Type 2 and Type 3 Average ($4^2D$-$3^2P$) Multiplet Spectra.

# APPENDIX E

## PLASMA CHANNEL FORMATION THROUGH LASER RESONANCE SATURATION

M. A. Cappelli, S. K. Wong, R. S. Kissack and R. M. Measures

Institute for Aerospace Studies
University of Toronto
4925 Dufferin Street
Downsview, Ontario, Canada
M3H 5T6

ABSTRACT

We have developed a computer code that models the three dimensional nature of a sodium plasma created by laser resonance saturation. This was accomplished by taking account of the temporal and spatial distortion suffered by the laser pulse as it propagates through a nonuniform sodium atom distribution. We have also undertaken the first measurements of the radial and axial electron density and temperature profiles arising in such a plasma and have been able to demonstrate that our computer code predictions are in reasonable agreement with these results. Absorption of the laser ulse is found to be quite significant for even a few centimeters of $10^{16}$ $cm^{-3}$ sodium atom density and that as a result quite low temperature plasmas can be produced for modest energy laser pulses.

## INTRODUCTION

Laser saturation of an atomic resonance transition clearly involves radiatively locking the resonance and ground state populations in the ratio of their degeneracies.[1] Lucatorto and McIlrath[2,3] were the first to show experimentally that this interaction represents an effective method of producing near total ionization of alkali atoms. Subsequent experiments have not only verified this observation but have shown that this form of laser ionization can be extended to other elements.[4-7] There is growing evidence that absorption and superelastic electron quenching collisions together represent the primary mechanism for rapidly extracting from the laser pulse the large amount of energy needed to achieve this high degree of ionization.[4-16] This mechanism was first suggested by Measures,[17] and is schematically illustrated in figure 1. A useful overview of the subject was provided by Jahreiss and Huber.[5]

Measures and coworkers,[19-21] have proposed that laser ionization based on resonance saturation (LIBORS) proceeds in four stages: (i) the laser rapidly "locks" the ground and resonance level populations roughly in the ratio of their respective degeneracies, (ii) there is a rapid growth of free electrons due to one or more "seed ionization" processes and these electrons very quickly acquire energy through "superelastic collision quenching" of the laser maintained resonance state population, (iii) these "hot" electrons proceed to collisionally excite and ionize the resonance state atoms and in addition the collisionally excited higher lying levels are "photoionized" by the laser field, finally (iv) "runaway" collisional ionization of the upper levels occurs once some critical free electron density is achieved and this leads to near complete ionization burnout of the species.

However, it should be noted that if a very high rate of seed ionization exists the 4 states telescope to 3 and the burnout stage precedes almost directly from seed ionization.[19]

During the ionization burnout stage superelastic heating can no longer balance collisional cooling due to depletion of the resonance state population and consequently the electron temperature is predicted[19] to fall significantly. This effect has also been predicted by Morgan[22] who has modelled the ionization using the Boltzmann equation rather than assuming that the free electrons have a Maxwellian velocity distribution.

In the original formulation of our LIBORS collisional-radiative computer code the sodium atom was represented by a 20-atomic level model and we assumed a step-like laser pulse.[19-21,23] An example of the temporal behaviour of the free electron density, free electron temperature, resonance state density, and ground state density predicted by this code modified to include a realistic flashlamp pumped dye laser pulse (such as used in the early experiments[6,7]) is presented in figure 2. Also shown on this figure is the assumed temporal growth of the laser irradiance. The influence of molecular nitrogen on this ionization process has also been considered by Measures et al[24] and Wong.[25] In an actual experiment the laser pulse propagates through a non-uniform atom density distribution and suffers appreciable absorption due to the strong nature of the interaction. This can lead to a considerable temporal and spatial distortion of the laser pulse. Consequently, the atoms at different locations along the path of the laser pulse are subject to progressively less energy and to a shorter period of excitation.

In order to better model the real effects associated with creating a plasma channel by laser resonance saturation we have undertaken the first analysis that takes account of both laser absorption and the non-uniform atom density distribution along the path of the laser pulse. We have also taken into account the spatial and temporal profile of the laser pulse.

In order to test this theoretical work we have attempted to computationally simulate as closely as possible experiments that we have undertaken using a specially designed sodium heat sandwich oven[26] and a Nd-YAG laser pumped dye laser.

## 5-LEVEL ATOM MODEL

In an attempt to keep the analysis economically viable we replaced our 20-level model of the sodium atom[19-21,23] with the simplified 5-level model[25] shown in figure 3. Although 5 levels are indicated in figure 3, we assume that the collisional coupling between levels 3 ($4^2S$), 4 ($3^2D$) and 5 ($4^2P$) is sufficiently rapid that their populations are maintained in a Boltzmann equilibrium. This assumption permits us to treat this trio of levels as a manifold and thereby reduce the number of atomic level rate

equations to three. In effect we consider only the collisional-radiative processes "into" and "out of" this (3-4-5) level manifold.

The remaining 15 high lying energy levels used in the 20-level model (not shown in figure 3) are partially taken into account by assuming that electron excitation to them (from any of the five lower levels) leads, in effect, to immediate ionization of the atom. We therefore introduce the 5-level "effective" electron collisional ionization rate coefficient for each of the low lying levels (m = 1 to 5) defined by the relation

$$K^*_{mc} = \sum_{n=6}^{21} K_{mn} \qquad (1)$$

where $K_{mn}$ represents the electron collisional rate coefficient between levels m and n. Note that $K_{m21}$ is the m-level electron collisional ionization rate coefficient according to the 20-level model of the sodium atom. The corresponding "effective" three body recombination rate coefficient to each of the low lying levels (m = 1 to 5) is similarly constituted to take account of recombination to the higher levels, followed by a rapid cascade down to the lower levels. We thus introduce

$$K^*_{cm} = \sum_{n=6}^{20} K_{cn} p(n,m) \qquad (2)$$

where $K_{cn}$ represents the three-body recombination rate coefficient to level n used in our 20-level LIBORS code and p(n,m) is introduced as the effective probability that a captured free electron arriving in level n subsequently decays to level m. In principle radiative recombination could be included into the effective recombination rates but for our conditions its omission was found to lead to negligible error.[25]

In calculating the electronic excitation rate coefficients we have averaged Seaton cross-sections[27] for the optically allowed transitions, and Gryzinski cross-sections[28] for all other transitions, over a Maxwellian velocity distribution. In the case of the resonance transition) the experimental value of Crandall et al,[29] was employed. Although both Seaton and Gryzinski collision rates were employed for transitions between

the 5 lower levels only Seaton collision rates were used for transitions that terminated above level 5.

We have found that close agreement can be obtained between the 5 and 20-level LIBORS codes if these probability factors are generally[†] given by the expression

$$p(n,m) = \frac{N_e K_{nm} + A_{nm}}{N_e(K_{nm} + \sum_q K_{nq} + K_{nc}) + A_{nm} + \sum_q A_{nq}} \qquad (3)$$

where $N_e$ is the free electron density, $A_{nm}$ the Einstein spontaneous transition probability between levels n and m, with q being the levels within the manifold that are optically connected to level n.

The 5-level model can thus be described by the following set of equations: first we have the three atomic level population rate equations,

$$\frac{dN_1}{dt} = (N_2 - gN_1)R_{21} + N_2C_{21} + N_5C_{51} + N_e(N_3K_{31} + N_4K_{41})$$

$$+ N_e{}^3K^*_{c1} - N_1[N_e\{\sum_{m=2}^{5} K_{1m} + K^*_{1c}\}] \qquad (4)$$

$$\frac{dN_2}{dt} = (gN_1 - N_2)R_{21} + N_e(N_1K_{12} + N_5K_{52}) + N_3C_{32} + N_4C_{42}$$

$$+ N_e{}^3K^*_{c2} - N_2[N_e\{\sum_{m=3}^{5} K_{2m} + K^*_{2c}\} + C_{21}] - N_2{}^2v(\sigma_L F + \sigma_A) - N_2\sigma^{(2)}_{2c}F^2 \qquad (5)$$

and

---

[†]In order to obtain the close agreement (indicated later) between the 5 and 20-level LIBORS codes it was found necessary to set $K_{nc} \approx 0$, for n = 17, 12 and 8, i.e., the 6f, 5f and 4f levels of sodium. As a consequence, p(n, 4) = 1 for n = 17, 12 and 8 because these levels are only optically coupled to level 4 of the manifold.

$$\frac{dN_3^*}{dt} = N_e\left[\sum_{m=3}^{5} (N_1K_{1m} + N_2K_{2m} + N_e{}^2K_{cm}^*)\right] - N_3(C_{32} + N_eK_{31} + P_{3c})$$

$$- N_4(C_{42} + N_eK_{41} + P_{4c}) - N_5(C_{51} + N_eK_{52} + P_{5c}) \qquad (6)$$

where we have introduced the (3-4-5) level manifold population density

$$N_3^* = N_3 + N_4 + N_5 \qquad (7)$$

As indicated we assume that the close spacing of these three levels ensures collisional equilibrium and consequently that the internal distribution of this manifold is described by a Boltzmann distribution. In which case

$$N_j = N_3^* / U_j(T_e) \qquad (8)$$

where

$$U_j(T_e) = \sum_{m=3,4,5} g_{mj} e^{-E_{mj}/kT_e} \qquad (9)$$

with $g_{mj} \equiv g_m/g_j$ and $E_{mj} = E_m - E_j$ ($j = 3$, 4 or 5). In order to streamline the equations as far as possible we also introduced the notation,

$$C_{nm} = N_eK_{nm} + A_{nm} \qquad (10)$$

and

$$P_{nc} = \sigma_{nc}F + N_eK_{nc}^* \qquad (11)$$

where $\sigma_{nc}$ is the single photon ionization cross section for level n and F is the laser photon flux density, i.e.,

$$F(t) = \frac{1}{h\nu} \int I^{\ell}(\nu,t)d\nu \qquad (12)$$

where $I^{\ell}(\nu,t)$ is the laser spectral irradiance at time t and $h\nu$ the laser photon energy. In the above equations we have also introduced the

resonance to ground level degeneracy ratio g and the stimulated emission rate per resonance state atom,

$$R_{21}(t) = \frac{B_{21}}{4\pi} \int I^{\ell}(\nu,t) L_{21}(\nu) d\nu \qquad (13)$$

where $B_{21}$ is the Milne stimulated emission coefficient and $L_{21}(\nu)$ is the line profile function (we shall further discuss this later) for the resonance transition.

The appropriate electron energy equation can be expressed in the following form:

$$\frac{d}{dt}(N_e \varepsilon_e) = N_e \sum_{\substack{n=2 \\ (n\neq m)}}^{5} \sum_{m=1}^{2} N_n K_{nm} E_{nm} + N_e{}^3 \sum_{m=1}^{5} K^*_{cm} E^{\#}_{cm} + \sum_{m=3}^{5} (E_{21} - E_{cm}) N_m \sigma_{mc} F$$

$$- N_e \sum_{\substack{m=1 \\ (n\neq m)}}^{2} \sum_{n=2}^{5} N_m K_{mn} E_{nm} - N_e \sum_{m=1}^{5} N_m K^*_{mc} E_{cm} - N_e{}^2 H_{ei}$$

$$- N_e [N_1 H_{e1} + N_2 H_{e2}] + S \qquad (14)$$

where $\varepsilon_e$ represents the free electron mean thermal energy (taken as $\frac{3}{2} kT_e$), and $H_{ei}$, $H_{e1}$ and $H_{e2}$ represent the rates of elastic energy transfer to ions and the ground and resonance state atoms through Coulomb scattering collisions[30] and hard sphere collisions,[31] respectively. S corresponds to the source of electron energy arising from the various seed ionization processes, i.e.,

$$S = (2E_{21} - E_{c2}) \{N_2 \sigma^{(2)}_{2c} F^2 + \tfrac{1}{2} N_2{}^2 v \sigma_L F\} + \tfrac{1}{2} N_2{}^2 v \sigma_A E_A \qquad (15)$$

Here $\sigma^{(2)}_{2c}$ represents the resonance state two photon ionization coefficient, $\sigma_L$ the laser assisted Penning ionization coefficient, and $\sigma_A$ the effective associative ionization cross section which is taken to be an F-dependent empirical fit to the experimental work of Roussel et al.[11] $E_A$ is the

effective energy of creation for the electrons liberated by this latter process and v represents the mean atom collisional velocity. Equation (14) is solved in conjunction with the ionization ($\dot{N}_e$) equatiion. A detailed discussion of the 20-level atomic code and a comprehensive review of the various seed ionization processes with the relevant cross sections used is provided by Cardinal.[31]

It should be noted that another fine adjustment in the form of a small reduction (of about 0.055 eV) in the three-body recombination energy was found to bring the results of the 5-level LIBORS code into excellent agreement with the 20-level code over a wide range of densities.[25] This modified energy is designated by $E^{\#}_{cm}$ in equation (14).

The electron-ion energy exchange rate $H_{ei}$ is proportional to $(T_e - T_i)$[30] and therefore it is necessary to evaluate the ion temperature. This is accomplished through simultaneously solving the ion energy equation,

$$\frac{d}{dt}(N_i \varepsilon_i) = N_e^2 H_{ei} - (N_o - N_e)N_e H_{ia} - N_A N_e H_{iA} + \varepsilon_a \dot{N}_i^I - \varepsilon_i \dot{N}_i^R \qquad (16)$$

where we assume that $N_e = N_i$ and $\varepsilon_i$ and $\varepsilon_a$ are the mean thermal energies of the ion and atom, respectively. The second and third terms in equation (16) takes account of elastic cooling collisions between the sodium ions and the background of sodium and argon buffer gas atoms. $(N_o - N_e)$ and $N_A$ represent the sodium and argon atom densities while $H_{ia}$ and $H_{iA}$ represent respective rates of elastic energy exchange between the ions and the background of neutral sodium and argon atoms[32,33]

$$H_{iA} = \langle \sigma v \rangle_{iA} \frac{4 m_i m_A}{(m_A + m_i)^2} \left(1 + \frac{m_i T_A}{m_A T_i}\right)^{1/2} k(T_i - T_A) \qquad (17)$$

where $\langle \sigma v \rangle_{iA}$ is the effective ion-argon collision frequency and $T_A$ the argon atom's translational temperature. A similar expression is used in the case of $H_{ia}$, with $m_i = m_a$ in this instance. The last two terms in Eq. (16) takes account of the net gain or loss of energy to the ions resulting from their creation from atoms or their conversion back to atoms.

This background density of argon atoms varies across the sodium vapor region such that the sum of the partial pressures equals the pressure of the argon in the water cooled peripheral region. The initial vapor temperature at each location is deduced from the optically measured sodium density profile using the vapor pressure curves provided by Nesmeyanov.(34) By a similar argument to that given above it follows that since $H_{iA}$ is proportional to the difference in temperature between the sodium ions and the argon atoms, the latter shall be computed. We have assumed that the argon's temperature is not changed appreciably. It should also be noted that an electron-argon elastic energy loss term was introduced into the free electron energy equation. To complete the set of energy equations we have also included an equation for the mean thermal energy of the neutral sodium atoms.

Combining equations (12) and (13) enables us to write the stimulated rate of emission per atom in level 2 in the form

$$R_{21}(t) = \frac{\lambda^2}{8\pi\tau_{21}} F(t) \int_{-\infty}^{\infty} L^{\ell}(x_{\ell}-x) L_{21}(x)dx \qquad (18)$$

where $\lambda$ is the appropriate wavelength and $\tau_{21}$ the radiative lifetime of level 2 and x is a dummy frequency variable introduced below with $x_{\ell}$ corresponding to the laser frequency.

In reality level 2 for the sodium atom comprises the two fine structure levels: $3^2P_{3/2}$ and $3^2P_{1/2}$ and so the reciprocal of the effective lifetime

$$\frac{1}{\tau_{21}} = \frac{1}{2} \left[A(3^2P_{3/2}, 3^2S_{1/2}) + A(3^2P_{1/2}, 3^2S_{1/2})\right]. \qquad (19)$$

Half the sum of the Einstein spontaneous transition probabilities for the two resonance transitions is taken because in equations (4) and (5) we use $N_2$, the total population of the $3^2P$ term.

The corresponding doublet line profile function for the sodium resonance lines,

$$L_{21}(x) = \left[\frac{2}{3} L_{3/2}(x) + \frac{1}{3} L_{1/2}(x + \Delta)\right] \qquad (20)$$

The dummy frequency variable

$$x \equiv \nu - \nu_{3/2} \tag{21}$$

where $\nu_{3/2}$ represents the center line frequency for the $(3^2P_{3/2} - 3^2S_{1/2})$ transition (at 589.0 nm) and $\Delta = \nu_{3/2} - \nu_{1/2}$ is the frequency separation of the doublet. $L_{3/2}(x)$ and $L_{1/2}(x+\Delta)$ are the respective line profiles of the individual resonance transitions. We have assumed a Lorentzian line profile function of the form

$$L_{3/2}(\nu - \nu_{3/2}) = \frac{1}{\pi} \cdot \frac{\gamma_a}{(\nu-\nu_{3/2})^2 + \gamma_a^2} \tag{22}$$

where $\gamma_a$ is the appropriate HMHW bandwidth [a combination of the Stark width and the resonance width].[25,26,35]

We have also introduced the spectral distribution function for the laser radiation

$$L^{\ell}(\nu_{\ell} - \nu) = \frac{I^{\ell}(\nu, z, t)}{h\nu F(z, t)} \tag{23}$$

and assumed that it is approximated by a Gaussian, i.e.,

$$L^{\ell}(\nu_{\ell}-\nu) = \frac{1}{\beta_{\ell}\sqrt{\pi}} e^{-[(\nu_{\ell}-\nu)/\beta_{\ell}]^2} . \tag{24}$$

In reality, there would be some degree of spectral hole burning expected as the laser pulse propagates through the vapor but as shown by Measures and Herchen[36] Wong,[25] the omission of this feature does not lead to appreciable error. Consequently, the convolution of the two profiles in (18) can be expressed in the form of a Voigt function,

$$V(\delta,u) = \frac{\delta}{\pi^{3/2}} \int_{-\infty}^{\infty} \frac{e^{-y^2}dy}{\delta^2 + (u-y)^2} \tag{25}$$

where

$$\delta \equiv \gamma_a/\beta_\ell, \quad y \equiv (x_\ell - x)/\beta_\ell, \quad u \equiv x_\ell/\beta_\ell \quad \text{and} \quad V(\delta, u)du = V(\delta, v)dv$$

It is important to notice that this Voigt function depends upon $\delta$ - the ratio of the atomic bandwidth to the laser bandwidth and to the frequency separation of the atomic and laser center frequencies normalized by the laser bandwidth, i.e.,

$$u = \frac{\nu_\ell - \nu_{3/2}}{\beta_\ell} \tag{26}$$

The form of equation (18) leads us to introduce an "effective cross-section" for stimulated emission of the resonance doublet,

$$\sigma_{21}^{\ell} = \frac{\lambda^2}{8\pi\tau_{21}} \int_{-\infty}^{\infty} L^{\ell}(x_\ell - x) L_{21}(x)dx \tag{27}$$

We recognized from the outset that attenuation of the laser pulse could lead to relatively sudden changes in the laser irradiance and that in many experiments short laser pulses are used. Consequently in our comparison of the 5 and 20-level computer codes we used the truncated laser pulse indicated as F in figure 4. With a laser pulse of this shape the comparison was tested fairly severely. Figure 4 indicates the excellent agreement obtained between the 5 and 20-level models for a sodium density ($N_0$) of $4\times10^{16}$ cm$^{-3}$. It is evident from figure 4 that $N_2/N_1$ falls from the saturated value of 3.0 at about the time of ionization burnout even though F is still increasing. This temporal minimum is attributed to the sudden increase in the superelastic quenching rate which for the given laser irradiance can overwhelm the stimulated emission rate as full ionization is achieved.

It is apparent from figure 4 that the 5-level LIBORS code mirrors very closely the predictions of the 20-level code in regard to the temporal behaviour of the parameters: $N_e$, $T_e$, $T_i$, $N_2$ and $N_1$. We feel that the small ($\lesssim$ 20%) difference in the lead time between the two sets of curves is quite acceptable. In order to check that this close agreement was not fortuitous to this particular density we ran comparisons at two additional densities ($N_0 = 5\times10^{15}$ and $10^{16}$ cm$^{-3}$) and found the same close

agreement.[25]

## RADIATIVE TRANSFER EQUATION FOR AN EXTENDED VAPOR REGION

The large cross section involved in laser resonance saturation leads to appreciable absorption of the laser pulse as it propagates through the atomic vapor. Consequently, any realistic simulation of plasma channel formation based on this interaction must take account of this fact and we are therefore led to consider the radiative transfer equation. For a laser pulse propagating in the z-direction we can write

$$\frac{1}{c}\frac{\partial F}{\partial t} + \frac{\partial F}{\partial z} = (N_2 - gN_1)R_{21} - N_2\sigma_{2c}^{(2)}F^2 - \frac{1}{2}N_2^2 v\sigma_L F - \sum_{m=3}^{5} N_m\sigma_{mc}F \qquad (28)$$

The first term on the right hand side takes account of the net loss of laser photons due to absorption in the resonance transition, the second term allows for two photon ionization of the resonance level, the third term involves laser assisted Penning ionization of the resonance level and the last term refers to single photon ionization of the levels within the (3-4-5) level manifold.

For the time scale of interest in our experiments the velocity of light c can be treated as infinite. Under these circumstances (28) is simplified to the steady state form given by

$$\frac{dF}{dz} = (N_2 - gN_1)\sigma_{21}^{\ell}F - N_2\sigma_{2c}^{(2)}F^2 - \frac{1}{2}N_2^2 v\sigma_L F - \sum_{m=3}^{5} N_m\sigma_{mc}F \qquad (29)$$

where $\sigma_{21}^{\ell}$ was given by equation (27).

It is quite clear that addressing the problem of laser resonance saturation for an extended vapor region involves the solution of the population and energy equations indicated earlier, together with this radiative transfer equation in both space and time. We decided to tackle this problem by dividing the irradiated vapor column into a series of slabs, see figure 5, each of which was assumed to have a uniform atom density equal to the average experimentally measured sodium atom density

for that segment of vapor. The thickness of each slab was determined by the requirement that at least 99% of the energy incident on any given slab be transmitted to the next slab[33] that the maximum value be limited to 1 mm

Within each slab the population and energy equations are numerically integrated (using an IMSL subroutine DGEAR[33]), subject to the laser pulse exiting the previous slab to provide the temporal history of the various parameters: $N_e$, $T_e$, $T_i$ $N_3^*$, $N_2$ and $N_1$. In this multislab model, equation (29) is solved and the laser photon flux density exiting the $i^{th}$ slab (bounded by $z_i$ and $z_{i-1}$)

$$F(z_i, t) = F(z_{i-1}, t)e^{-p_i \Delta z} \tag{30}$$

and is seen to be expressed in terms of the incident value $F(z_{i-1}, t)$. In this equation

$$p_i = \left[(gN_1 - N_2)\sigma_{21}^{\ell} + N_2\sigma_{2c}^{(2)}F(z_{i-1}, t) + \frac{1}{2}N_2^2 v\sigma_L + \sum_{m=3}^{5} N_m\sigma_{mc}\right]_i \tag{31}$$

and

$$\Delta z = z_i - z_{i-1} \tag{32}$$

This is permissible because the loss of laser energy through two photon ionization is small compared to that extracted through resonance pumping. The right-hand side of equation (31) is evaluated using the mean values of the parameters associated with the $i^{th}$ slab. The value of $F(z_i, t)$ for each time step is stored and then used for calculating the temporal variation of the parameters in the subsequent $(i+1)^{th}$ slab.

The incident temporal laser profile used in these calculations was chosen to approximate the experimental laser pulse by an analytical curve of the form

$$F^{\ell}(o, t) = \varepsilon_{\ell} a t^b e^{-ct^2} \tag{33}$$

where b and c were constants determined from the experiment and $\varepsilon_\ell$ is the energy fluence in the laser pulse "a" is determined from the relation,

$$\int_0^{\tau_\ell} a t^b \, e^{-ct^2} \, dt = 1 \qquad (34)$$

## EXPERIMENTAL FACILITY

The experimental facility developed for this research is schematically illustrated in figure 6. The second harmonic of a Neodymium-YAG laser (JK HY750) was used to pump a dye laser (Quanta-Ray PD1). Using Kiton Red-620 dye (Exciton Chemical Co.) an output of about 40 mJ at a 10 Hz repetition rate was obtained over a wavelength range that included the two sodium D lines at 589.0 and 589.6 nm. The dye laser's spectral full width half maximum FWHM was measured to be about 0.02 nm.

A specially designed heat sandwich oven was used to generate a disc-shaped zone of sodium vapor. This oven is in the form of a rectangular box with circular heater plates and steel wicks, top and bottom, surrounded by cooling water coils to prevent the sodium vapor from reaching the four windows that provide 360° optical access. A more detailed description of the method of measuring the sodium atom density distribution is provided elsewhere.[26]

The electron density measurements were undertaken using a sideways mounted SPEX 1700 II monochromator. This enables the entrance slit of the monochromator to sample a thin horizontal slab of the plasma emission at a height y (scanned by adjusting the input optics) above the axis of the laser beam. The magnification of the optics was 1:1 with the SPEX entrance slit at 1 cm × 40 μm.

The signal from the RCA C31034 photomultiplier mounted on the SPEX monochromator was processed by an EG&G 4420 Signal Averager that was typically gated to sample the emission in a 2 ns interval, some 65 ns after the start of the laser pulse. Since the laser pulse duration was less than 40 ns, the influence of the laser field (through the dynamic Stark effect) should be minimal and spontaneous and electron collision induced decay of the resonance state population should minimize optical depth effects.

In order to evaluate the radial profile of the free electron density $N_e(4r)$, spectral scans of the $4^2D$-$3^2P$ multiplet were taken for 15 lateral (y) positions across the plasma column. The spectral resolution was estimated to be 0.05 nm (FWHW) with 16 laser shots being averaged to constitute one intensity measurem,ent (at a given wavelength) and 128 such measurements comprise one spectral scan.

## COMPARISON OF COMPUTATIONAL AND EXPERIMENTAL RESULTS

The present form of our LIBORS computer code predicts the state of the plasma formed along the direction of propagation for a given sodium atom distribution and a temporally prescribed laser field. In an experiment the laser field also has a radial variation and this has to be taken into account if we wish to model the three dimensional nature of the interaction. To accomplish this we have assumed that the incident laser pulse has a Gaussian radial distribution (the justification for this is presented elsewhere[33]), and the same temporal history given by equation (33), at each radial position.

A series of computer runs for a range of incident laser energy fluences was then undertaken. The state of the plasma at any position can then be predicted from these computer runs by assigning tne appropriate laser energy fluence to each radial position. By way of example we have displayed in figure 7 the predicted axial variation in the free electron density $N_e(z)$ corresponding to four radial positions (r = 0, 1.25, 2.55 and 3.55 mm) 65 ns after the start of the laser pulse for the experimentally based sodium atom distribution $N_o(z)$ also shown. The incident laser pulse used to generate these results wasa assumed to have the temporal variation given by equation (33) with b = 2.64, c = $6.5\times10^{-3}$ and $\tau_\ell$ = 40 ns and a Gaussian radial profile with an energy of 25 mJ and $r_o$ = 2.5 mm. These four radial positions corresponded to incident laser energy fluences of: 127.3, 95, 55 and 17 (mJ $cm^{-2}$) for this particular laser pulse.

A comparison of the free electron density achieved at equidensity axial locations in figure 7 reveals that both the electron density and the radius of the plasma column core diminishes as the laser pulse penetrates further into the sodium vapor. This effect is even more obvious in figure

8 where the predicted full radial profile of the electron density created by this laser pulse is displayed.

This reduction and narrowing of the core plasma density is a direct consequence of the absorption suffered by the laser pulse as it propagates through the sodum vapor (from -ve to +ve z values). In figure 9 we present the axial variation of the fraction of transmitted laser energy fluence for several incident values of laser energy fluence for the sodium atom distribution shown in figure 7. It can be seen that the smaller the incident laser energy fluence the greater its percentage attenuation in propagating through the sodium vapor. It follows that the radial profile of a laser pulse will tend to steepen as it propagates since its high intensity core will be proportionately less reduced than its weaker outer region.

In contrast to the rapid decline of the core electron density with axial position, the low electron density halo, see figure 8, is predicted to fall less rapidly with axial position. This behaviour can be understood in terms of the shoulder in the dependence of $N_e$ on the incident laser energy fluence for a given sodium atom distribution. This is illustrated for the simulation under consideration in figure 10, where the variation of $N_e$ at t = 65 ns and Z = -4, 0 and 4 cm are plotted as a function of the incident laser energy fluence.

We can interpret the $N_e$-shoulder seen on the Z = 4 cm curve [$30 < \varepsilon_\ell < 110$ (mJ $cm^{-2}$)] in terms of our four stage model of LIBORS discussed earlier.[19] For $\varepsilon_\ell > 110$ (mJ $cm^{-2}$) full ionization burnout is approached, while in the range: $30 < \varepsilon_\ell$ 110 (mJ $cm^{-2}$) the degree of ionization attained is determined by the energy invested in saturating the atoms. This resonance state energy is then converted into ionization through superelastic collisional heating of those electrons produced by the seed ionization process. In essence each atom can only contribute one laser photon in this regime (compared to being cycled many times with longer more intense laser radiation) and so the degree of ionization attained is almost independent of the laser energy fluence under these conditions. This suggestion is borne out when the computer predicted energy loss per cm path length is compared with the energy required to saturate the atoms per cm at this location.

AD-A172 945 THE APPLICATION OF LASER SATURATION TO THE EFFICIENT 2/2
GENERATION OF SHORT (U) TORONTO UNIV DOWNSVIEW
(ONTARIO) INST FOR AEROSPACE STUDIES R M MEASURES
UNCLASSIFIED MAY 86 AFOSR-TR-86-0906 AFOSR-85-0020 F/G 20/5 NL

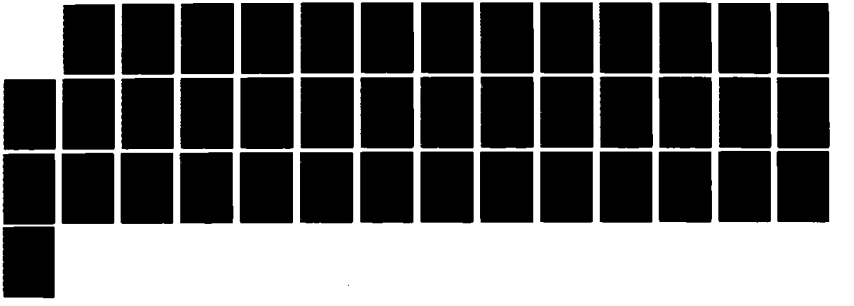

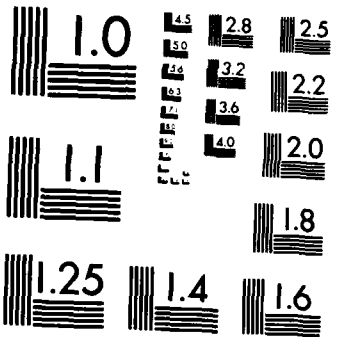


MICROCOPY RESOLUTION TEST CHART
NATIONAL BUREAU OF STANDARDS-1963-A

In figure 11, we display the experimentally measured free electron density radial profiles at Z = -2 and 2 cm, 65 ns from the start of the incident laser pulse. These results were derived by fitting convoluted Stark and instrumental profiles to radially inverted using the Abel transform $4^2D$-$3^2P$ lateral emission spectra[37] for the same conditions as used in the computational work. Also shown in figure 11 are two empirical profiles fitted to these data. A comparison of figure 11 with that of figure 9 reveals that the experimental $N_e$-radial profiles fall off more sharply than the predicted radial profiles. In light of the above discussion this led us to rerun our computer code with a reduced value for the associative ionization cross-section $\sigma_A$. To simplify matters we used a constant value $\sigma_A = 1.5\times10^{-15}$ cm$^2$ rather than scale the irradiance dependent curve suggested by Roussel et al.[11] This is justified for our computations since $\sigma_A$ had its maximum value of $5\times10^{-15}$ cm$^2$ for most of the conditions of interest, the exception being large radial positions ($r \gtrsim 3$ mm) at axial locations, Z > 2 cm.

In figure 12(a) we present both the experimental $N_e$-radial profile (at Z = -2 cm and t = 65 ns) and the two computed profiles: for $\sigma_A = \sigma_A(F)$, derived from Roussel et al,[11] and $\sigma_A = 1.5\times10^{-15}$ cm$^2$, while in figure 12(b) we present the corresponding profiles at Z = 2 cm. It is evident that the experimental values of $N_e(r)$ fall, to some extent, between the two computational curves at both Z = -2 and 2 cm. The experimentally derived radial profile is seen to be steeper than either of the computational profiles, in keeping with our earlier observation. Indeed both computed profiles underestimate the peak ionization and overestimate the ionization at large radial positions. We should, however, point out that our sodium atom density measurements are only accurate to about 20%[26] and that our assumed radius of the laser pulse also is subject to comparable uncertainty. We will address this further in the Discussion and Conclusion section.

In addition to the radial measurements of the free electron density we have also recorded the $4^2D$-$3^2P$ multiplet spectrum at five (y=0) axial locations (Z = -4, -2, 0, 2, 4 cm). These spectra can be used to give us a fairly good idea of the variation of the peak (r = 0) electron density along the path of the laser beam. This is accomplished by matching the

spectrum at each Z-location to that evaluated from the one dimensional radiative transfer equation for a uniform plasma of electron density $N_e$ and radius $r_o$.[37] In effect $N_e$ and $r_o$ are used as fitting parameters. Figure 13 presents these two sets of $4^2D$-$3^2P$ multiplet spectra. The computed Stark broadened profiles (full curves) are seen to approximate the experimental spectra (+) in regard to: the ratio of peak heights, the peak to minimum ratio and the widths of the profiles.

Confirmation that these spectra, which are integrated along the line of sight for y = 0 (as opposed to the radially inverted spectra used for the radial profile measurements) can be used to approximately assess the axial (r = 0) electron density is obtained when we compare the predictions at Z = -2 and 2 cm from figure 13 with the actual radial profiles presented as figure 11.

The axial values of $N_e$ can be seen to decline rapidly for Z > 0 and the asymmetry with regard to equidensity locations is in keeping with our other observations and with our computational predictions. These results confirm that attenuation of the laser pulse is a very real effect, even for distances of a few centimeters, once the atom density is around $10^{16}$ $cm^{-3}$.

If we assume that the plasma is in LTE, then the experimentally measured radial electron density distributions at Z = -2 and 2 cm can be used with the Saha equation and the initial atom density to determine the corresponding radial profile of the free electron temperature. These are displayed with the two computed $T_e(r)$ profiles in figure 14(a) and (b). In both cases the experimental data is quite well flanked by the two computational $T_e$-profiles.

The temperatures indicated in these results are somewhat lower than we had previously expected from LIBORS but appears to confirm other observations of low electron temperatures.[4,5,38,39] This is particularly so for Z = 2 cm, where the mean temperature is about 4000K. These low temperatures are predicted by our LIBORS code after penetrations of several centimeters of vapor and represent another manifestation of reduced laser energy fluence resulting from absorption of the laser pulse. This is clearly seen in figure 15 where the computer predicted axial variation of $N_e$ and $T_e$ (for r = 0) are presented with that of $\varepsilon_\ell$ for $\sigma_A = 1.5\times10^{-15}$ $cm^2$. Also shown is the measured axial variation of $N_o$ that was used in the computer code. The slight upturn in $T_e$ predicted at Z = -5 and 4 cm is a

result of the ionization not proceeding to the burnout stage. The reliability of the computer calculations is questionable at these low densities since the free electrons may not Maxwellianize in the time allowed. In figure 16 we present a comparison of the computer predicted axial variation (at $r = 0$) of $N_e$ and $T_e$ with that of the experimentally derived values.

The cmputational work used the associative ionization cross section of Roussel et al[11] and is found to give results that are in close agreement with the experimental values. The deviation observed for $Z > 0$ could be due to the uncertainty in the sodium atom density distribution. A slightly large $N_o(z)$ would increase the computed $N_e$ values for $Z < 0$, but lower them for $Z > 0$ due to attenuation of the laser pulse.

## DISCUSSION AND CONCLUSIONS

We have developed a computational model of "laser ionization based on resonance saturation" (LIBORS) for sodium vapor that takes into account both the nonuniform atom distribution and absorption of the laser field. This computer code has been used to provide the first insight into the three dimensional nature of this interaction.

We have also undertaken the first measurements of both the radial and axial profiles of the free electron density in a sodium plasma created by laser resonance saturation. From these measurements we have deduced the corresponding radial and axial electron temperature profiles.

We have used our LIBORS cmputer code to model the sodium plasma formed along the path of the laser pulse used in our experiments and have compared the code predicted radial and axial profiles of electron density and temperature with the results derived from our experiments. In general the agreement is very good, especially if allowance is made for the experimental uncertainties and the limited accuracy of the many cross-sections used in the code.

A detailed comparison reveals that the computer code (using $\sigma_A$ of Roussel et al[11] tends to underpredict the $r = 0$ value of the free electron density for $Z < 0$, while overpredicting the value for $Z > 0$. This is consistent with a few percent underestimate of the sodium atom density. This would lead to larger values of $N_e$ for $Z < 0$, but lower values of $N_e$ for $Z > 0$ due to greater attenuation of the laser pulse. The

overprediction of the code with respect to the free electron density at large radial positions could be accounted for by an overestimate on our behalf of the radius of the incident laser pulse.

We believe that these results demonstrate that our LIBORS computer code is capable of fairly accurately predicting the three dimensional behaviour of this new mode of laser ionization. In particular, both our computer code and our experiments clearly reveal that absorption of laser energy due to the strong nature of the interaction leads to a decline in the free electron density and temperature along the path of the laser pulse. This can, for modest values of laser energy fluence, lead to quite low values of both $N_e$ and $T_e$ after the laser pulse has penetrated just a few centimeters of vapor at an atom density of about $10^{16}$ $cm^{-3}$. This could well explain why some researchers have failed to observe appreciable ionization[40] or have measured low values of $T_e$.[4,5,38,39]

Our results clearly indicate that if LIBORS is to be used to generate fairly uniform plasma channels, then the laser energy fluence has to be sufficient to achieve close to full ionization along the path of the atomic vapor. If plasma channels of several meters length are required,[41,42] this could require very large pulses of laser energy, and other techniques such as near resonant multiphoton ionization could be quite competitive, even if they do not achieve full ionization during the laser pulse duration.

In comparing LIBORS with near resonant multiphoton ionization it has to be recognized that in the former case ionization is achieved through a laser driven collisional process which invariably leads to populating most of the intermediate levels — all of which lose energy by radiative decay. Near resonant multiphoton ionization can lead to direct ionization with almost no excitation of intermediate states for short times. However, it is difficult to achieve full ionization by this means especially at high densities. Consequently LIBORS may be the best technique for creating long, dense, relatively cool plasmas.

ACKNOWLEDGEMENTS

This work was supported by the U.S. Air Force Office of Scientific Research (under grant number AFOSR 85-0020) and the Natural Science and Engineering Research Council of Canada.

## REFERENCES


1. Measures, R. M., 1968, J. Appl. Phys., Vol. 39, 5232.
2. Lucatorto, T. B. and McIlrath, T. J., 1976, Phys. Rev. Letters, 37, 428-431
3. McIlrath, T. J. and Lucatorto, T. B., 1977, Phys. Rev. Letters, 38, 1390-1393.
4. Skinner, C. H., 1980, J. Phys. B: Atom. Molec. Phys., 13, 55-68.
5. Jahreiss, L. and Huber, M. C. E., 1983, Phys. Rev. A, 28, 3382-3401.
6. Bréchignac, C., Cahuzac, Ph., and Débarre, A., 1985, Phys. Rev. A 31, 2950-2956.
7. Lucatorto, T. B. and McIlrath, T. J., 1980, Appl. Optics, Vol. 19, 3948.
8. Krebs, D. J. and Shearer, L. D., 1981, J. Chem. Phys. 75, 3340-3344.
9. Bréchignac, C. and Cahuzac, Ph., 1982, Optics Commun., 43, 270-273.
10. Krasinski, J., Stacewicz, T. and Stroud, C. R. Jr., 1980, Optics Commun. 33, 158-162.
11. Roussel, F., Breger, P., Spiess, G., Manus, C. and Geltman, S., 1980, J. Phys. B: Atom. Molec. Phys. 13, L631-L636.
12. Stacewicz, T. and Krasinski, J., 1981, Optics Commun. 39, 35-40.
13. Carré, B., Roussel, F., Breger, P. and Spiess, G., 1981, J. Phys. B: Atom. Molec. Phys. 14, 4289-4300.
14. Carré, B., Roussel, F., Breger, P. and Spiess, G., 1981, J. Phys. B: Atom. Molec. Phys. 14, 4271-4288.
15. LeGouët, J. L., Picqué, J. L., Wuilleumier, F., Bizau, J. M., Dhez, P., Koch, P. and Ederer, D. L., 1982, Phys. Rev. Lett., 48, 600-603.
16. Kumar, J., Silfvast, W. T. and Wood, O. R. II, 1982, J. Appl. Phys., 53, 218-222.
17. Measures, R. M., 1970, J. Quant. Spectrosc. Radiat. Transfer, 10, 107-125.
18. Measures, R. M., 1977, J. Appl. Phys., 48, 2673-2675.
19. Measures, R. M. and Cardinal, P. G., 1981, Physical Review A, 23, 804-815.
20. Measures, R. M., Cardinal, P. G. and Schinn, W. G., 1981, J. Appl. Phys. 52, 1269-1277, 1981, and 52, 7459.

21. Measures, R. M., 1982, "Laser Resonance Saturation: An Efficient and Rapid Means of Ionization and Electron Heating". Invited paper at the Society for Optical and Quantum Electronics LASER'S 82 Meeting, New Orleans, Dec. 12-17.

22. Morgan, W. L., 1983, Appl. Phys. Lett., Vol. 42, No. 9, 790-791.

23. Measures, R. M., Drewell, N. and Cardinal, P., 1979, J. Appl. Phys., 50, 2662-2669.

24. Measures, R. M., Wong, S. K. and Cardinal, P. G., 1982, J. Appl. Physics 53, 5541-5551.

25. Wong, S. K., 1985, "A Computational Study of the Influence of Molecular Nitrogen and Laser Absorption on Plasma Channel Formation Created by Laser Resonance Saturation of Sodium Vapor", UTIAS Report No. 292.

26. Cappelli, M. A., Cardinal, P. G., Herchen, H. and Measures, R. M., 1985, Rev. Sci. Instrum. 56, 2030-2037.

27. Seaton, M. J., 1962, "Atomic and Molecular Processes", Edited by D. R. Bates, Academic Press, New York.

28. Gryzinski M., 1965, Phys. Rev. 138, A336.

29. Crandall, D. H., Dunn, G. H., Gallagher, A., Hummer, D. G., Kunasz, C. V., Leep, D. and Taylor, P. O., 1974, Astrophys. J. 191, 789.

30. Morgan, E. J. and Morrison, R. D., 1965, Phys. Fluids, 8, 1608.

31. Cardinal, P. G., 1985, "A Study of Laser Ionization Based on Resonance Saturation", UTIAS Report No. 299.

32. Cravath, A. M., 1930, Phys. Rev. 36, 248-250.

33. Kissack, R. S., 1986, University of Toronto, Institute for Aerospace Studies Report No. 305.

34. Nesmeyanov, An. N., 1963, "Vapour Pressure of the Elements (Translator, J. I. Carasso), Academic Press.

35. Griem, H. R., 1974, "Spectral Line Broadening by Plasmas", McGraw-Hill, Toronto.

36. Measures, R. M. and Herchen, H., 1983, J. Quant. Spectrosc. Radiat. Transfer 29, 9-17.

37. Cappelli, M. A. and Measures, R. M., 1986, "Electron Density Radial Profiles Derived from Stark Broadening in a Sodium Plasma Produced by Laser Resonance Saturation" (to be published).

38. Bachor, H. A. and Kook, M., 1981, J. Phys. B14, 2793.

39. Landen, O. L., Windfield, R. J., Burgess, D. D., Kilkenney, J. D., and Lee, R. W., 1982, Phys. Rev. A, 32, 2963.

40. Bowen, J. L. and Thorne, A. P., 1985, J. Phys. B: At. Mol. Phys. 18, 35-50.
41. Olsen, J. N. and Leeper, R. J., 1982, J. Appl. Phys., Vol. 53, 3397.
42. Yonas, G., 1978, G. Yonas, Sci. Am., Vol. 239, 50.

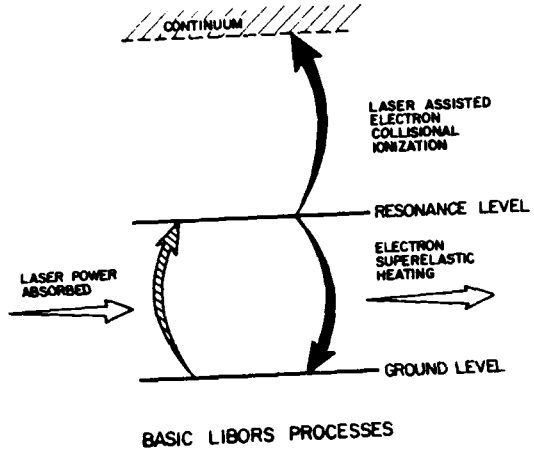


Fig. 1 Schematic Representation of Ionization and Electron Heating Attained Through Laser Resonance Saturation.

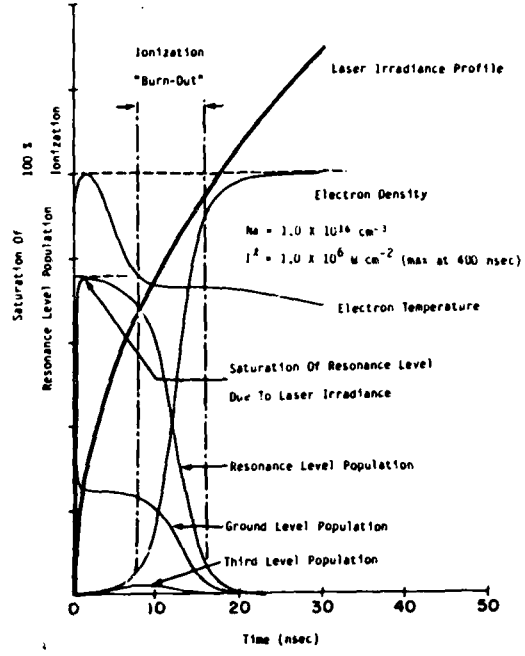


Fig. 2 Temporal Variation of Various Parameters Resulting from Laser Resonance Saturation.

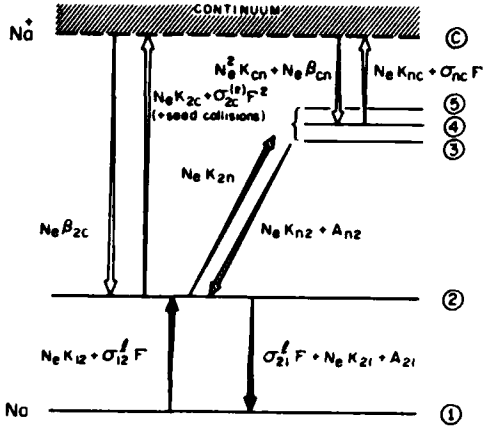


Fig. 3 Five Level Model of Sodium Atom.

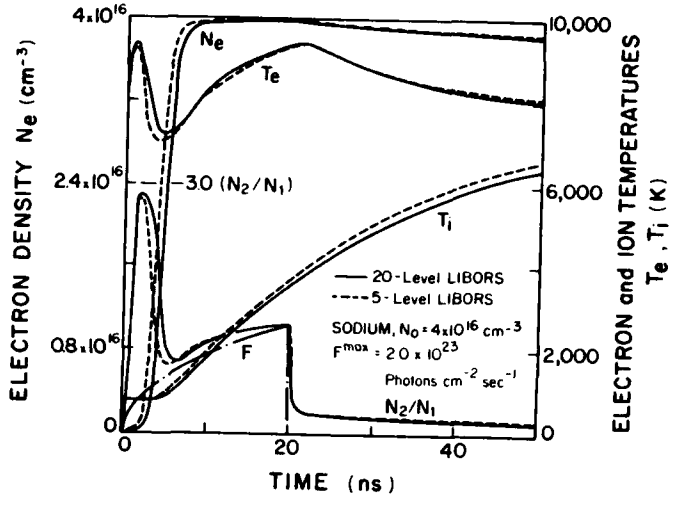


Fig. 4 Comparison of Computer Predicted Temporal Histories of Various Parameters Based on 5 and 20-Level Models of Sodium Atom (———— 20-level, ———— -- ———— 5-level) $N_0 = 4 \times 10^{16}$ cm$^{-3}$ and $F_p = 2 \times 10^{23}$ photons cm$^{-2}$ s$^{-1}$.

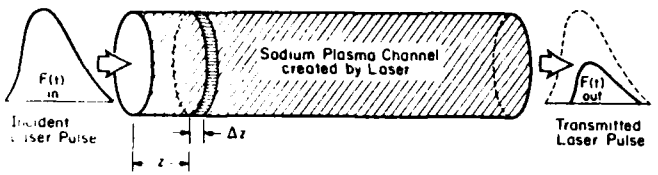


Fig. 5 Multislab Model Used for LIBORS Computer Calculations Showing Attenuation of Laser Pulse.

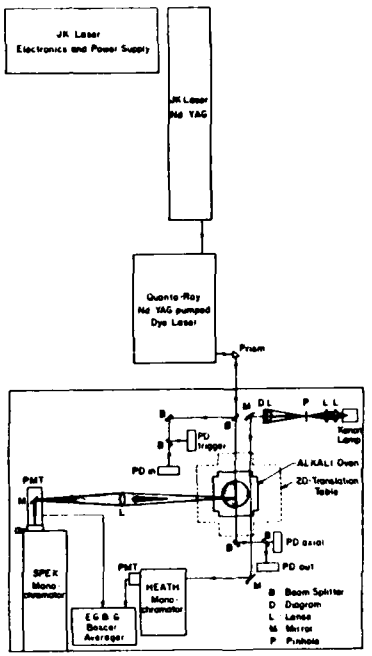


Fig. 6 Schematic of LIBORS Experimental Facility.

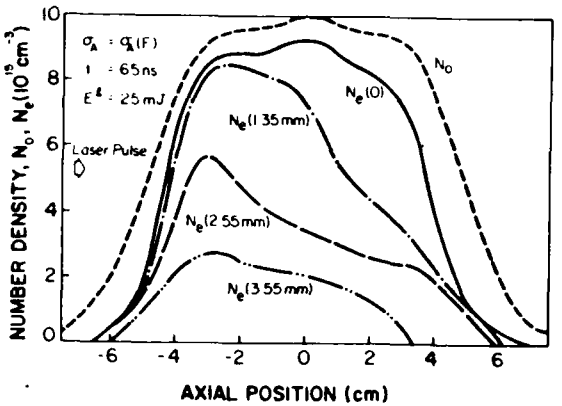


Fig. 7 Axial Variation of Free Electron Density $N_e$ at Four Radial Positions (r = 0, 1.35, 2.55 and 3.55mm) predicted by LIBORS code at t = 65ns. Also shown is the Axial Sodium Atom Density Distribution $N_o(z)$ Used in the Computation.

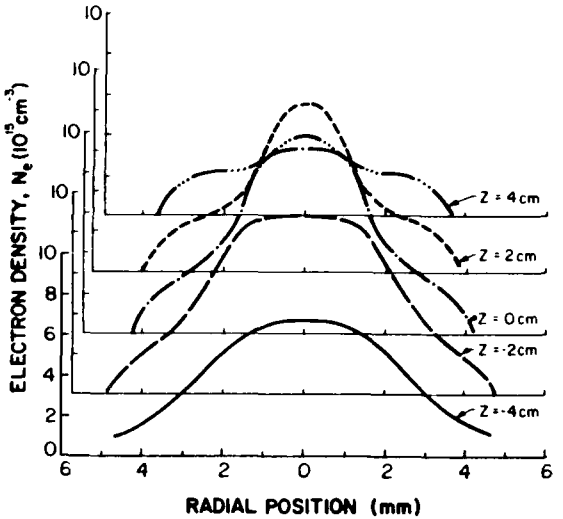


Fig. 8 Full Radial Profiles of the Free Electron Density Predicted at Five Axial Locations (Z = -4, -2, 0, 2, 4 cm) Along the Path of a 25mJ Laser Pulse, $N_o$=$10^{16}$cm$^{-3}$, t 65ns.

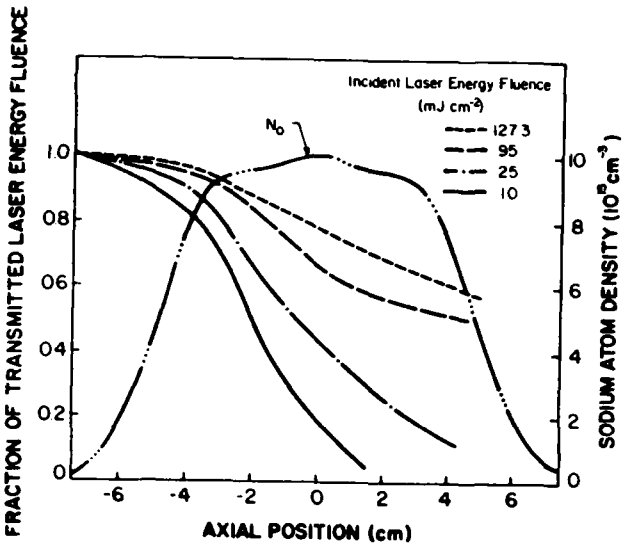


Fig. 9 Fraction of Transmitted Laser Energy Fluence as Function of Axial Location for Four Values of Incident Laser Energy Fluence. Also Shown is the Sodium Atom Distribution Assumed Along the Path of the Laser Pulse.

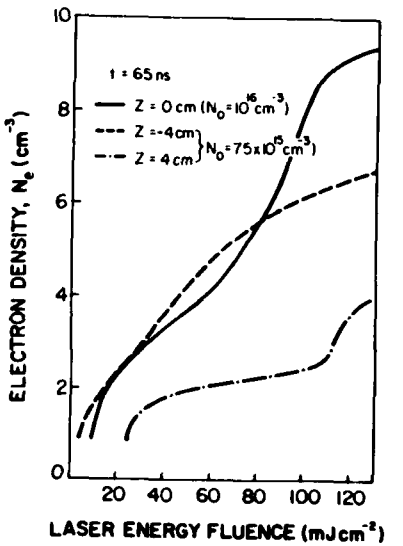


Fig. 10 Variation of the Free Electron Density (achieved at Z = -4, 0 and 4 c and t = 65ns) with the Incident Laser Energy Fluence.

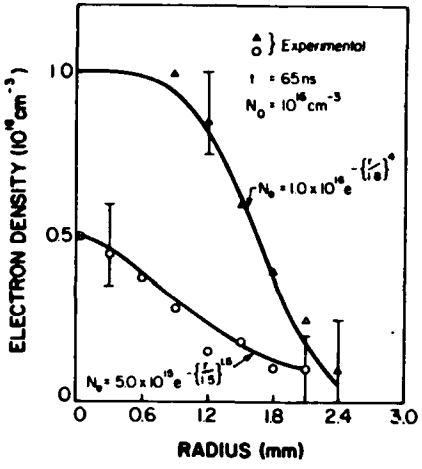


Fig. 11 Free Electron Density Radial Profiles Attained at Z = -2 and 2 cm for $N_o = 10^{16} cm^{-3}$ and t = 65ns, $E^{\ell}$=25mJ.

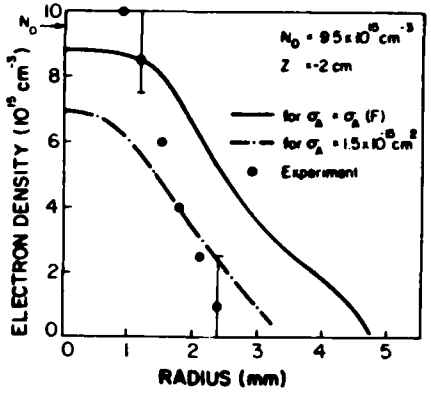


(a)

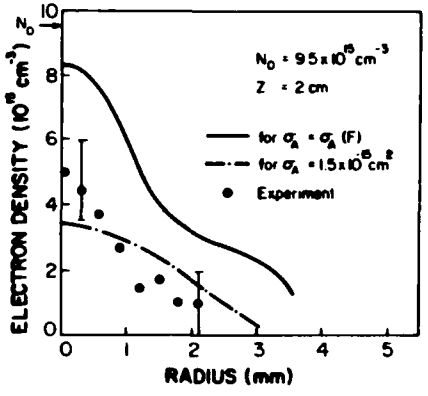


(b)

Fig. 12 Free Electron Density Radial Profile at Z = -2 cm (a) and Z = 2 cm (b) where $N_o = 9.5 \times 10^{15}$ $cm^{-3}$ and t = 65ns as determined by: Experiment and LIBORS computer code with $\sigma_A = \sigma_A(F)$ ———— and $\sigma_A = 1.5 \times 10^{-15} cm^2$ —— – ——.

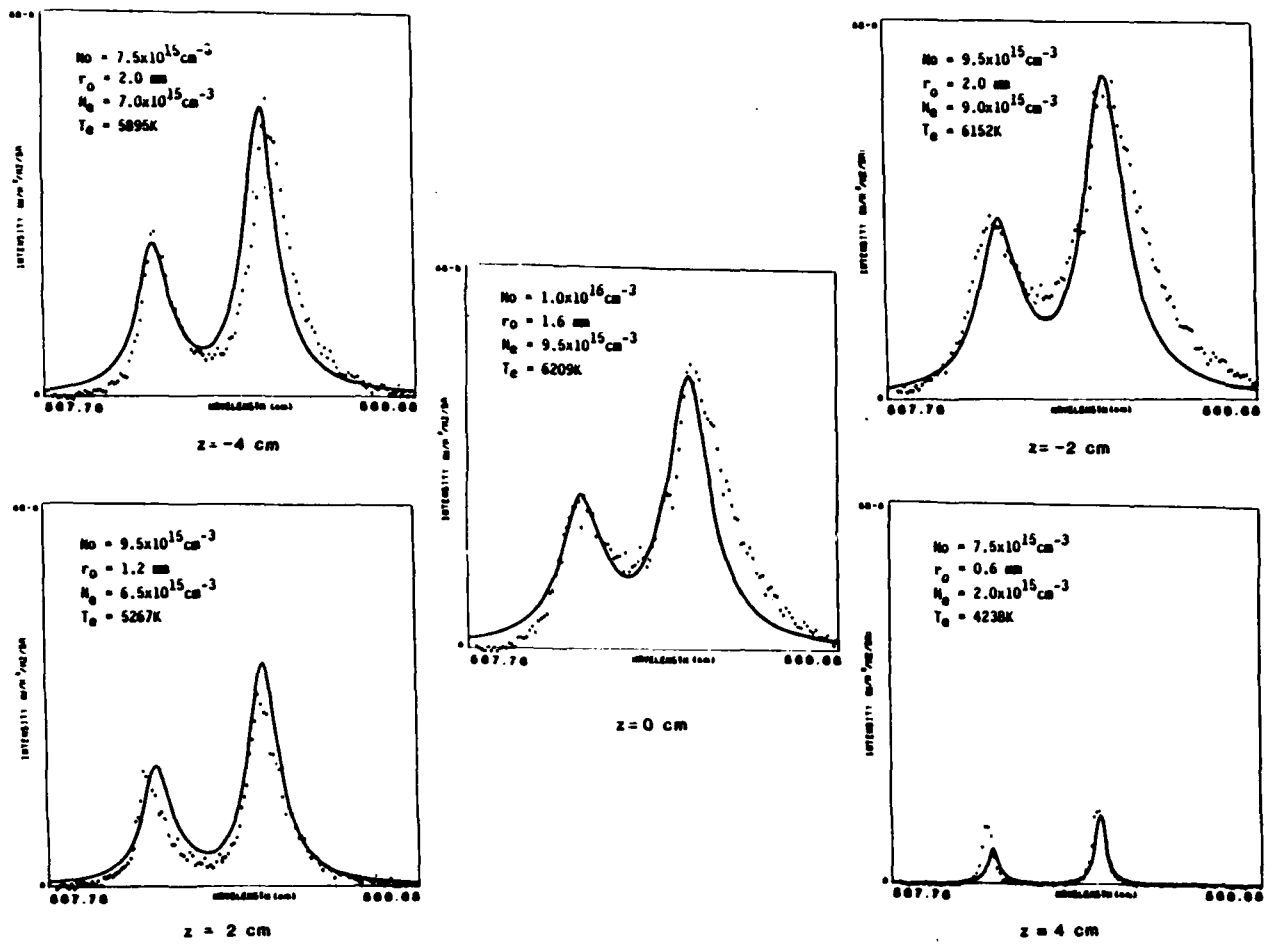


Fig. 13 Comparison of Experimentally Measured $4^2D$-$3^2P$ Multiplet Spectra at Z = -4, -2, 0, 2 and 4cm for a Sodium Atom Distribution with $N_e^{Peak}=10^{16}cm^{-3}$ at t = 65ns, where $E^{\ell}$ = 25mJ, with Computer Simulation of the Same Spectra Under Identical Conditions.

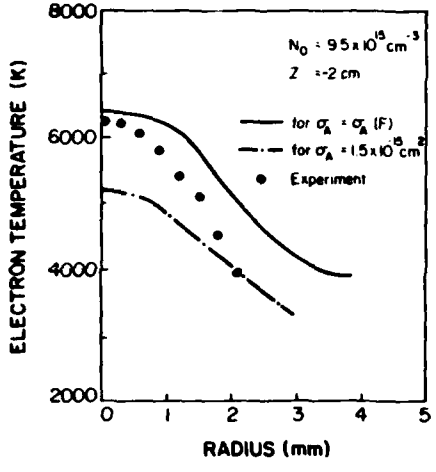


(a)

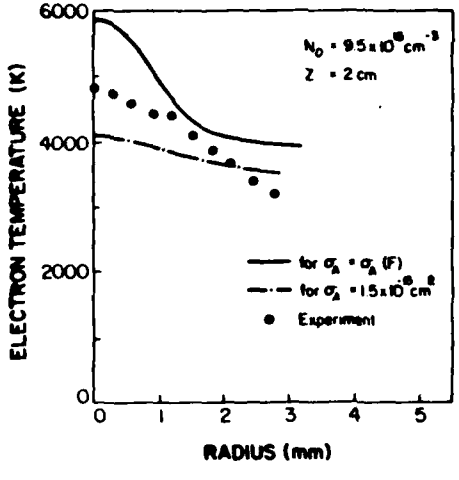


(b)

Fig. 14 Electron Temperature Radial Profile at Z = -2cm (a) and Z = 2cm (b) where $N_0 = 9.5 \times 10^{15}\ cm^{-3}$ and t = 65ns as Determined by: Experiment (o) and LIBORS Computer Code with $\sigma_A = \sigma_A(F)$ ———— and $\sigma_A = 1.5 \times 10^{-15} cm^2$ — — — —.

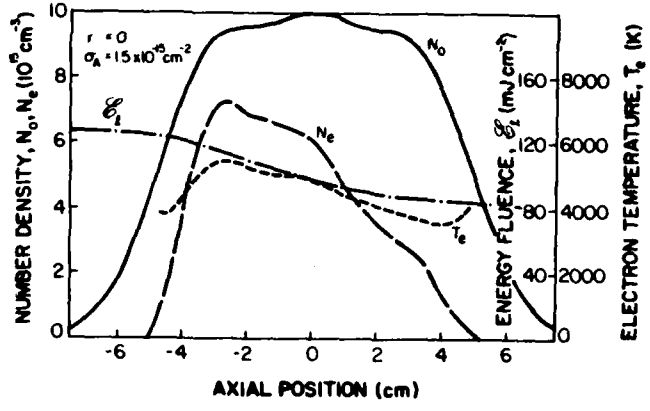


Fig. 15 Axial Variation of the Free Electron Density and Temperature As Predicted by LIBORS Computer Code at r = 0 and t = 85ns for $\sigma_A = 1.5 \times 10^{-15}\ cm^2$. Also shown is the Assumed Sodium Atom Density Distrubition and the Decline in the Laser Energy Fluence with Axial Location.

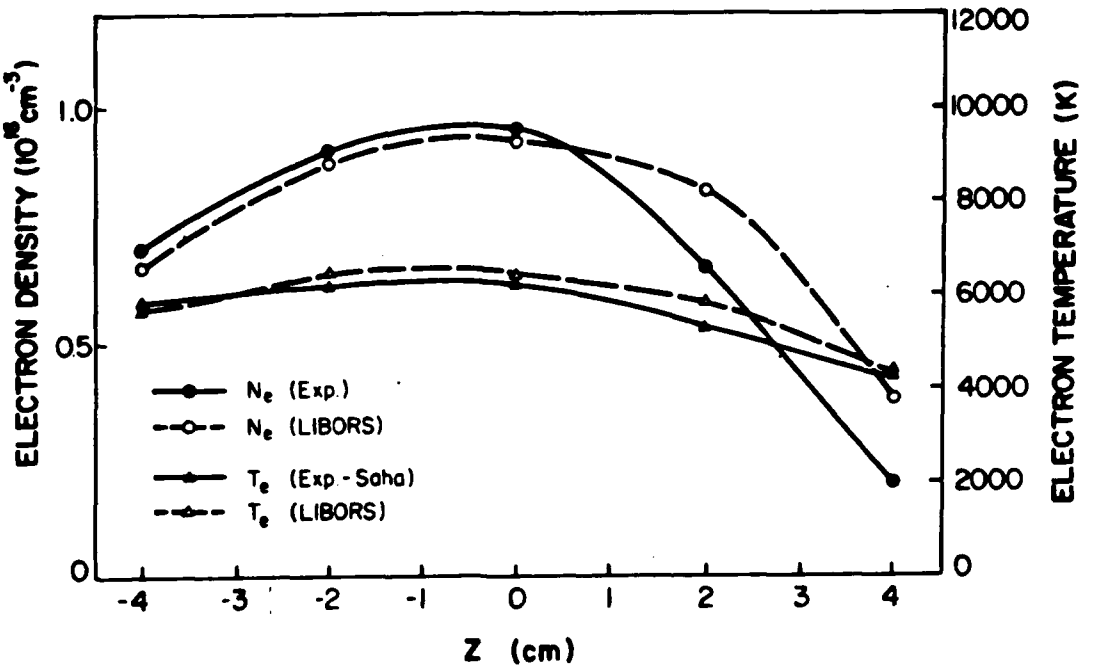


Fig. 16 Comparison of the axial variation (for r = 0) of the free electron density and temperature determined by experiment and predicted by our LIBORS computer code.

APPENDIX F

# SUPERELASTIC COLLISIONAL EXCITATION OF A STRONTIUM PLASMA BY ONE AND TWO PHOTON LASER PUMPING

K. A. Menard and R. M. Measures

Institute for Aerospace Studies, University of Toronto
4925 Dufferin Street
Downsview, Ontario, Canada
M3H 5T6

## Abstract

Fast superelastic electron heating by collision quenching of one and two photon laser pumped states has been demonstrated in a relatively cold strontium plasma created by two photon ionization of strontium vapor contained within a crossed heat pipe oven.

## INTRODUCTION

Laser saturation of an atomic resonance transition involves radiatively locking the resonance and ground state populations in the ratio of their degeneracies.[91] Lucatorto and McIlrath[2] were the first to show experimentally that this interaction represents an extraordinarily effective method of producing near total ionization of alkali atoms along the path of the laser pulse. Subsequent experiments have not only verified this observation but have shown that this form of laser ionization can be extended to other elements.[3-6]

Measures[7,8] first proposed that a combination of laser pumping of the resonance state and superelastic electron collision quenching of the resonance state represent the primary mechanism for converting laser energy into free electron energy which in turn creates a high degree of ionization[3-15] Measures and Cardinal,[16] Measures et al[17] and Measures[18] have proposed that "laser ionization based on resonance saturation" (LIBORS) proceeds in four stages: (i) the laser rapidly "locks" the ground and resonance level populations roughly in the ratio of their respective degeneracies, (ii) there is a rapid growth of free electrons due to one or more "seed ionization" processes and these electrons very quickly acquire energy through "superelastic collision quenching" of the laser maintained resonance state population, (iii) these "hot" electrons proceed to collisionally excite and ionize the resonance state atoms and in addition the collisionally excited higher lying levels are "photoionized" by the laser field, finally (iv) "runaway" collisional ionization of the upper levels occurs once some critical free electron density is achieved and this leads to near complete ionization burnout of the species. Further theoretical confirmation of this work has been provided by Moryan[19] who modeled the ionization using the Boltzmann equation rather than assuming that the free electrons have a Maxwellian velocity distribution.

Measures et al[20] have also shown that superelastic laser energy conversion is also capable of very rapidly exciting and heating a plasma if an ion resonance line is laser pumped, and Measures et al[21] indicated that, under certain circumstances, this form of laser interaction could be very competitive with inverse bremsstrahlung for coupling laser energy into a plasma. Measures et al[21] also suggested that multiphoton pumping could be used to broaden the scope of this form of laser interaction. We suspect that Sorokin et al[22] inadvertently verified this possibility several years earlier when they observed VUV emission from high lying nf-4d lines in SrII following two photon pumping of the $6^2S_{1/2}$ level.

In the present paper we report the results of experiments involving both one and two photon laser pumping of SrII created by the same laser through two photon ionization of strontium vapor.[23]

## EXPERIMENTAL FACILITY AND RESULTS

The third harmonic output of a Nd-YAG pulsed laser system (JK HY750) was used to pump a dye laser (Quanta-Ray PDL-1) using Stilbene 420. The 40 ns, 2 mJ laser pulses at a 10 Hz repetition rate were focussed into a stainless steel "crossed heat pipe" oven that is heated to about 800°C and contains strontium vapor. Cooled argon buffer gas at about 50 torr is used to prevent the strontium from condensing on the four windows of the crossed heat pipe oven. Emission at right angles to the laser beam was viewed by a photomultiplier (RCA 4526) mounted on a Czerny-Turner monochromator (SPEX 1700 II) for spectral discrimination. A Boxcar Signal Averager (EG&G-PARC 4420) was used for data acquisition and a microcomputer (Apple II Plus) for data recording and processing. A schematic overview of the facility is presented as figure 1. The mean strontium atom density was determined by measuring the temperature of the central zone of the crossed heat pipe oven with a thermocouple and this was checked by measuring the spectral hole width burned in a collimated beam of broadband radiaton from a Xenon lamp. The technique used is similar to that reported recently by Cappelli et al[24] for sodium.

When the dye laser was tuned to either the $5^2S_{1/2}$-$5^2P_{1/2}$ resonance lines (421.67 nm) or the two photon transition, $5^2S_{1/2}$-$6^2S_{1/2}$ (418.97 nm) and fired through the strontium vapor, a visible breakdown could be seen and is assumed to result from two photon ionization. A partial Grotrian diagram showing the transitions of interest is presented as figure 2. With the dye laser wavelength tuned to the $5^2P_{1/2}$ ion resonance transition (421.67 nm), a weak, noisy signal was detected at the $5^2F_{5/2}$-$5^2D_{3/2}$ wavelength (562.45 nm) and a slightly stronger signal at the $5^2F_{5/2,7/2} \rightarrow 5^2D_{5/2}$ wavelength (565.20 nm). To study the sensitivity of this excitation process to laser wavelength, the signal was temporally averaged over the length of the laser pulse, using the gated sampling mode of the Boxcar Averager and the laser

was tuned from 421.17 nm to 422.23 nm. The spectrally integrated signal at 565.20 nm rose sharply on the blue side and reached a maximum at the resonance wavelength, see figure 3(a). On the red side, the signal descended very slowly and, in fact, was clearly detectable 0.5 nm away from the peak. When the neutral density was reduced [figure 3(b), (c)], the signal weakened in intensity and the profile became more symmetrical. Three photon excitation of the $5^2F$ levels appears to be ruled out by the observation that the emission at 565.20 nm failed to increase when the laser was tuned for exact three photon resonance at 422.14 nm.

Further insight into the mechanism of excitation was gained by monitoring the emission from the $6^2S_{1/2}$-$5^2P_{3/2}$ transition at 430.67 nm as the laser was tuned over the same range (i.e., 421.17 to 422.23 nm), see figure 4. The emission is seen to exhibit the same laser wavelength behaviour as observed with the 565.20 nm emission. In addition the emission at 565.20 nm is seen, in figure 5(a), to be very long lived compared to the duration of the laser pulse when the laser is tuned to 421.67 nm.

When the dye laser was tuned between 418.49 and 419.56 nm, a well defined spike in the emission from $6^2S_{1/2}$-$5^2P_{1/2}$ at 430.67 nm was observed for $\lambda_L$ = 418.97 nm, corresponding to excitation of the two photon $5^2S_{1/2}$-$6^2S_{1/2}$ transition, see figure 6. In addition significant long lived emission was observed on the $5^2F_{5/2,7/2}$-$5^2D_{5/2}$ transition at 565.20 nm when the laser was tuned to this wavelength, see figure 5(b). Note the scale is the same for figures 5(a) and 5(b).

## CONCLUSIONS

Our observations strongly suggest that the SrII $5^2F$ level excitation mechanism is not radiative but collisional in origin. Indeed we propose that strong pumping of the ion resonance line at 421.67 nm creates an energy reservoir, in the form of an excess of $5^2P_{1/2}$ level population, that is used to heat the free electrons present in the plasma through superelastic quenching collisions. The asymmetry in the sensitivity to laser wavelength could be attributed to refractive index self-focussing effects. The disappearance of this asymmetry with decreasing strontium density is in keeping with this hypothesis.

We also propose that two photon laser pumping of the $6^2S_{1/2}$ level also appears to cause superelastic heating and concomitant excitation of the $5^2F$ levels. Indeed according to figure 5, this process is 50% as effective as pumping the resonance level, if we use the ratio of the peak signals at 565.20 nm as a guide. We conclude that both one and two photon resonance laser pumping of low lying ion levels can be used to rapidly excite high lying levels of the ion through superelastic laser energy conversion, Measures et al.[20] Under certain conditions (initial dense, cold plasma) this could represent a new method of efficiently producing intense short wavelength emission from a plasma using visible wavelength lasers.


## ACKNOWLEDGEMENTS

This work was supported by the U.S. Air Force Office of Scientific Research (under grant number AFOSR 85-0020) and the Natural Science and Engineering Research Council of Canada.


## REFERENCES


1. Measures, R. M., 1968, J. Appl. Phys., Vol. 39, 5232.
2. Lucatorto, T. B. and McIlrath, T. J., 1976, Phys. Rev. Letters, 37, 428-431
3. Skinner, C. H., 1980, J. Phys. B: Atom. Molec. Phys., 13, 55-68.
4. Lucatorto, T. B. and McIlrath, T. J., 1980, Appl. Optics, Vol. 19, 3948.
5. Bréchignac, C. and Cahuzac, Ph., 1982, Optics Commun., 43, 270-273.
6. Jahreiss, L. and Huber, M. C. E., 1983, Phys. REv. A, 28, 3382-3401.
7. Measures, R. M., 1970, J. Quant. Spectrosc. Radiat. Transfer, 10, 107-125.
8. Measures, R. M., 1977, J. Appl. Phys., 48, 2673-2675.
9. Krebs, D. J. and Shearer, L. D., 1981, J. Chem. Phys. 75, 3340-3344.
10. Krasinski, J., Stacewicz, T. and Stroud, C. R. Jr., 1980, Optics Commun. 33, 158-162.
11. Roussel, F., Breger, P., Spiess, G., Manus, C. and Geltman, S., 1980, J. Phys. B: Atom. Molec. Phys. 13, L631-L636.
12. Stacewicz, T. and Krasinski, J., 1981, Optics Commun. 39, 35-40.
13. (a) Carré, B., Roussel, F., Breger, P. and Spiess, G., 1981, J. Phys. B: Atom. Molec. Phys. 14, 4289-4300.
    (b) Carré, B., Roussel, F., Breger, P. and Spiess, G., 1981, J. Phys. B: Atom. Molec. Phys. 14, 4271-4288.

14. LeGouët, J. L., Picqué, J. L., Wuilleumier, F., Bizau, J. M., Dhez, P., Koch, P. and Ederer, D. L., 1982, Phys. Rev. Lett., 48, 600-603.
15. Kumar, J., Silfvast, W. T. and Wood, O. R. II, 1982, J. Appl. Phys., 53, 218-222.
16. Measures, R. M. and Cardinal, P. G., 1981, Physical Review A, 23, 804-815.
17. Measures, R. M., Cardinal, P. G. and Schinn, W. G., 1981, J. Appl. Phys. 52, 1269-1277, 1981, and 52, 7459.
18. Measures, R. M., 1982, "Laser Resonance Saturation: An Efficient and Rapid Means of Ionization and Electron Heating". Invited paper at the Society for Optical and Quantum Electronics LASER'S 82 Meeting, New Orleans, Dec. 12-17.
19. Morgan, W. L., 1983, Appl. Phys. Lett., Vol. 42, No. 9, 790-791.
20. Measures, R. M., Wizinowich, P. L. and Cardinal, P. G., 1980, J. Appl. Phys. , 51, 3622-3628.
21. Measures, R. M., Drewell, N., and Cardinal, P., 1979, Appl. Optics, 18, 1824-1827.
22. Sorokin, P. P. et al, 1974, Laser Spec., Proc. 2nd Int. Conf., 46.
23. Menard, K. A., University of Toronto, M.A.Sc. Thesis, 1986.
24. Cappelli, M. A., Cardinal, P. G., Herchen, H. and Measures, R. M., 1985, Rev. Sci. Inst., 56, 2030-2037.

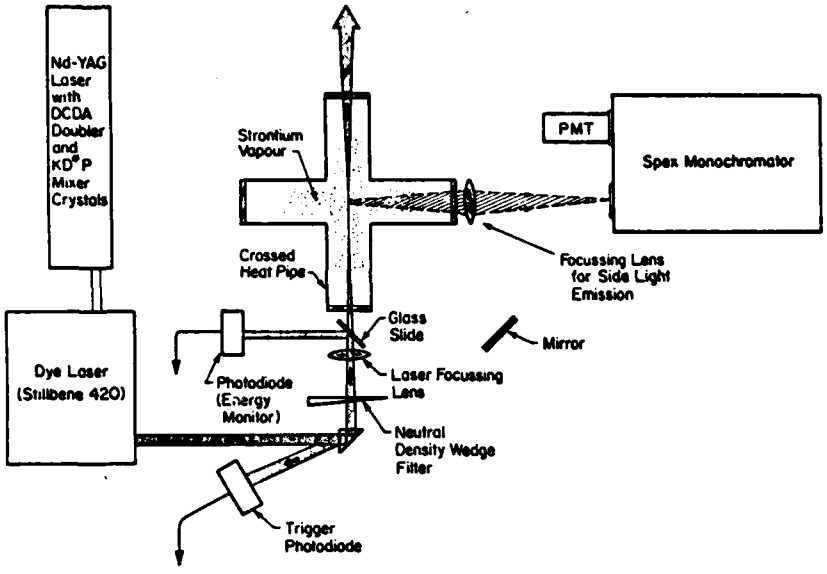


Figure 1. Schematic View of Strontium Multiphoton Pumping Experimental Facility.

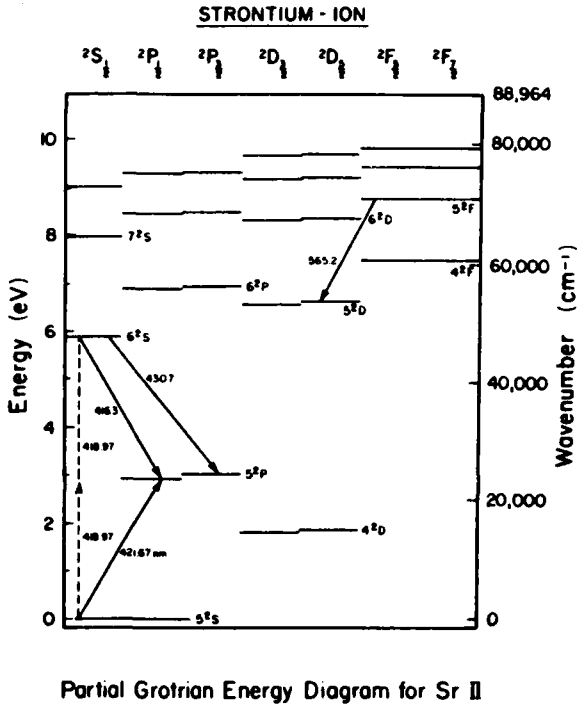


Partial Grotrian Energy Diagram for Sr II

Figure 2. Partial Grotrian Energy Level Diagram of Strontium Ion.

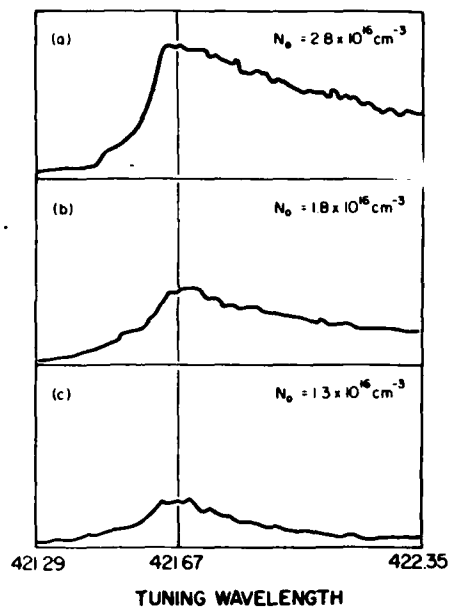


Figure 3. Variation of Sr II ($5^2F_{5/2,7/2}$-$5^2D_{5/2}$) 565.20nm Emission from a Strontium Plasma as a Function of the Exciting Laser Wavelength for Three Values of the Initial Strontium Atom Density. Ion Resonance Line Wavelength at 421.67nm.

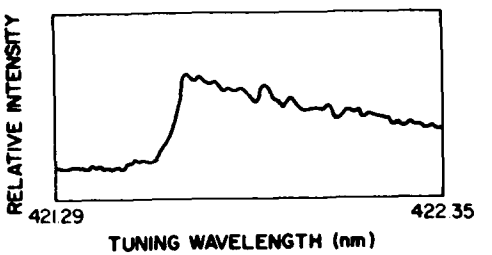


Figure 4. Variation of Sr II ($6^2S_{1/2}$-$5^2P_{1/2}$) 430.67nm Emission from a Strontium Plasma as a Function of the Exciting Laser Wavelength for an Initial Strontium Atom Density of $2.8 \times 10^{16} cm^{-3}$. Ion Resonance Line Wavelength 421.67nm.

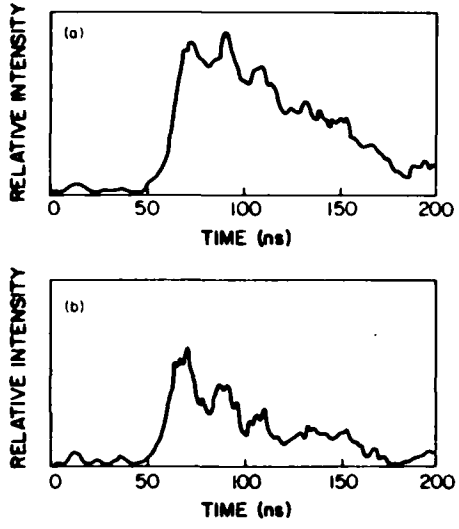


Figure 5. Temporal Variation of 565.20nm Emission when the Laser Wavelength Tuned to (a) the Ion Resonance Line at 421.67nm, and (b) the ($5^2S_{1/2}$-$6^2S_{1/2}$) Two Photon Transition at 418.97nm.

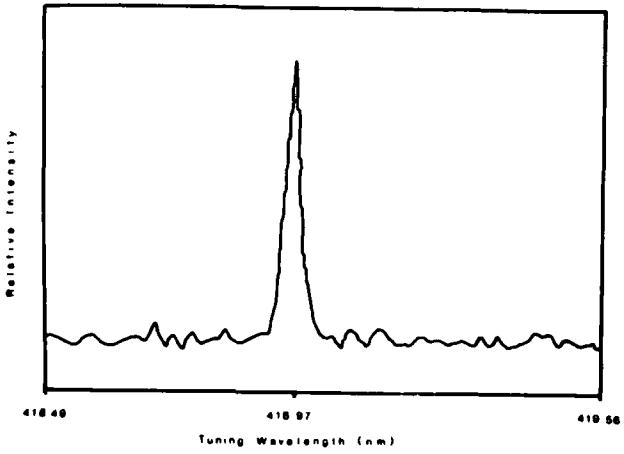


Figure 6. Variation of the 430.67nm Emission from a Strontium Plasma as a Function of the Laser Wavelength in the Vicinity of the Two Photon Transition Wavelength (418.97nm).

# PARAMETRIC GENERATION WITHIN A STRONTIUM PLASMA CREATED BY TWO PHOTON IONIZATION

by

K. A. Menard and R. M. Measures

University of Toronto, Institute for Aerospace Studies
4925 Dufferin Street
Downsview, Ontario, Canada
M3H 5T6

## ABSTRACT

An experiment has been performed to demonstrate a third-order nonlinear optical effect involving the ground state of the strontium ion. Evidence of strong and slightly tunable parametric generation from a doubly resonant four wave mixing process is provided when a single wavelength laser is used to two-photon ionize strontium and simultaneously pump close to the 5s → 6s two-photon resonance of the ion. This result appears to conform with a semi-classical wave equation decription, although there is evidence that a population rate equation analysis will also be necessary if the process is to be modeled more accurately.




## Introduction

Multiphoton induced "nonlinear optical" (NLO) effects in atomic vapours, have been studied for the past 15 years. However, little attention has been directed towards multiphoton interaction in atomic ions, although a medium of this nature offers the potential for shorter wavelengths.

The study of NLO effects in plasmas actually predates that in atomic vapours [1], and was associated with free electron nonlinear polarization. When a laser is tuned to be in close resonance with one or more transitions in an ion, then the nonlinear susceptibility of that ion can become dominant. The present study is concerned with the generation of nonlinear parametric processes in a Strontium plasma created by two photon ionization of Strontium vapor by the same laser.

Freeman et al [2] reported observation of 4-wave parametric mixing in Ba II using essentially the same scheme as Boker et al [3] with an additional laser to couple two photons to the $6^2F_{5/2}$ levels. The auto-ionization transition $6^2P_{3/2}12p \rightarrow 6^2P_{1/2} + e^-$ creates an inversion on the $6^2P_{1/2} \rightarrow 5^2D_{3/2}$ transition and the resulting ASE sums with two 451 nm photons to yield a 167 nm photon on the $6^2F_{5/2} \rightarrow 5^2D_{3/2}$ transition of BaII.

Alkaline earth ions are employed for these interactions because the neutral atom can often be two photon ionized by laser radiation that is tuned close to one of the resonance transitions of the ion. Furthermore, in many cases the ion's first excited S-state is almost double its resonance energy. This characteristic, which is fairly unique to these species, can have a significant effect in enhancing third order NLP's, as a consequence of the strong sensitivity in the susceptibilities to intermediate resonances. Although there is a limitation to the enhancement due to single photon absorption [4], we shall see in theory that they can be advantageous in certain schemes of interest.

The work reported herein has exploited most of the above attractive features in the element strontium to observe a four-wave mixing process in the Sr ion, see figure 1. To our knowledge, this represents the first time four-wave difference mixing has been demonstrated in any ion using a single

laser, and the first time the ground state of an ion has been used to generate difference mixing.

Multiphoton Ionization

When sufficiently intense radiation interacts with an atomic system, a high-order theory is necessary to describe such phenomena as multiphoton absorption and nonlinear parametric processes. If the interaction involves elastic, virtual scattering phenomena the quantity of interest is normally the semiclassical susceptibility factor, whereas interactions based on inelastic, real or absorption processes are discussed in terms of the absorption cross-section. We have found it suitable to use the asorption cross-section to describe the ionization process and the susceptibility to describe the subsequent parametric interactions [5].

When an external laser field with a photon energy $h\omega$ (which equals or just exceeds half the neutral ionization potential) is applied to strontium vapor one of the SrI ground state electrons will be photoionized while the remaining 5s electron forms the $5^2S_{1/2}$ state. The result is the formation of strontium ions in their ground state, and free electrons of energy,

$$\epsilon_e = 2h\omega - E_{c1} \tag{1}$$

where $E_{c1}$ represents the neutral strontium atom's ionization energy. The probability per unit time for this event to occur can be expressed as,

$$R_{c1} = \sigma_{c1}(\omega)\, F^2 \tag{2}$$

where $\sigma_{c1}(\omega)$ is the generalized two photon ionization (TPI) cross-section at frequency, $\omega$, and F is the laser photon flux density (photons $sec^{-1}cm^{-2}$). To compute the value of $\sigma_{c1}(\omega)$, one needs to formulate the wavefunctions which couple the ground state to the continuum. Recently, Kim and Lambropoulos [6] have considered this problem for alkaline earth systems, and although they offer the general framework for describing the process, one must normally resort to a multi-configuration Hartree-Fock (MCHF) numerical method to compute actual values. In addition, the



structure of the continuum in Sr I, just above threshold, has not been well studied, making it difficult to set up the type of configuration interactions likely to occur. There is, for example, an auto-ionizing level slightly beyond threshold which Esherick [7] and Ewart and Purdue [8] have both independently observed; however, there is some question as to the $(4d)^2$ assignment.

More recently, there have also been some attempts to measure the multiphoton cross-sections in Alkaline Earths [9]; however, it appears none have been performed for the two-photon energies of interest. In view of these problems, we shall adopt the method of Leuchs [10] which follows that of Gold [11] to get a typical order of magnitude estimate of the TPI cross-section.

If we consider a first order transition, it would occur at a rate,

$$R^{(1)} = \sigma_1^{(1)} F \tag{3}$$

where $\sigma_1^{(1)}$ is the appropriate single photon cross section. Now assuming the laser frequency is detuned from any single-photon resonances (in Sr I, the closest separation is $\sim 1000\ cm^{-1}$), the atom will spend a short time $\Delta t$ in a virtual excited state in accordance with the uncertainty principle. If a second photon is now incident on the atom within this time, the probability of a second absorption will be $\sigma_2^{(1)}F$. The overall rate is thus,

$$R^{(2)} = \sigma_1^{(1)} F\, \Delta t\, \sigma_2^{(1)} F \tag{4}$$

and since a typical $\sigma^{(1)}$ in the visible range is of the order of an atomic dimension squared,

$$\sigma_1^{(1)} = \sigma_2^{(1)} = 10^{-16}\ cm^{-2} \tag{5}$$

and $\Delta t$ is roughly the inverse of an atomic frequency,

$$\Delta t = \omega^{-1} = 10^{-16} \tag{6}$$

the overall cross-section is of the order of $10^{-48}$ $cm^2 sec$. This agrees quite well with typical off-resonance values determined by perturbation theory [12] and will allow us to estimate the expected ion density in our scheme.

*To obtain the necessary flux density, for a significant transition rate, it was necessary in our experiments to focus the incident radiation.* Now, assuming negligible recombination during the time of interest, the rate of growth of ions can be expressed as,

$$dN_i = ( N_0 - N_i ) \sigma^{(2)} F^2 dt \qquad (7)$$

where $N_i$ is the ion density at time t, $N_0$ is the initial neutral atom density, $\sigma^{(2)}$ is the TPI cross section, and $F = F(r,z)$ represents the *laser photon flux density.*

The solution to this equation has the general form

$$N_i = N_0(1-\exp( -\int \sigma^{(2)} F^2 dt ) \qquad (8)$$

but for an order of magnitude calculation let us assume F to be a square pulse. In which case

$$F^2 = \frac{\ln [N_0 / ( N_0 - N_i)]}{\sigma^{(2)} t} \qquad (9)$$

If we now approximate the values appropriate to our experiment,

$\sigma^{(2)} = 10^{-48}$ $cm^2/sec$ $\quad\quad$ $\omega = 4.4959 \times 10^{15}$/sec

$\tau = 15$ ns $\quad\quad$ $w_0 = 100$ μm (beam radius at focus)

$F =$ Energy per pulse/$h\omega \tau\pi w_0^2$ $\quad\quad$ Energy per pulse = 5 mJ

we can determine the highest density expected under the above assumptions, i.e.,



$$(N_0 - N_i) / N_0 = \exp [F^2 \sigma^{(2)} t] \approx 1\% \qquad (10)$$

Since our typical neutral densities were of the order of $10^{16}$ $cm^{-3}$, we can thus expect ion densities in the $10^{14}$ $cm^{-3}$ range.

## Parametric Oscillation and Mixing

To formulate a description for NLO processes, we shall use an approach that is similar to the three-wave solution of Bloembergen [13], and Byer [14] However, we shall deal with the general case of two, different attentuation constants for the signal and idler fields, and show how the expressions for these constants arise implicitly from the wave equations, where normally the constants are invoked phenomenalogically.

Finally, we shall discuss the possibility of 'lasing' on the idler frequency, and the possibility of having two signal and idler pairs. Although Ward and Smith [15] have also discussed the criteria for idler lasing, we offer an analysis that avoids the somewhat confusing *expressions that stems from their imaginary wave vector method.*

Let us consider the ion medium to be dielectric, non-magnetic and conducting: In such case, Maxwell's equations become,

$$\nabla \cdot E = \rho \qquad (11) \qquad\qquad \nabla \times E = -\frac{\partial B}{\partial t} \qquad (12)$$

$$\nabla \cdot B = 0 \qquad (13) \qquad\qquad \nabla \times B = \mu_0[\epsilon_0 \frac{\partial E}{\partial t} + J] \qquad (14)$$

where E, B, J, and ρ represent the Electric field intensity, Magnetic - induction. Current density and Charge density respectively. Substituting (14) into (12) and using the curl-curl rule gives the wave equation for the E field

$$\nabla^2 E = \frac{1}{c^2} \frac{\partial^2 E}{\partial t^2} + \frac{1}{\epsilon_0} \frac{\partial J}{\partial t} \qquad (15)$$

Following the method of Bloembergen [13], let

$$J = J_{cond} + \frac{\partial P}{\partial t} \tag{16}$$

where $J_{cond}$ is the static contribution due to conduction, and let P, the Polarization, represent the linear plus nonlinear contribution,

$$P = P^{L} + P^{NL} \tag{17}$$

We then obtain, using the constitutive equations,

$$J_{cond} = \sigma E \tag{18}$$

$$P^{L} = \epsilon_o \chi^{(1)} E \tag{19}$$

the wave equation,

$$\nabla^2 E = \frac{1}{c^2}\left[\left\{1 + \chi^{(1)}\right\}\frac{\partial^2 E}{\partial t^2} + \frac{1}{\epsilon_o}\frac{\partial^2 P^{NL}}{\partial t^2} + \frac{\partial(\sigma E/\epsilon_o)}{\partial t}\right] \tag{20}$$

Difference Mixing

Equation (20) represents a general purpose non-linear wave equation in a conducting, non-magnetic medium. To apply it to the problem of doubly resonant 4-wave amplification, we need to define all the polarizations involved.

Using only terms in third order and retaining only the dominant ones, we have [15],

$$P^{(3)}(\omega_p) = \epsilon_o \chi^{(3)}_1(-\omega_p;\omega_s,\omega_i,-\omega_p)E_p^* E_s E_i + \epsilon_o \chi^{(3)}_2(-\omega_p;\omega_p,\omega_p,-\omega_p)E_p^* E_p^2 \tag{21}$$

$$P^{(3)}(\omega_i) = \epsilon_o \chi^{(3)}(-\omega_i;\omega_p,\omega_p,-\omega_s)E_p^2 E_s^* \tag{22}$$



$$P^{(3)}(\omega_s) = \epsilon_o \chi^{(3)}(-\omega_s;\omega_p,\omega_p,-\omega_i)E_p^2 E_i^* \tag{23}$$

In equation (21), the first term represents energy which the laser can gain from the parametric signals while the second represents the two-photon absorption loss. In equations (22) and (23), the terms represent energy extracted from the laser at the idler and signal frequencies respectively.

If we now assume the waves to have a solution of the form (plane wave approximation),

$$E_s = E_{so}\exp(ik_s z - i\omega_s t) \tag{24}$$

$$E_i = E_{io}\exp(ik_i z - i\omega_i t) \tag{25}$$

$$E_p = E_{po}\exp(ik_p z - i\omega_p t) \tag{26}$$

and define the following variables,

$$\alpha_a = \frac{\omega^2}{c^2 k_a \epsilon_o} \text{Im}\ \chi^{(1)}(\omega_a) \tag{27}$$

$$\Delta k = 2k_p - k_s - k_i \tag{28}$$

$$k_a = \frac{1}{c^2}\left[1 + \frac{1}{\epsilon_o}\text{Re}\ \chi^{(1)}(\omega_a)\right] - \frac{i\sigma}{c}\frac{\omega_a}{\epsilon_o} \tag{29}$$

where $\alpha_a$ is the linear absorption term at frequency $\omega_a$, $k_a$ the associated wave number, and $\Delta k$ is the wave vector mismatch, the reduced wave equations for each of the fields are determined by substituting (24), (25), and (26) into equation (20). The algebra is straight forward if we use the slow wave approximation,

$$\frac{\partial^2 E}{\partial t^2} << 2k\frac{\partial E}{\partial z}$$

The resulting equations are,

$$\frac{dE_s}{dz} = \frac{i\,\mu_o\omega_s^2}{2k_s} E_p^2 E_i^* \chi^{(3)}(\omega_s)\, e^{i\Delta kz} - \frac{\alpha_s}{2} E_s \qquad (30)$$

$$\frac{dE_i}{dz} = \frac{i\,\mu_o\omega_i^2}{2k_i} E_p^2 E_s^* \chi^{(3)}(\omega_p) e^{i\Delta kz} - \frac{\alpha_i}{2} E_i \qquad (31)$$

$$\frac{dE_p}{dz} = \frac{i\,\mu_o\omega_p^2}{2k_p} E_p^* \left[E_s E_i \chi_1^{(3)}(\omega_p) e^{i\Delta kz} + E_p^2 \chi_2^{(3)}(\omega_p)\right] - \frac{\alpha_p}{2} E_p \qquad (32)$$

To solve (30), (31) and (32), we assume as usual, a neglible pump beam depletion over the irradiated column:

$$E_p(z,t) = E_p(t)$$

In other words, we assume only a small fraction of the laser pump pulse is actually used to photo-ionize and pump the ions, i.e.,

$$\frac{I_p}{h\omega_p} >> 4\, N_1\, L\, p_t \qquad (33)$$

where $I_p$ is the laser irradiance, L the column length, $p_t$ probability of two photon absorption + conversion per unit time, and $N_1$ the ion ground state density

Assuming (33) to be valid, we can substitute the conjugate of (30) into the derivative of (31) to obtain

$$\frac{d^2E_i}{dz^2} + \frac{\alpha_i}{2}\frac{dE_i}{dz} + \frac{i\beta_i\alpha_s}{2} E_s^* e^{i\Delta kz} - \beta_i\beta_s^* E_i + \beta_i \Delta k\, E_s^* e^{i\Delta kz} = 0 \qquad (34)$$



where we define

$$\beta_{i,s} = \frac{\mu_o\omega_{i,s}^2}{2k_{i,s}} \chi^{(3)}(\omega_{i,s})\, E_p^2 \qquad (35)$$

Using a manipulated form of (31),

$$E_s^* e^{i\Delta kz} = \frac{1}{i\beta_i}\left[\frac{dE_i}{dz} + \frac{\alpha_i E_i}{2}\right]$$

to substitute into (34), we arrive at,

$$\frac{d^2E_i}{dz^2} + b\frac{dE_i}{dz} + c\,E_i = 0 \qquad (36)$$

where $$b = \frac{1}{2}(\alpha_i + \alpha_s) - i\Delta k \qquad (37)$$

$$c = \frac{\alpha_i\alpha_s}{4} - \beta_i\beta_s^* - i\frac{\alpha_i\Delta k}{2} \qquad (38)$$

The solution is thus,

$$E_i = E_{i1}e^{\gamma_+ z} + E_{i2}e^{\gamma_- z} \qquad (39)$$

where,

$$\gamma_\pm = \frac{-b \pm \sqrt{b^2-4c}}{2} \qquad (40)$$

If we let

$$E_i(0) = E_{i0} \qquad (41)$$

and compare,

$$\frac{dE_i}{dz} = \gamma_- E_{i1} e^{\gamma_- z} + \gamma_+ E_{i2} e^{\gamma_+ z} \tag{42}$$

with

$$\left.\frac{dE_i}{dz}\right|_{z=0} = -\frac{\alpha_i E_{i0}}{2} + i\beta_i E^*_{s0} \tag{43}$$

we find,

$$\gamma_- E_{i1} + \gamma_+ E_{i2} = \frac{-\alpha_i E_{i0}}{2} + i\beta_i E^*_{s0} \tag{44}$$

Thus,

$$E_{i1} = \frac{(\gamma_+ + \alpha_i/2)E_{i0} - i\beta_i E^*_{s0}}{2\Gamma} \tag{45}$$

$$E_{i2} = \frac{-(\gamma_- + \alpha_i/2)E_{i0} + i\beta_i E^*_{s0}}{2\Gamma} \tag{46}$$

where,

$$(\gamma_+ - \gamma_-)/2 = \Gamma \tag{47}$$

Substituting (45) and (46) into (39) now gives,

$$E_i(z) = \frac{E_{i0}}{4\Gamma}(b-\alpha_i)(e^{\gamma_+ z} - e^{\gamma_- z}) +$$

$$\frac{E_{i0}}{2}(e^{\gamma_- z} + e^{\gamma_+ z}) + \frac{i\beta_i E^*_{s0}}{2\Gamma}(e^{\gamma_+ z} - e^{\gamma_- z}) \tag{48}$$

which becomes with some back substitution



$$E_i(z)e^{(\alpha_i+\alpha_s)z/4} e^{-i\Delta kz/2} = E_{i0}(\cosh \Gamma z +$$

$$\frac{((\alpha_s-\alpha_i)-2i\Delta k)}{4\Gamma} \sinh \Gamma z + \frac{i\beta_i E^*_{s0}}{\Gamma} \sinh \Gamma z \tag{49}$$

and in a similar manner, the solution for the signal field is found to be,

$$E^*_s(z)e^{(\alpha_i+\alpha_s)/4} e^{-i\Delta kz/2} = E^*_{s0}(\cosh \Gamma^* z +$$

$$\frac{((\alpha_s-\alpha_i)-2i\Delta k)}{4\Gamma^*} \sinh \Gamma^* z) + \frac{i\beta_s E_{i0}}{\Gamma^*} \sinh \Gamma^* z \tag{50}$$

where,

$$\Gamma = [\frac{\delta}{4} + \beta_i\beta^*_s - (\Delta k/2)^2]^{1/2} \tag{51}$$

$$\delta = \frac{(\alpha_i-\alpha_s)^2}{4} + i(\alpha_i-\alpha_s)\Delta k \tag{52}$$

At this point, let us interpret the nature of these equations. Firstly, the exponential containing $-i\Delta kz/2$ can be neglected since it will disappear when irradiance is considered. The second exponential, however, is real and in the normal case represents the Beer-Lambert attentuation process. On the right hand side, the $E_{s0}$ and $E_{i0}$ constants are the initial $z = 0$ values of the fields. Since we are considering the case when only the laser pump field is incident to the medium, we associate these values with either noise from the pump field, spontaneous emission from pump field absorption, or collisionally induced radiative processes.

Special Cases Involving Parametric Gain

The $\Gamma$ value is normally called the "parametric gain" factor. When $\Gamma$ is real ($\Gamma = \Gamma^*$), the above equations indicate that refractive index effects on the phase velocities are sufficiently overcome (by the induced polarizations of the bound electrons) to create gain. In general, the equations for the idler and signal are well coupled; but here let us consider several special cases. To simply the analysis, let us assume the mismatch, $\Delta k$, to be very small. A particular case of physical significance arises if $\beta_i$, $|\alpha_i| \ll |\alpha_s|$; or more specifically, assume the intermediate state(s) is not significantly populated relative to the ion ground state, and that parametric gain is small. If, furthermore, tne $|\Gamma|z$ product is quite large, such that the negative exponentials in $\Gamma$ can be neglected, we have the following:

$$E_s(z) = \frac{E_{s0}}{2} \exp\{[\Gamma - \frac{(\alpha_s+\alpha_i)}{4}]z\} \left[1 + \frac{(\alpha_i-\alpha_s)}{4\Gamma} + \frac{i\beta_s E_{i0}}{\Gamma E_{s0}}\right] \quad (53)$$

$$E_i(z) = \frac{E_{i0}}{2} \exp\{[\Gamma - \frac{(\alpha_s+\alpha_i)}{4}]z\} \left[1 + \frac{(\alpha_s-\alpha_i)}{4\Gamma} + \frac{i\beta_i E_{s0}}{\Gamma E_{i0}}\right] \quad (54)$$

And since $\alpha_s$ will also dominate the expression for $\Gamma$,

$$\Gamma = \frac{\alpha_s - \alpha_i}{4} \quad (55)$$

then,

$$\frac{|E_s(z)|}{|E_i(z)|} \approx \frac{2|\beta_s|}{\alpha_s} = \frac{\mu_0 \omega_s^2 \chi^{(3)}(\omega_s) |E_L|^2}{k_s \alpha_s} \quad (56)$$

This expression conforms within a factor of 2, with that given by Bloembergen, following the consideration that he treated the other extreme, $\alpha_i \gg \alpha_s$.

As noted by Bloembergen, this is a very interesting result. Even



though the damping in the signal wave is severe enough to dominate the parametric gain, there can still be strong gain in the idler and much weaker gain in the signal.

Even more interesting, is to assume $\alpha_s$ is negative, corresponding to the case of a population inversion between the intermediate and upper level. Although equations (53) and (54) still apply, it is more fruitful to insert (55), to obtain,

$$|E_s(z)| \approx 2 E_{i0} \exp\left[-\frac{\alpha_s z}{2}\right] \left(\frac{|\beta_s|}{\alpha_s}\right) \quad (57)$$

and

$$|E_i(z)| \approx E_{i0} \exp\left[-\frac{\alpha_i z}{2}\right] \quad (58)$$

The conventional laser gain equation is revealed and in addition a combination process is obtained whereby a parametric signal appears on the cascade transition.

Let us now look at the case when two intermediate levels exist (labelled 1 and 2) with the arrangement where susceptibilities controlling the mixing between parametric pairs are insignificant. The analysis is then very simple since each pair is generated independently of the other, and in the above stated attentuation regime, their relation will be:

$$\frac{|E_{s1}|}{|E_{s2}|} \approx \frac{E_{i10}}{E_{i20}} \exp\left[\frac{(\alpha_{i2}-\alpha_{i1})z}{2}\right] \frac{|\beta_{s1}|}{|\beta_{s2}|} \frac{\alpha_{s2}}{\alpha_{s1}} \quad (59)$$

$$\frac{|E_{i1}|}{|E_{i2}|} \approx \frac{E_{i10}}{E_{i20}} \exp\left[\frac{(\alpha_{i2}-\alpha_{i1})z}{2}\right] \quad (60)$$

so that,

$$\frac{|E_{s1}|}{|E_{i1}|} \approx \frac{|\beta_{s1}|}{|\beta_{s2}|} \frac{\alpha_{s2}}{\alpha_{s1}} \frac{|E_{s2}|}{|E_{i2}|} \quad (61)$$

where,

$$\frac{\beta_{s1}\alpha_{s2}}{\beta_{s2}\alpha_{s1}} = \left[\frac{\omega_{s1}}{\omega_{s2}}\right]^2 \frac{\chi^{(3)}(\omega_{s1})}{\chi^{(3)}(\omega_{s1})} \frac{\text{Im } \chi^{(1)}(\omega_{s2})}{\text{Im } \chi^{(1)}(\omega_{s2})} \qquad (62)$$

The last two equations represent quite a remarkable result. If the susceptibilities of the system are power independent, then the field ratios of the signal and idler pairs are linearly related through fixed atomic properties. That is, there is no explicit dependence on pump power, gain length ,or initial field conditions.

Experimental Facility

At the heart of our experimental facility is a JK (LUMONICS) HY750 Nd-Yag laser system. The second harmonic generator houses a DCDA water soluble, non-critically phase matched crystal, which maintains the vertical polarization. The third harmonic generator contains a critically phase-matched KDP type crystal which has a horizontally polarized output. The dye laser is a Quanta-Ray, Model PDL-1, requiring a vertically polarized pump beam.

A specially designed Crossed Heat Pipe (CHP) Oven was used to confine a fairly homogeneous column of strontium vapour. The device is made from two cross-butted, stainless steel tubes, each having a length of 24", O.D. 2", and I.D. 1 3/4". Each arm of the CHP oven contains a stainless steel cylindrical mesh that permits the condensed liquid metal to be rapidly drawn back to the central hot zone where evaporation can then re-occur. A more detailed explanation is provided by Cooper [16].

Unfortunately, we have found that strontium is not very suitable for working in heat pipe mode as it tended to crystallize rather than condense. To achieve longer and more stable operations, we have found in agreement with [17], that an overpressure of buffer gas permits increased performance. Generally the CHP oven was operated at about 800°C with an argon buffer gas pressure of about 50 torr.

The photodetection system comprised an RCA 4526 photomultiplier and spectral discrimination was accomplished with a SPEX 1700-II Czerny-Turner



monochromator. Signal triggering was performed by a high speed Hewlett-Packard No. 5082-4220 silicon planar PIN type photodiode, which was also suitable for relative pulse energy measurement when terminated into a 1 MΩ impedence. An overview of the experimental facility is presented as figure 2. A Princeton EG&G Box Car Averager (Model 4420) was used for data acquisition, with a laser repetition rate of 10 Hz.

The neutral strontium density was ascertained in two ways, Gomes [33]: the first used a digital voltmeter to monitor the thermocouple outputs. By consulting a standard table of type K thermocouple readings, the temperature of the central pipe outside region can be determined to about ± 5°K accuracy.

The second involved a measurement of the spectral hole produced by the strontium 4607 A resonance line when the column of vapour was illuminated with an apertured (collimated) broad band Xenon lamp. This technique is described by Cappelli et al [19]. From a knowledge of the optically transparent spectral profile (pipe off), the optically thick spectral profile (pipe on), and the vapour zone length, the neutral strontium density can be determined. From the vapour pressure curve, the temperature can then be calculated and compared with that measured by the voltmeter.

Since both methods yielded temperatures in good agreement (less than 5% discrepancy), we concluded that the central thermocouple would suffice as the neutral density indicator, so long as the crystallization was not severe.

Experimental Results

The laser frequency was first set below the TPI threshold (45932 $cm^{-1}$) and then slowly scanned to the first ion resonance level (23715.19 $cm^{-1}$). A breakdown, predominantly green in colour, of the Strontium vapour was observed to rapidly flicker in intensity until the threshold for TPI was reached.

As the laser frequency approached the value of the ion resonance transition, the luminous intensity increased and shifted to a predominately blue-white colour. The most intense breakdown occurred

when the laser frequency precisely matched the ion resonance value and then slowly levelled off as the frequency was further increased.

The side-on detection arrangement was used and the laser tuned to the two-photon resonance (47736.53 $cm^{-1}$) of Sr II at a wavelength of 418.97 nm. When the monochromator was set to monitor the $6^2S_{1/2} \rightarrow 5^2P_{3/2}$ transition at 430.67A strong emission was observed [figure 3(a)] with high sensitivity to laser tuning (figure 4). Strong signals were also obtained on the $6^2S_{1/2} \rightarrow 5^2P_{1/2}$ transition at 416.3 nm [figure 3(b)], as well as the cascade transitions $5^2P_{3/2} \rightarrow 5^2S_{1/2}$ at 407.89 nm [figure 3(c)] and $5^2P_{1/2} \rightarrow 5^2S_{1/2}$ at 421.67 nm [figure 3(d)]. The relative intensity peak values [1.8 (421.67 nm), 1.45 (416.3 nm), 3.8 (407.89 nm), 3.3 (430.67 nm)] compare favourably with the relative gf values for the transitions .716, .315, 1.47 and .731, while the measured emission half-lives of 7, 6, 8 and 7 (ns) are very different from the accepted values of 7.9, 7.0, 1.6 and 7.8 ns, respectively.

All signals were found to increase with neutral density. The sensitivity to laser intensity was also studied in the case of the 430.67 nm line (figure 5), and interestingly, the relation can be seen to be close to parabolic.

## Doubly Resonant Difference Mixing in Sr II

With the end-on configuration (i.e., the emission emerging close to colinear with the residual pump laser radiation is directed towards the photodetection system, see figure 2) and the laser is tuned to the two-photon ($5^2S_{1/2} \rightarrow 6^2S_{1/2}$) resonance in Sr II, an intense diverging beam was detected at 430.67 nm in the forward direction. No focussing, imaging, or filtering was required to isolate the signal, and the gain on the PMT had to be reduced to avoid saturation, and the monochromator slits were closed down to 10 μm. Using a pinhole aperture at the exit window of the pipe and a 22 cm. imaging lens, certain regions off axis from the pump laser gave comparable signals, in fact, to the pump laser intensity signal.

In addition to the 430.7 nm signal, three other strong emission signals were detected at 407.9 nm, 416.3 nm and 421.7 nm with significantly



less intensity. The relative intensities of the four signals were approximately 100, 10, 2, and 0.5 respectively.

With the pump laser tuned to the two-photon resonance, temporal traces of the 430.7 nm line were acquired as a function of incident intensity. This involved monitoring a small portion of the incident light on a photodiode, while a wedge type neutral density filter was translated into the beam. As indicated in figure 6 peak emission signal is seen to have an abrupt threshold and then appears to saturate rather quickly. Further evidence for saturation provided as a comparison of the temporal history of the 430.67 nm emission with that of the laser pulse, see figure 7. The 430.67 nm signal is seen to peak and practically decay away by the time the laser pulse attains its maximum intensity.

To differentiate between possible mechanisms that might generate this intense, near colinear 430.67 nm emission, the mirror close to the SPEX monochromator was rotated for rear light collection. However, no detectable signal was observed at 430.67 nm.

The 430.67 nm signal was also studied as a function of neutral density. In all cases, the signal was found to monitonically increase with neutral density, and no saturation or threshold effect was observed in the measurement interval.

Using the end-on arrangement and slit widths of 10 μm, a further experiment was undertaken to measure the spectral profile of the 430.67 nm signal as a function of laser pump frequency. This involved setting the EG&G signal averager to sampling gate mode, and gating the signal over the time duration of the pulse, while the monochromator was scanned over the 0.64 nm range, centered near the line transition centre. This procedure was repeated in 1-2 wave number increments of the laser frequency over the range for which the signal was detectable. The resulting family of curves is shown in figure 8, where the resolution of the monochromator was approximately 0.02 nm for this slit setting.

## Discussions and Conclusions

We believe that the observed strong end-on emission at 430.67 nm has a parametric origin (four-wave difference mixing) rather than arising from

stimulated emission. This conclusion is based on the following considerations:

(1) The strong 430 (430.67) nm end-on emission was accompanied by two weaker, nearly collimated beams of radiation at the ion resonance wavelengths of 407.89 and 421.67 nm. Since a population inversion with respect to the ground state is a highly unlikely possibility, the origin of these two weaker beams is also assumed to be parametric.

(2) The 430 nm radiation was observed to be slightly tunable, and fairly broad spectrally, figure 8; both features are characteristic of parametric processes.

(3) No 430 nm radiation was observed to be emitted from the laser pulse "incident end" of the CHP oven, whereas one would expect stimulated emission to emerge in approximately equal proportions from both ends, assuming negligible laser beam attenuation.

(4) The spontaneous side-arm emission from the $6^2S_{1/2}$ level at 430 nm was observed to increase fairly monitonically with the laser pulse intensity. One would not expect this to be the case if a population inversion threshold was exceeded.

(5) The axis of the laser pulse and 430 nm beams appeared to be slightly angled as determined by a spatial analysis of their intensity ratios. This observation would be consistent with a phase match dependent process.

(6) Many similiar results have been observed in neutral atomic species and most were determined to be parametric based processes.

Since the results conform with parametric theory, the equations presented earlier provide a suitable framework for which to model this process. However, this analysis is deficient in that it fails to take account of the populations of the various levels induced by this parametric interaction. A more complete analysis allowing for this effect might account for the saturation behaviour of the parametric signals. To do this one would have to account for the variation in the populations, modify the N in the susceptibility factors and phase factor by terms of the form $[N_1 - (g_1/g_2)N_2]$ and couple the parametric radiative transfer equations to population rate equations in a manner similar to the work of Puell et al



[20] for Third Harmonic Generation. In our case this saturation effect is so severe that the signal intensity drops virtually to zero at the peak of the laser pump intensity, see figure 7.

A second deficiency of the theory appears to be in the estimate of ionization yield. There is evidence that electron-impact processes could be quite important and contribute to the ionization, in which case the ionization percentage could be significantly higher than expected.

In summary we have demonstrated that a single wavelength laser, of modest intensity, can create both an ion medium and parametric processes within that medium. We believe that our results represent the first demonstration of a parametric mixing process in Sr II, and the first time "difference mixing" has been demonstrated involving the ground state of an ion. Although a saturation effect was found to limit the gain we expect the process to be intensity scaleable by simply increasing the beam waist of the laser pump pulse. The alkaline earth ions have been shown to have unique properties involving the position of the intermediate states. According to an initial evaluation of this effect on parametric gain processes, this allows high gain to be obtained at low densities making such ions a very attractive medium for these types of interactions, Menard [5].

Our encouraging results lead us to propose other schemes which may prove fruitful in the quest for efficient short wavelength generation. One possibility is THG in Mg II using the same two-photon resonant enhancement technique, yielding radiation near 95.5 nm, while pumping at 287 nm. Another is THG in Be II yielding 75.6 nm radiation with a 227 nm pump. And, although phasematching would be more difficult to achieve for THG, the common techniques (dispersive gases) used for atomic vapours [21] should be equally effective in an ionic medium.

More advanced possibilities involve the doubly ionized group III elements which could be formed by similar photo-ionizing techniques and which have similar properties to the group II singly ionized ions. With B III, for example, the two photon resonance ($2^2S_{1/2} \rightarrow 3^2S_{1/2}$) corresponds to 180,201.8 $cm^{-1}$ and the B IV limit is 305,931 $cm^{-1}$. Thus it may be feasible to sum mix two photons at 111 nm with one photon near 100 nm to obtain 35.7 nm. And similarily with the group IV series, one can approach the soft

x-ray region with, for example, C IV, by mixing two photons turned to the $2^2S_{1/2} \rightarrow 3^2S_{1/2}$ transition ( $\lambda$ = 66.0 nm) with another at $\lambda$ = 50 nm to generate 19.9 nm radiation. Schemes such as these do not seem unreasonable when one considers the work of Boker [22] whereby 35 nm radiation was generated in a gas jet by 7 photon harmonic conversion.

Acknowledgements

This work was supported by the U.S. Air Force Office of Scientific Research (under grant number AFOSR 85-0020) and the Natural Science and Engineering Research Council of Canada.

References

1. P. Rosen, Phys. Fluids vol 4, 341 (1961).
2. R. R. Freeman, J. Boker, W. E. Cooke, Phys. Rev. A, vol. 26, no. 5, 3029 (1982).
3. J. Boker, R. R. Freeman, and W. E. Cooke, Laser Tech. for EUV Spec., 153 (1982).
4. C. R. Vidal, App. Optics, vol. 19, 3897, 1980.
5. K. A. Menard, University of Toronto, M.A.Sc. Thesis, 1986.
6. Y. S. Kim and P. Lambropoulos, Phys. Rev. A., vol. 29, no. 6, 3159 (1984).
7. P. Esherick, Phys. Rev. A., vol. 15, no. 5, 1920 (1977).
8. P. Ewart and A. F. Purdue, J. Phys. B: Atom. Molec. Phys., vol. 9, No. 15, L437 (1976).
9. I. I. Bondar et al, J. Phys. B.: Atom. Molec. Phys. vol. 17, 2049 (1984).
10. G. Leuchs, Laser Physics Proceedings, Hamilton New Zealand, 174 (1983).
11. A. Gold, Proc. Int. School of Phys: Quantum Optics, 397 (1969).
12. H. B. Bebb, Phys. Rev., vol. 149, no. 1, 25 (1966).
13. N. Bloembergen, Nonlinear Optics, (Benjamin, New York, 1965).
14. R. L. Byer and R. L. Herbst, Nonlinear Infrared Generation (chap 3); Ed. by Y. R. Shen, Springer-Verlag, New York, 1977.



15. A. V. Smith and J. F. Ward, IEEE J. Quantum Electronics, vol. QE-17, no. 1, 525 (1981).
16. R. C. Vidal, J. App. Phys. vol. 44, 2225 (1973).
17. G. Gerber, R. Moller and H. Schneider, J. Chem. Phys., vol. 81, no. 4, 1538, (1984).
18. P. Gomes, UTIAS M.A.Sc. Thesis, 1986.
19. M. A. Cappelli, P. G. Cardinal, H. Herchen and R. M. Measures, Rev. Sci. Instrum. Vol. 56, 2030, 1985.
20. H. Puell, H. Shiengraber and C. R. Vidal, Phys. Rev. A, 22, 1165 (1980).
21. R. B. Miles and S.E. Harris, IEEE J. Quantum Electronics, vol. QE-9, no. 4, 470 (1973).
22. J. Boker, P. H. Bucksbaum and R. R. Freeman, Optics Lett., Vol. 8, 217-219, 1983.

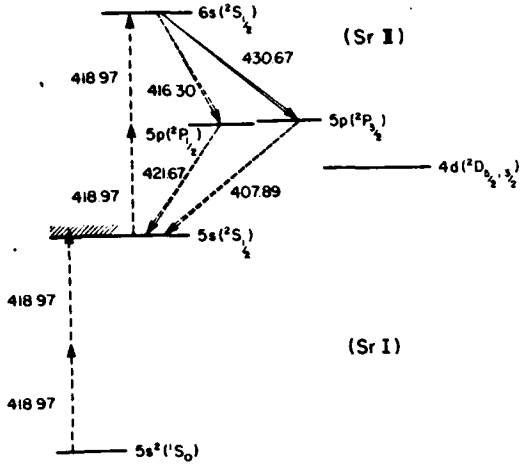


Figure 1. Partial Grotrian Energy Level Diagrams for Sr I and Sr II.

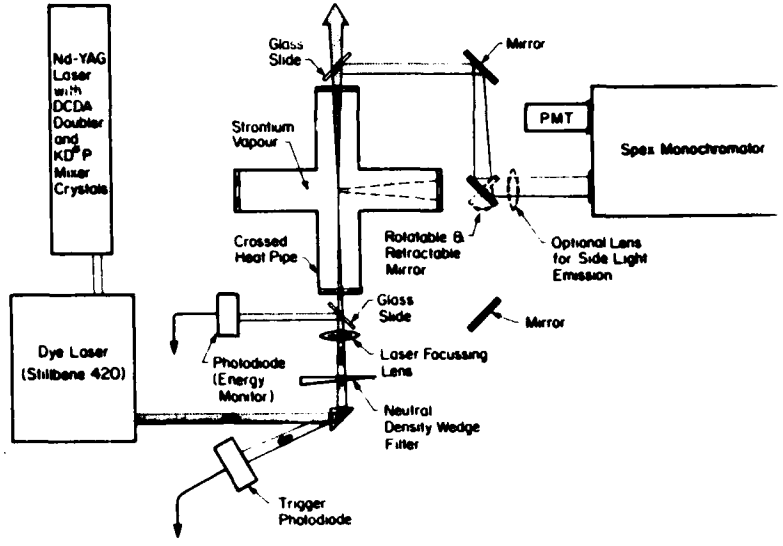


Figure 2. Schematic View of the Strontium Multiphoton Interaction Facility.

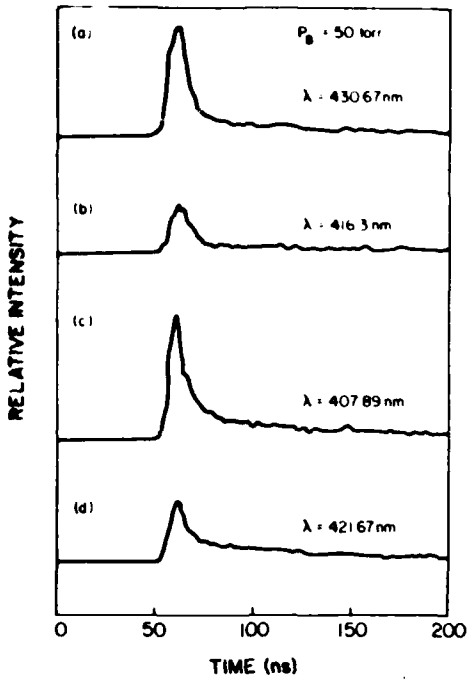


Figure 3. Temporal Variation of the 430.67, 416.30, 407.89 and 421.67nm Side-Emissions from a Strontium Plasma Pumped by a Laser Tuned to the 418.67nm Two Photon Transition in Sr II.

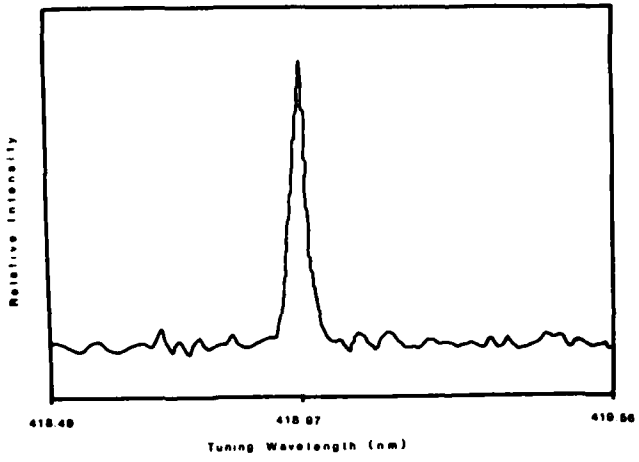


Figure 4. Sensitivity of the 430.67nm Emission from a Strontium Plasma to the Laser Wavelength in the Vicinity of the Two Photon Transition Wavelength, 418.97nm.

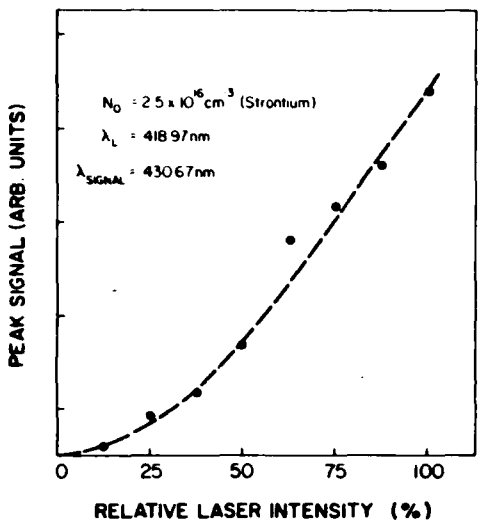


Figure 5. Dependence of Peak Spontaneous (Side) Emission at 430.67nm, from a Strontium Plasma on the Relative Laser Energy. 100% Corresponds to the Maximum Available Energy in the Laser Pulse ($\lambda_L$ = 418.97nm).

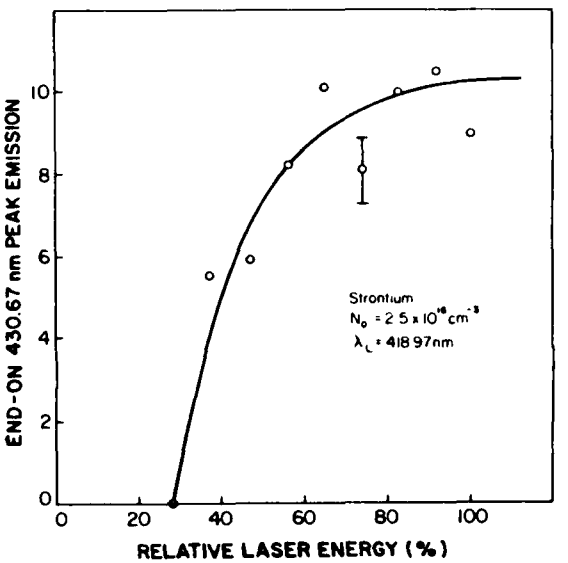


Figure 6. Dependence of "End-On" Peak Emission at 430.67nm on the Relative Laser Energy ($\lambda_L$ = 418.97nm).

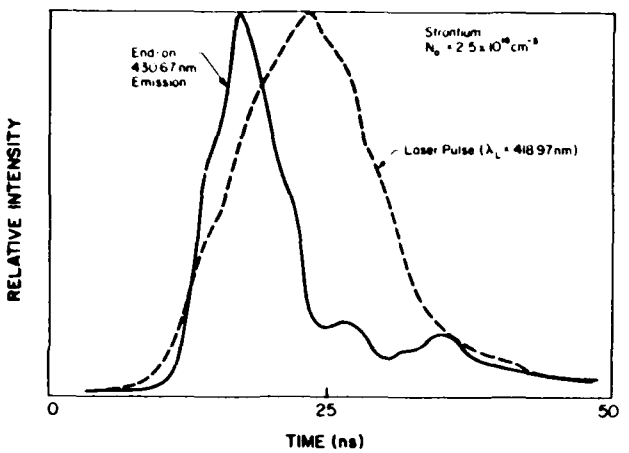


Figure 7. Comparison of the Temporal Histories of the Incident Laser Pulse at 418.97nm and the End-On 430.67nm Emission from a Strontium Plasma.

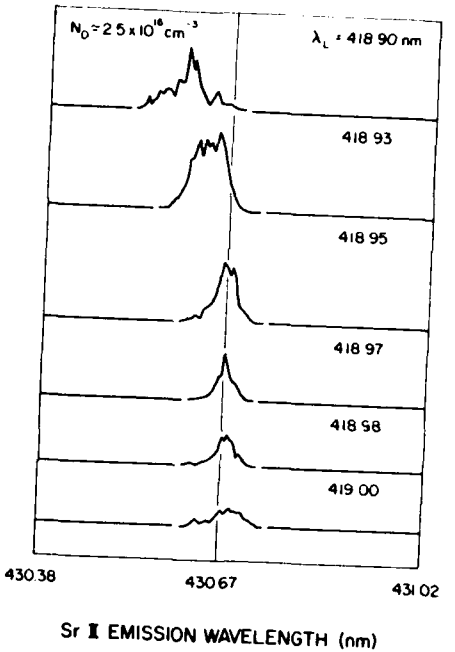


Figure 8. Several End-On Emission Spectra, in the Vicinity of 430.67nm, For a Strontium Plasma Pumped by Laser Pulses of Different Wavelength ($\lambda_L$).

END

11-86

DTIC